# LABORATORY STUDIES ON THERMAL FRACTURING BEHAVIOR IN WELL STIMULATION OF ENHANCED GEOTHERMAL SYSTEMS

A Thesis

by

YUNXING LU

Submitted to the Office of Graduate and Professional Studies of
Texas A&M University
in partial fulfillment of the requirements for the degree of

MASTER OF SCIENCE

| | |
|---|---|
| Chair of Committee, | Minsu Cha |
| Committee Members, | Marcelo Sanchez |
| | Kan Wu |
| Head of Department, | Robin Autenrieth |

August 2017

Major Subject: Civil Engineering

# ABSTRACT

Thermal fracturing is aim to increase the permeability of the reservoir formation through thermal stress cracking. It occurs in enhanced geothermal system (EGS) wells and other types of geothermal wells where the temperature difference between injection fluid and reservoir temperature is high. Although the hydraulic fracturing is the effective technology to improve the production wells with low permeability in EGS, thermal fracturing is observed to further enhance the permeability of reservoir. However, the mechanism of thermal fracturing in downhole conditions is still not well understood. In the thesis, we aim to provide a deeper understanding of the thermal fracturing and thermal shock mechanisms by an experimental study in a laboratory environment mimicking EGS wellbores.

The laboratory study investigates the behavior of thermal fracturing stimulation by using room temperature water injected into hot concrete and granite blocks without confining pressure. An experimental test system and test procedures were developed and used to apply thermal shock to wellbores in block specimens with elevated temperatures. Water usage, borehole pressure, and temperature were monitored continuously during the fracturing process. The direct and indirect assessments of fractures were made by visual inspection, bubble leakages, pressure decay, and acoustic signatures before and after the experiments. In addition, the mechanical and thermal properties are measured and analyzed before and after treatment.

Experimental data showed that the permeability of the treated specimens was enhanced by the macro/micro cracks induced by thermal loading during thermal

stimulations. The profiles of borehole pressure decay obtained before and after each stage of stimulation show that the thermal shock increased the permeability of treated specimens. The thermally driven fractures were usually initiated from the borehole surfaces and propagated adjacent to the boreholes to some extent. Those fractures was confirmed by the acoustic measurement and visually demonstrated by bubble leakage tests. These "seed" fractures created during the thermal stimulations may help reduce the breakdown pressure levels of pressure-based fracturing methods, and improve fracturing efficiency by creating multiple thermal fracture surfaces around a wellbore.

CONTRIBUTORS AND FUNDING SOURCES

## Contributors

*Part 1, faculty committee recognition*

This work was supervised by a thesis committee consisting of Professor Minsu Cha and Professor Marcelo Sanchez of the Department of Civil Engineering and Professor Kan Wu of the Department of Petroleum Engineering.

*Part 2, student/collaborator contributions*

All work for the thesis was completed by the student, in collaboration with Dani Dawson, Jack Kong, Dong Wang, Yong Deng, Xi Luo, Xijun Shi, Jimmy Liu, and the rest of Aggies in the Department of Civil Engineering.

## Funding Sources

Graduate study was supported by a fellowship from Texas A&M University and the funding contributions from Texas Engineering & Experiment Foundation.

TABLE OF CONTENTS

Page

Page

LIST OF FIGURES

Page

LIST OF TABLES

Page

# 1. INTRODUCTION

## 1.1 Motivation and background

The extensive high-temperature resource that exists in the hot, dry rock is always challenging to utilize economically and optimally due to the low permeability of the wellbore face and reservoir in the enhanced geothermal system (EGS) (Duchane and Brown, 2002, Fragaszy et al., 2011). Thermal fracturing is a concept that tries to maximize the effect of the application of traditional hydraulic fracturing in the EGS. It relies on a large thermal gradient that between the injection fluid and reservoir temperature to initiate fractures in the rock under downhole conditions.

The rapid cooling will occur when the cold water is injected into the hot reservoir. This process will make the rock surface to shrinkage and generate the local tensile stress. Once this stress is sufficiently build up that exceeds the tensile strength of rock, the new fractures will generate. These fractures could penetrate deeper inside the reservoir by the following up borehole pressure. The thermal stimulation has been applied in many enhanced geothermal system fields, such as in Los Humeros, Mexico; Hellisheidi high-temperature field, Iceland. It has been proved that it is very efficient to improve the permeability in the EGS reservoir by re-opening the existing fractures, opening new fractures or cleaning the debris in the flow channel. However," the thermal stimualtion mechanism that occurred in the field and the preferred methodology for the thermal stimulation application is still not well understood" (Siratovich, 2014).

## 1.2 Literature review

The thermal stimulation has been applied in many enhanced geothermal system fields, such as in Los Humeros, Mexico; Hellisheidi high-temperature field, Iceland. It has been proved that it is very efficient to improve the permeability in the EGS reservoir by re-opening the existing fractures, opening new fractures or cleaning the debris in the flow channel. However, the thermal stimualtion mechanism that occurred in the field and the preferred methodology for the thermal stimulation application is still not well understood (Siratovich, 2014). The literature review in this chapter will include the most important aspects that related to the thermal stimulation. It will give the relevant knowledge to understand the performance of the Enhanced Geothermal System better. "Although it is known that thermal shock could initiate the fracture in the rocks, the mechanism that responsible for the successful thermal stimulation is not well understood" (Siratovich et al., 2015). "To date, there also has not been one preferred methodology for application of thermal stimulations that account for the end of borehole conditions and surface infrastructure, injection fluid availability, and well completion" (Siratovich et al., 2011).

Cryogenic fracturing is one of the waterless or reduced-water fracturing technologies in hydrocarbon reservoirs. The method employs sharp thermal gradient surrounding wellbore created from liquid nitrogen injected to or flowed through wellbore (Alqahtani et al., 2017). Thermal shock on wellbore surfaces induces tensile fractures on the surfaces. It is aimed to improve reservoir permeability by thermal shock and also alleviate the concerns of formation damage, water consumption and environment impact that are

associated with the water-based fracturing in the unconventional resources. Wang et al. (2016) reviewed the current key theories and features of waterless fracturing technologies.

Cha et al. (2014) experimentally investigated the cryogenic fracturing stimulation by using liquid nitrogen to initiate and propagate fractures on unconfined rock specimens by strong thermal gradient. The cryogenic fracturing conducted in their study were able to create cracks in rock blocks and change the rock properties. The rock properties will also affect the effect of the cryogenic stimulations. The visible fractures were generated in the cement block by the repeated thermal shock. Those fractures were also detected and demonstrated by the acoustic signal and CT scan. However, no visible fractures were observed in the sandstone blocks after several cyclic of treatments. But the signature from the acoustic measurements suggested that there were invisible fractures generated inside the sandstone block by the thermal gradient.

Further experimental studies on cryogenic fracturing were performed under true triaxial loading and an environment better mimic wellbores of oil and gas reservoirs (Cha et al., 2016b). The cryogenic fracturing under triaxial loading revealed that the permeability enhanced, breakdown pressure reduced, fracture direction and internal stress field were altered due to cryogenic treatments (Alqatahni et al., 2016). A study using transparent specimens allowed to observe radial and vertical (longitudinal) fractures adjacent a wellbore (Cha et al., 2016a).

## 1.3 Objectives and scope of the thesis

The thesis aims to emulate the thermal stimulation of geothermal reservoir through laboratory based investigations and have a better understanding of how the fracture initiate

and propagate. Studying the laboratory scale tests of permeability enhancement by injecting the cold water into hot reservoir rock, we will provide a deeper understanding thermal fracture mechanism in the enhanced geothermal system.

In Chapter 1, the previous studies, especially on the thermal fracturing mechanism and case studies, of thermal fracturing in geothermal field are reviewed and summarized.

In Chapter 2, we present an experimental rig designed to resemble EGS thermal stimulations in laboratory scale and show results gathered from laboratory concrete blocks. No confining pressure is applied to specimens in this study. Acoustic signal, mechanical properties and thermal properties are measured and analyzed before and after the treatment.

In Chapter 3, to have more understanding that how thermal stimulation in EGS may occur, we designed and developed an integrated system to emulate thermal stimulation under wellbore condition in laboratory scale. We present a laboratory study of the role of thermal stress on fracture imitation and propagation. The acoustic amplitude and acoustic velocity are profiled to describe the physical properties. Thermal conductivity, expansion of thermal diffusivity are also measured before and after the thermal stimulation.

In Chapter 4, we applied thermal shock on granite core specimens by heating and quenching them. Then we observed how micro and macro properties are altered by some methods. We characterized mechanical and thermal properties before and after quenching tests. The physical properties measured include elastic wave velocities, dynamic modulus, thermal conductivities, the coefficient of thermal expansion, specific heat, and surface texture.

In Chapter 5, the key findings and implication in this study are concluded.

# 2. WELLBORE THERMAL STIMULATION IN CONCRETE BLOCK SPECIMENS

## 2.1 Introduction

Thermally induced fractures during EGS well stimulation may help improve its permeability in the reservoir. Thermal fractures or thermal effect have been indicated by geophysical indicators in the field, and some numerical studies have been performed by researchers (Pasikki et al., 2010, Siratovich et al., 2015, Enayatpour and Patzek, 2013, Arshad et al., 2016), but the mechanism of thermal fractures in downhole conditions is still not well understood. In particular, there is no controlled laboratory study in an environment resembling EGS wellbore conditions (e.g., the cold water injected into the hot reservoir wellbore).

In this chapter, we present an experimental rig designed to resemble EGS thermal stimulations in laboratory scale and show results gathered from laboratory concrete blocks. The apparatus allows specimens to be heated to up to 280 °C and then flow the cold water under low flow pressure (< 20psi) through a borehole drilled in cubic specimens. Concrete blocks are used for test specimens as common synthetic rocks. There is no confining pressure applied to specimens in this study. Acoustic velocities and amplitudes are profiled to assess cracks and damages created due to thermal flows. Thermal properties such as thermal conductivity and specific heat are also measured before and after the thermal stimulation. By flowing room-temperature water into the hot specimen, thermal fractures or thermal damage and were induced. With increasing cycles of thermal stimulations, we observed decreased acoustic velocities and changed the mechanical

properties of our specimens. The laboratory tests of thermal stimulation reasonably resemble the field conditions provide deeper insight in to thermal fracturing mechanism.

## 2.2 Experimental studies

### 2.2.1 Experimental design and equipment

Unlike pressure-induced fracturing, e.g., hydraulic fracturing, to maximize thermal gradient and thus thermal fracturing, water needs to keep flowing through a borehole by a circulation path to the outside to quickly cool a borehole. The thermal shock is caused by injecting and flowing room-temperature tap water under low borehole pressure into a wellbore of a hot specimen that is placed in an oven. Fracturing by borehole thermal shock uses local tensile stress resulting from sharp thermal gradient to initiate fractures. With flowing water continuously through the borehole without pressurization, the borehole will be cooled as quickly as possible to maximize the thermal gradient near wellbores. Injected water become warmed and exit through an outlet.

A borehole with 1-inch diameter and 6-inch depth is drilled by using a diamond embedded coring drill bit from the center of the top surface on each block. A 1" OD stainless steel tube used as a borehole casing was inserted 2 inches into the borehole and mounted to the borehole wall using epoxy to seal and resist fluid pressure and high temperature. To achieve a flow-through path, we built a tube/fitting design that enables effective flow through a coaxial inlet and outlet (Figure). Water enters the borehole through the central smaller-diameter inlet tubing, which passes through a larger-size cross-shaped fitting. Then warmed water exits through the annulus between the inlet tubing and

the casing, and then through the space in the cross fitting (Figure). Flow rate can be controlled by an amount of opening of the inlet valve.

The integrated experimental apparatus for the test is shown in Figure 2.1. A pressure transducer is attached to the wellhead to monitor the borehole pressure (Figure 2.1). In this thermal shock setup, the pressure inside the borehole may first increase due to the evaporation of the water and then decrease to the pressure that is similar to the flow pressure. Because the maximum borehole fluid pressure during the entire test including pressure decay tests will not exceed 100 psi, it can be safely applied to unconfined specimens. This experiment equipment employs transport, control, and measurement systems rated for high temperature. We have set up continuous monitoring and logging of parameters inside the borehole including pressure, water flow rate and consumption, temperature. Thermocouples were located at the inlet, borehole air, borehole wall, outlet, and specimen surfaces to monitor the dynamic evolution of temperatures.

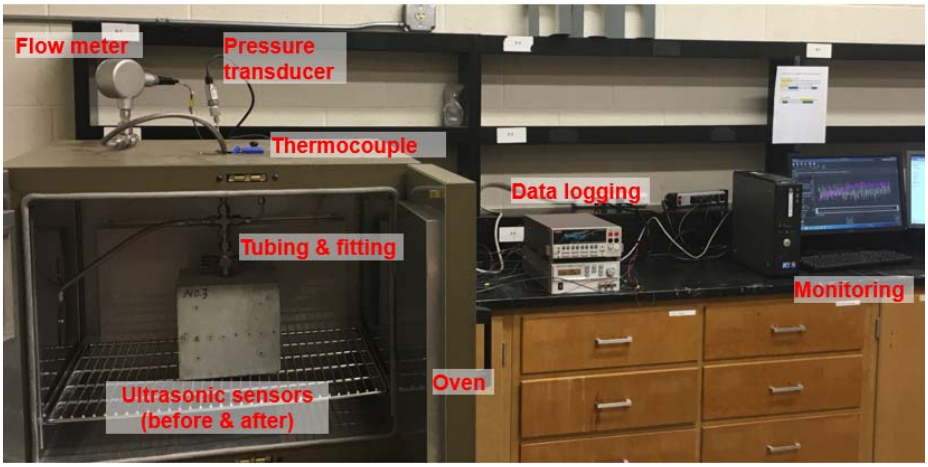


Figure 2.1 The integrated experimental system for the lab test.

The monitoring of the stimulation tests is done manually and digitally by visual gauges that provide the user with information on temperatures and pressures inside the system while under operation. Digital data is collected by the Keithley data acquisition device (main body - Keithley 7700; A/D board - Keithley 2701), which allows obtaining data from thermocouples, pressure transducers and flow meter (Figure 2.1 - at the center). For acoustic measurements, an OLYMPUS pulser, ultrasonic transducers, and a DSO-X 2004A digital oscilloscope are used (Figure 2.2). Figure 2.3 shows a schematic of the experimental setup for through-transmission acoustic measurement. The typical waveform that is captured in the acoustic tests is provided in Figure 2.3.


Figure 2.2 Equipment used for acoustic measurement - pulser, ultrasonic transducers, and the digital oscilloscope.

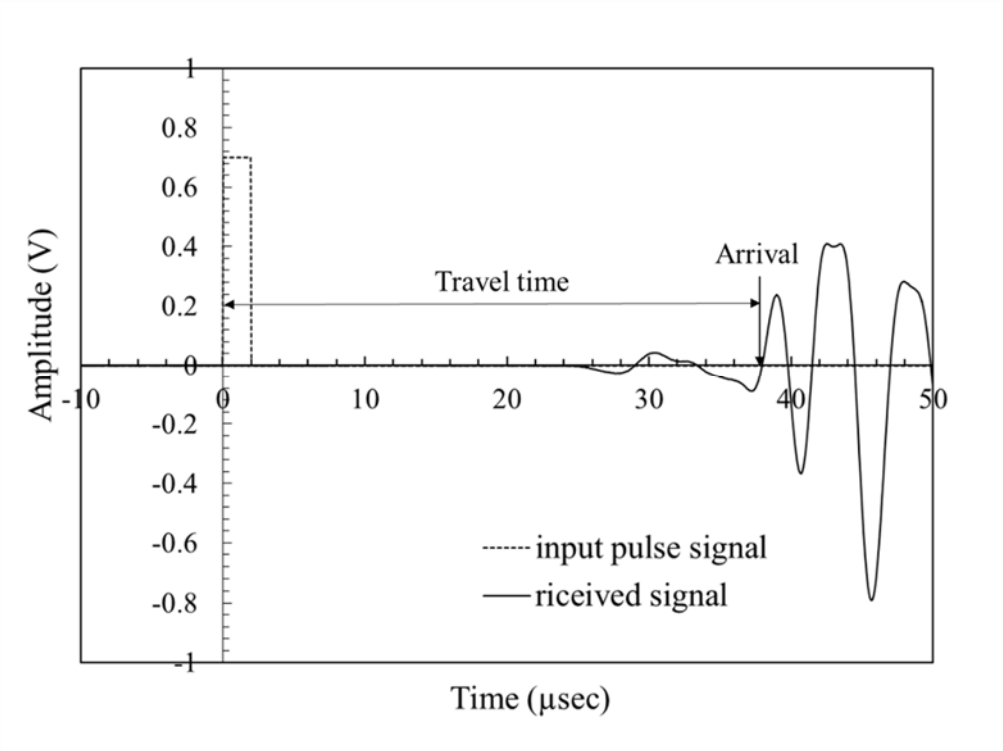


Figure 2.3 Typical input pulse and received signals from acoustic tests.

2.2.2 Specimens

Concrete blocks were also used for specimens as surrogates for rocks. A large specimen size (8"×8"×8") was selected to create sufficient thermal gradient in the specimen for an extended time. It is very important that all the specimens were prepared in a similar way to allow meaningful comparison between tests. There may be a few variable parameters to investigate and analyze for types of fracture mechanisms. Fresh concrete with water to cement ratio of 0.55, and sand to cement ratio of 2.5 was poured into an 8"×8"×8" mold and sealed in a plastic bag. After 24 hours, the seal and mold were removed, and the concrete was cured either in the air or under water (ASTM, 2014a).

Portland cement (commercial grade Portland Cement Quikrete Type I/II) is used (the time for drilling, setting time, and curing time are all recorded). A few specimens were prepared with temperature sensors embedded into concrete.

Some index properties of intact specimens were obtained for test specimens. Elastic constants were obtained from measurements of elastic wave velocities (ASTM, 2008a, Cha and Cho, 2007). Thermal conductivities and specific heat capacity were obtained by using a hot-disc thermal analyzer (model). Splitting tensile strength and unconfined uniaxial compressive strength were obtained using procedures from the ASTM standards (ASTM, 2008b, ASTM, 2014b).

Several researchers (Powers, 1969, Lamond and Pielert, 2006, Bazant and Kaplan, 1996) have worked on the properties of concrete. According to their results, typical properties of normal strength Portland cement concrete are listed in Table 2-1.

Table 2-1 Typical properties for concrete (provide literatures and web sources for all values).

| Properties* | |
|---|---|
| Density (kg/m³) | 2240-2400 |
| Unconfined compressive strength (MPa) | 20-40 |
| Tensile strength (MPa) | 2-5 |
| Dynamic Young's Modulus (GPa) | 14-41 |
| Dynamic constraint Modulus (GPa) | 30-70 |
| Dynamic shear Modulus (GPa) | 10-25 |
| Poisson's ratio | 0.1-0.2 |
| P-wave velocity (Km/s) | 4-6 |
| S-wave velocity (Km/s) | 2-3 |
| Thermal conductivity (W/m·K) | 1.5-2.6 |
| Volumetric specific heat (MJ/(m³K) | 1.4-1.7 |
| Thermal diffusivity ($mm^2/s$) | 1.0-1.3 |
| Coefficient of thermal expansion (/K) | $0.4\text{-}0.7\times10^{-5}$ |

* Typical underwater cured concrete (gravel + sand + cement +water)

According to our measurements, the properties of the specimens used in the tests are tabulated in Table 2-2.

Table 2-2 Properties of the air-cured mortar concrete block specimens used in the tests.

| Properties* | |
|---|---|
| Density (kg/m³) | 2223 |
| Dynamic constraint modulus (GPa) | 40 |
| Dynamic shear Modulus (GPa) | 14 |
| P-wave velocity (m/s) | 4.0-4.2 |
| S-wave velocity (m/s) | 2.5-2.7 |
| Thermal conductivity (W/m·K) | 1.7-1.9 |
| Volumetric specific heat (MJ/(m³K) | 1.65 |
| Thermal diffusivity (mm2/s) | 1.1 |
| Coefficient of linear thermal expansion (K-1) | 0.55×10-5 |

* Air-cured mortar concrete (Sand + cement + water)

2.2.3 Fracture characterizations

*Pressure decay test*

The pressure decay test is performed to evaluate the permeability of concrete specimens. We perform a pre-stimulation pressure decay test on all specimens at their intact conditions before heating and stimulations. Then, pressure decay tests are performed after heating, after water flow, during cooling, and after completing a test. For the specimens that have the continuing heating period, we also have the intermediate pressure decay test to observe the fractures closed up phenomenon during the reheating process. Tests provide the rate of pressure decay, indicating the changes in effective air permeability of the specimen in the vicinity of boreholes. Pressure decay tests were performed by pressuring the borehole to 40 psi, shutting in the wellbore, and allowing the pressure to draw down gradually.

*Acoustic measurement*

Acoustic measurements provide the velocities and waveforms of compressional and shear waves of solid materials. By comparing these signatures before and after performing the thermal stimulation, the existence of fractures within the rock specimen medium can be qualitatively estimated. Additionally, with known rock density, the dynamic elastic modulus and Poisson's ratio can be calculated from these two velocities.

*Bubble leakage tests*

We found that induced bubble leakage tests can be utilized to show that permeation path or cracks created due to the thermal stimulation. To do this, the borehole is pressurized to about 40 psi by air. A liquid detergent mixed with water that is used to detect leaks in pressurized pipeline or tank is used for the bubble tests can detect minute leakage on specimen surfaces. Before the leakage tests, the bubbling agent is applied all over the surfaces. Minute cracks created during the thermal stimulation are located by the generation of bubbles in those spots of the outer surfaces. The tests are performed before and after stimulations to compare.

2.2.4 Procedures

Procedures followed for the experiments of wellbore thermal stimulation in concrete specimens are detailed below.

① Before specimen heating

- Before putting the specimen in the oven

    1) Pressure decay test with the short rig

2) Leak detection test (at 40 psi constant borehole pressure) with the short rig

- After putting the specimen in the oven and fully assembling the rig

1) Pressure decay test

② During specimen heating

- Data logging: Temperature (slow logging)
- Observe epoxy damage/contacts
- Pressure decay test right before treatment
- For granite block sample, should heat at least for 20 hrs.

③ During treatment (flow of water through a borehole)

- Flow rate (2-3 options: e.g. 1, 2, 3 GPM)
- Flow duration (2-3 options: e.g., 20, 40, 60 minutes)
- Target temperatures (Two options: 200 °C and 280 °C (max))
- Data logging: Temperature, flow rate and borehole pressure (intermediate)
- Observe processes and take photos

④ After treatment

- Pressure decay test right after treatment
- Two intermediate pressure decay tests
- Data logging: Temperature (slow logging)
- Continue heating for 6-10 hours
- Pressure decay test right before cooling

⑤ Cooling (two options: closed oven door / open oven door)

- Data logging: Temperature (slowest logging)
- One pressure decay test when the specimens are cooled a bit, but still warm (maybe after 3-5 hrs).
- Cool down sample to ambient temperature (75 °F or 24 °C). Then do pressure decay test
- Take out the specimen, and then perform:

    1) Pressure decay test with the short rig

    2) Leak detection test (again at 40 psi borehole pressure) with the short rig.

We started from preliminary tests to understand system and specimen behaviors. Then as we gather more understanding, we added more measurement and procedures to better capture the stimulation behavior. Thus, some experiments have more or fewer data due to different test conditions. The details for specimens in which experimental procedures deviated from the procedures stated above are described as follows:

- Specimen 13: This specimen was subjected to heating and cooling, without water injection. We ran this test in an attempt to determine a baseline to compare with the subsequent tests to see the how the temperature changes might influence the specimen, such as the creation of the micro-fractures, changes in the physical properties with the temperature change etc.
- Specimen 3: Test procedures were simpler as the first specimen to test. Includes measurements of the borehole temperatures (hanging in the borehole and attached to the borehole surface) and temperature on specimen surface (right surface), and

borehole pressure measurement; acoustic measurement before and after the thermal stimulation.

- Specimen 12: In addition to the procedures in #3, a thermocouple is added to the outlet tubing; also added the pressure decay test before and after thermal stimulation; increased the cycles of injection. The procedures that are different from the #3 are described as follow:
    1. When the borehole temperature arrives 200°C, the test started.
    2. First, open the inlet and outlet valve at the same time; let the water flow for seven minutes (recording the temperature, pressure change and water loss).
    3. After seven minutes, remove injection hose and close the inlet and outlet valve (the pressure inside the borehole will increase and use the outlet valve to adjust to 75-80 psi. Then start the pressure decay test).
    4. After the pressure decay test, wait for the thermal recovery until the borehole temperature back to 200°C.
    5. Then repeat from the first step, repeat for two times
- Specimen 14: in additional to the procedures and equipment in #12, a thermocouple is added to the oven to measure the exact oven temperature; a flow meter was added to measure the flow rate that was injected into the borehole; the cooling period temperature after the thermal stimulation was recorded.
- Specimen 15: in additional to the procedures in #14, a thermocouple is added on the right and left surfaces to measure the outside surface temperature of the

specimen; the pressure decay test was performed after the specimen cooled to the room temperature.

Beginning from the Specimen 16, the test procedure of the unconfined air-cured specimens were more consistent. Thus the #18, #19, #20 were followed the procedures that same with the "standard" procedure described above.

## 2.3 Results

This section presents the data that gathered from the thermal stimulation tests for air cured, water cured, and concrete blocks embedded with temperature sensors. Data include temperature, pressure, flow rate, an acoustic signal and experimental photos that show the feature and characteristic of the fracture on the specimens. Because this type of experiment in enhanced geothermal system was first performed in the lab, it has been developing until appropriate procedures are identified. These procedures are trying to replicate the situations that are performed in the field. In this section, we discuss and analysis the data that gather from those specimens

### 2.3.1 System behavior – temperature / pressure / flow

Monitoring of some environmental parameters such as borehole pressure, temperatures at various spots, and water flow allows understanding the behavior of the laboratory setup. We present the representative data and cases to discuss.

*Temperature*

As shown in Figure 2.4, the specimen was heated for 16 hours before subjected to water flow. Pressure decay tests were performed before the heating and at the end of heating period to observe how the heating process affects the permeability of the specimen.

Two thermocouples were placed on the left and right faces of the specimen. The thermocouple on the right face was placed in the center, and the thermocouple on the left face was placed in the upper corner. The reason for different locations of the sensors on the two faces is that we want to investigate the temperature propagation in specimen surfaces during the heating. Figure 2.4 also indicates that the surface has a faster temperature increase rate than the borehole temperature.

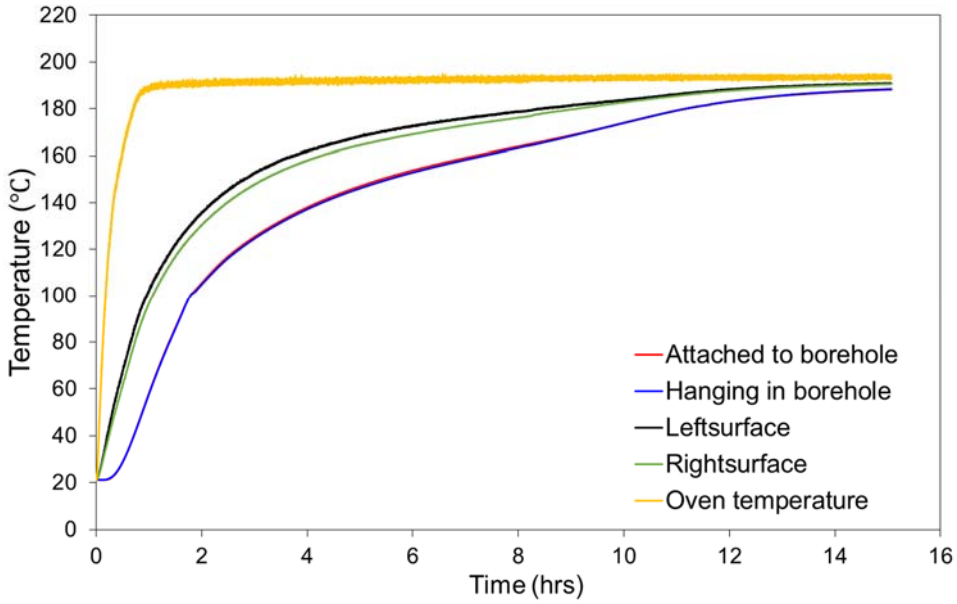


Figure 2.4 Temperatures in borehole and outer faces during heating (Test #15; Specimen #7).

Upon water injection, the borehole temperature decreased rapidly. The flow of tap water through the borehole started at t=52 sec, and borehole temperature dropped from 188 ºC to 27 ºC rapidly (Figure 2.5). The temperature of the water that came out of the outlet suddenly increased from 20 ºC to 78 ºC, and then decrease gradually to the

temperatures similar to those in borehole, which become stable at 25 ºC. Throughout the thermal treatment by the water flow, the difference of temperatures between the borehole wall and the block faces is observed to be large up to 160 ºC (Figure 2.5). This rapid heat transfer created a drastic thermal shock to the borehole surface and made it contract. This shrinkage subjects the surface of the borehole to a tensile stress. If the thermal gradient between the cooled borehole surface and adjacent hot part of the concrete is large enough, the specimen will fail in tension. Water injection stopped at t=12.7 mins. Once the water flow into the borehole is stopped, the temperature began to increase quite fast. A pressure decay test was performed soon after the water injection to measure the permeability of the specimen.

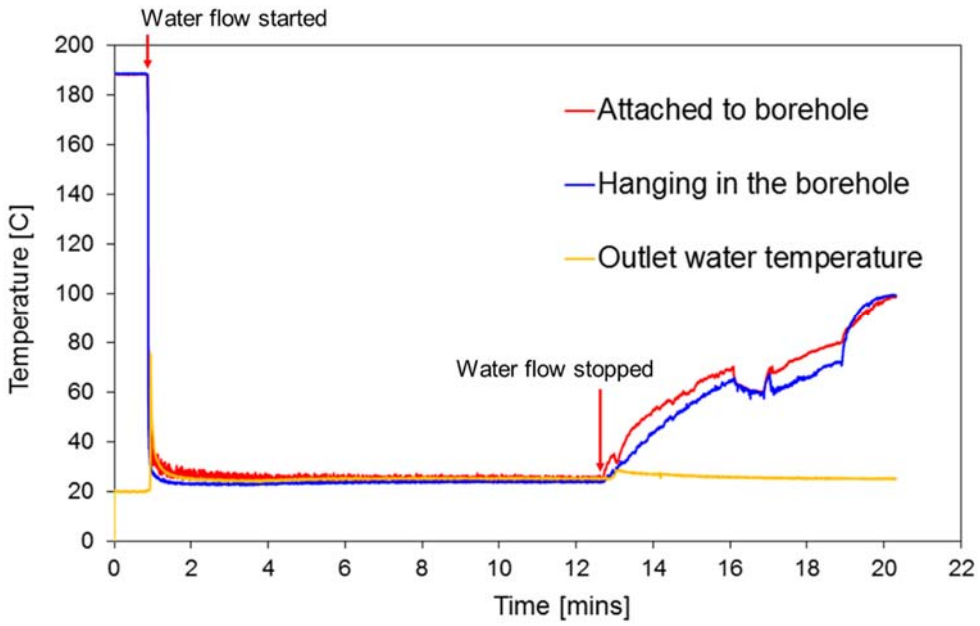


Figure 2.5 Borehole temperature change during water injection (Test #15; Specimen #7).

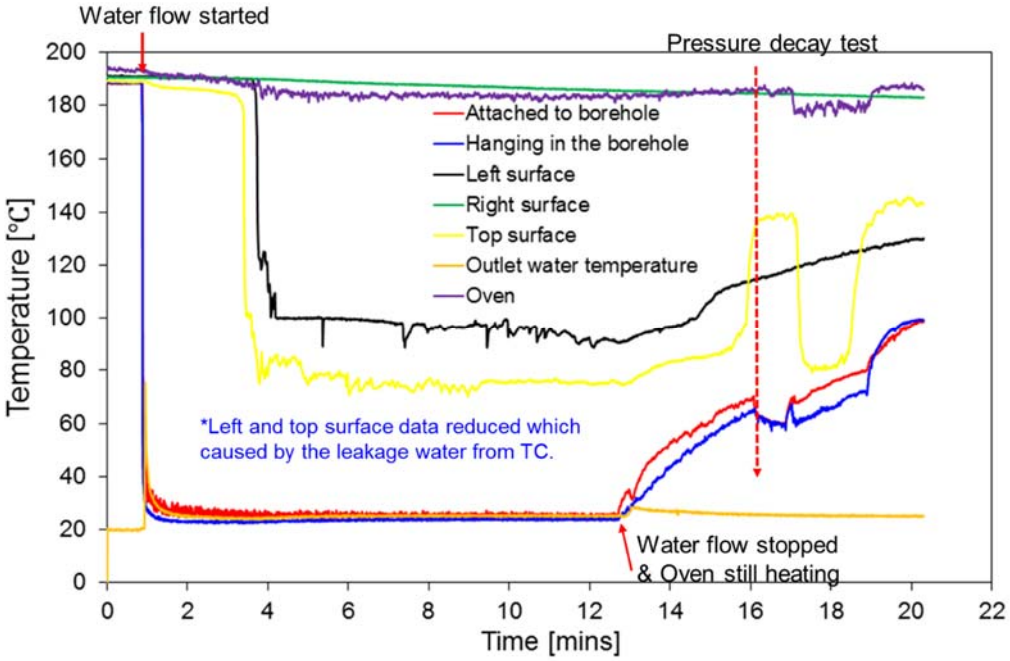


Figure 2.6 Temperatures in borehole and outer faces during water injection (Test #15; Specimen #7).

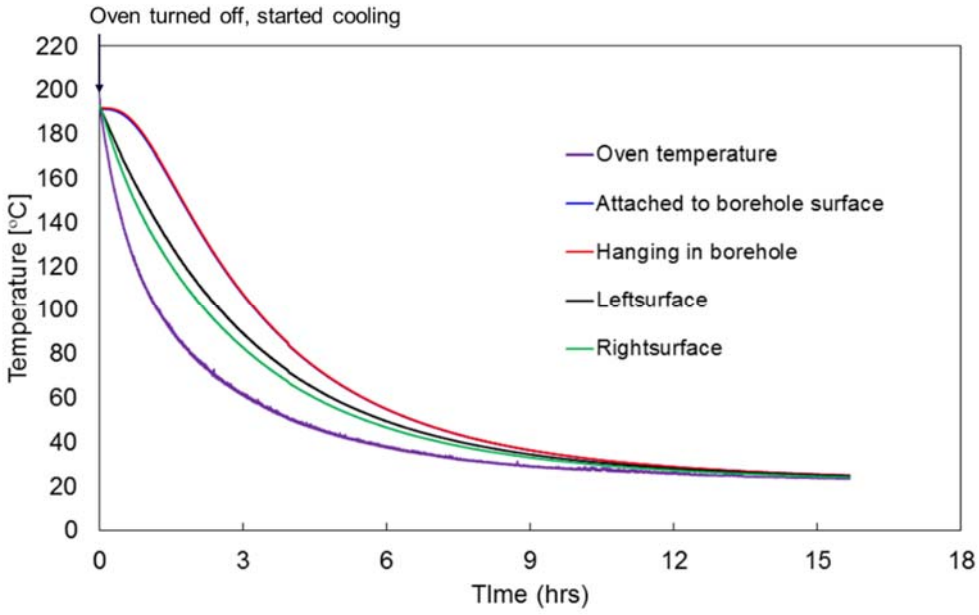


Figure 2.7 Temperatures in borehole and outer faces during cooling period (Test #15; Specimen #7).

We observed the small temperature difference between borehole space and the borehole wall Figure 2.5. When cold fluid contacts a hot solid surface with a large temperature difference, immediate vaporization created at the contact delays thermal conduction at the contact. This phenomenon is called Leidenfrost effect or film boiling effect. In our tests where room-temperature water contacts with much hotter rock surfaces, there is only minor Leidenfrost effect compared to liquid nitrogen contact on room-temperature wellbore surface as observed (Cha et al., 2014). Delays in temperature conduction due to such film boiling effects are unfavorable for thermal shock fracturing.

*Flow and borehole pressure*

Tap water is flown from water faucet to the borehole. The pressure in the borehole is mainly created from the pressure in the flow of water. From the pressure profile (Figure 2.8), we see a spike when water initially enters the borehole. This probably is caused by the rapid evaporation of water in the borehole. As the wellbore become cooler, the pressure in the borehole became steady and is mostly caused by the water flow pressure (Figure 2.8 & 2.9). The faucet opening was reduced after at three minutes after starting flow water. The pressure had the same trend with the flow rate. This indicates that the pressure in the borehole is mostly caused by the fluid flow pressure. The low fluid pressures (about six psi) in the borehole have little effect in initiating and propagating fractures.

The amount of faucet opening is kept the same, and the flow rate remained fairly constant through the thermal stimulation. The water was collected at the outlet after it flows through the borehole. The flow rates measured by the meter was compared with the flow rates calculated from the collected water and flow time, and they are in reasonable

agreement. The small difference is probably due to turbulent flows created in the flow lines, which affect measurements by a flow meter. For example, in Figure 2.8, the flow rate recorded by the flow meter in the Test 15 was around 0.78 GPM. The water volume that flew through the borehole was around 8 Gallons and flow time is about ten mins. Thus, the calculated flow rate was around 0.8 GPM, which was similar to the flow rate by the flow meter.

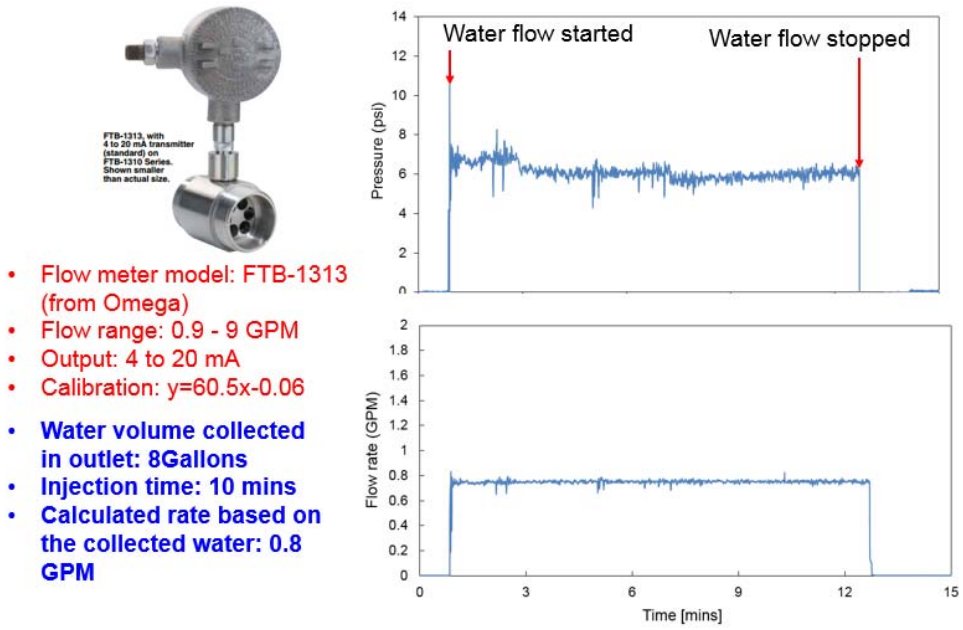


Figure 2.8 Borehole pressure and flow rate during thermal stimulation (Test #15; Concrete #7).

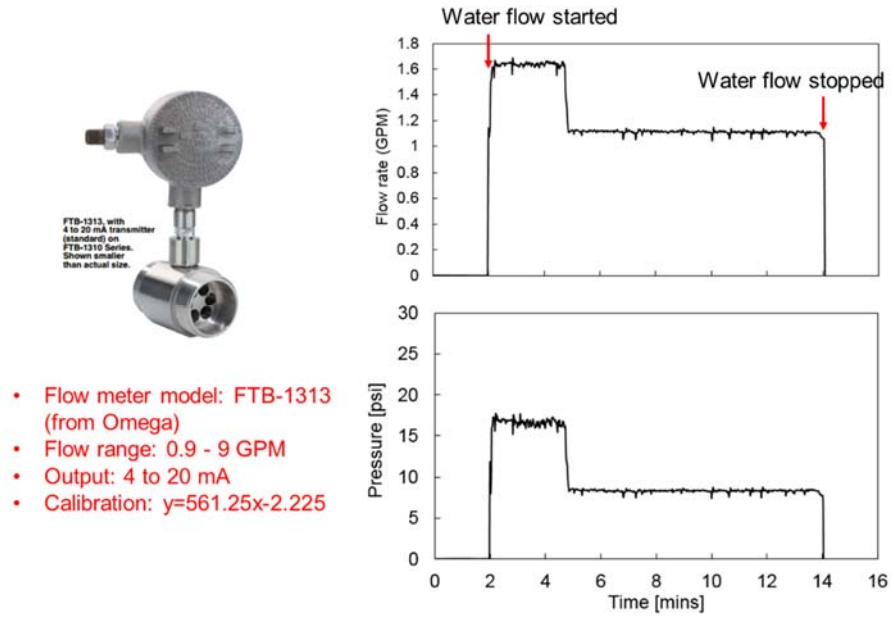


Figure 2.9 Borehole pressure and flow rate during thermal stimulation (Test #6; Concrete #15).

There was a pressure spike (around 12 psi, occurred at 2 mins) when the cold water was injected into the hot specimen. However, due to the higher pressure (around 17 psi) that caused by the higher flow rate (around 1.6 GPM) was appied in at the early time of this test (from 2 mins to 5 mins), the pressure spike (around 12 psi) was not show very clearly in the Figure 2.9).

Specimen 12 is the only specimen that had two cycles of treatments and it is the only specimen that broken (failure) by the combination stimulation methods: thermal shock and gas (air) fracturing. During the pressure decay test, after the borehole pressure arrived 80 psi, this specimen broke apart. It indicates that its breakage pressure is 80 psi, which is much lower than before (500 psi). It suggests that more treatments weaken the specimen, subsequently resulting in a lower fracturing pressure.

Thermal shock can explain this increase of the likelihood that of failure with more treatments. As the borehole surface rapidly cools, the thermal expansion coefficient of the specimen dictates how much the surface of the borehole will shrink. This shrinkage subjects the surface of the specimen to a tensile stress. It can be determined from test 3 (Concrete Specimen #12) there is clear indication that the thermal fracturing treatment increased the permeability of the specimen as the pressure decay test took significantly less time than that before the first treatment. Furthermore, an increase in the number of thermal fracturing treatments increases the likelihood that the specimen would fail due to small fractures that have formed during previous treatment, which added up, significantly weakened the specimens. The fracture profile of test 3 captured front of thermal fracture of the first water flow, which strongly proves it. Increasing the cycles of thermal fracturing treatment and waiting for the thermal recovery between each injection are also suggested by the industrial geothermal field and be proved an efficient method to open up new fractures or widen the existing fractures in the reservoir.

During the thermal stimulation, there was always leakage water that covered the top surface of the sample. Two reasons are causing the water leakage. The first is cracks that are resulting from the thermal stress grow beyond the epoxy coat. So the water flows out from these cracks and then accumulate on the top surface. In other situation, where the epoxy have been weakening or even broken by thermal stress, the cracks occurred on epoxy coat during water flow and caused by the borehole pressure and fluid pressure. Under this situation, air leaking was audibly heard and physically felt through the concrete around epoxy near the borehole during pressure decay test. To prevent water leakage and

to keep epoxy in excellent condition after the thermal stimulation, it suggests that the epoxy coat should be at least one-inch length and quarter inch thickness.

### 2.3.2 Fracture Characterizations

*Visual observations of fractures*

After thermal stimulation, often there are visible fractures on the outside surface of the concrete blocks. Usually, these fractures are initiated from the borehole and then propagate from inside of the concrete to the outside surface (shown in Figure 2.10). It is noticed that the fracture that occurred on the surface, especially on the top surface, are tortuous, not like the linear fracture. This fracture tortuosity reflects the curvature of how the fracture grows near the borehole and reflects the fracture complexity.

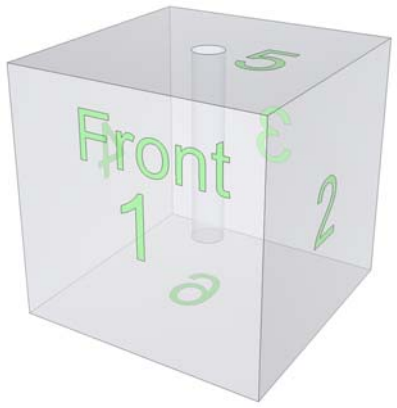


Figure 2.10 Face numbering convention for the block specimens.

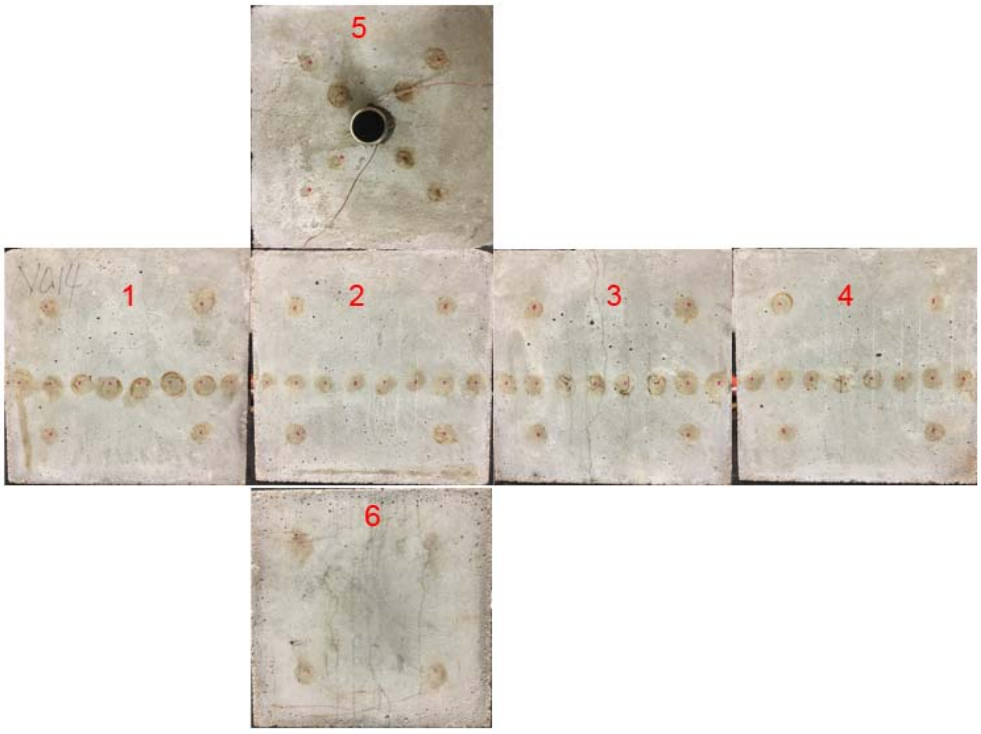


Figure 2.11 Fracture observations of Specimen #14.

*Pressure decay test*

Pressure decay tests are performed to evaluate changes in the permeability of the concrete specimens. We performed a pre-stimulation pressure decay test on all specimens at their intact condition. We also performed a post-stimulation pressure decay test after treatments. For specimens that underwent continued heating period after treatment, we also had one or more intermediate pressure decay tests to observe that the fractures close during the reheating in the wellbore. These tests provide the rate of pressure decay, indicating the changes in effective air permeability of the specimen in the vicinity of the

borehole. Pressure decay tests were performed by pressurizing a borehole to 40 psi, shutting in the wellbore, and allowing the pressure to draw down.

Thermal shock can increase the propagation of fractures with increasing cycles of treatments. There is a clear indication which can be determined from test 3 (Concrete Specimen #12) that the thermal fracturing treatment increased the permeability of the specimen as the pressure decay took significantly less time than that before the first treatment (Figure 2.13). When increasing the cycles of treatment, it will further enhance the permeability of specimen and lower the breakthrough pressure. After the borehole was performed the first treatment, some micro fractures and macro fractures caused by thermal stress initiated on the borehole wall. After waiting for thermal recovery for several hours, the temperature of the specimen reached the high temperature again. Performing the second treatment at this moment will propagate the existing fractures and thus further enhance the permeability.

The fractures caused by the thermal shock increase the permeability of specimen. This is because the fractures will increase the air flow path when doing the pressure decay tests. The permeabilities are particularly enhanced right after the treatment when the borehole is significantly colder than outer surfaces of the block, which is still hot.

However, when a specimen is continued to be heated after stopping water injection, the permeability of the specimen decreased again (Figure 2.14). This is because as the wellbore temperature increases, the thermal gradient decreases, making the fractures close again and thus permeability decreases.

When the temperature cools to room temperature, it is found that permeability increase a bit compared to the permeability of the specimen at the continued heating (hot borehole). However, this situation tends only to apply when the fractures are a vertical direction. When the fractures are horizontal directions, the ambient temperature permeability will decrease due to by the gravity made the transverse cracks sealed when thermal gradient disappeared after temperature back to ambient temperature.

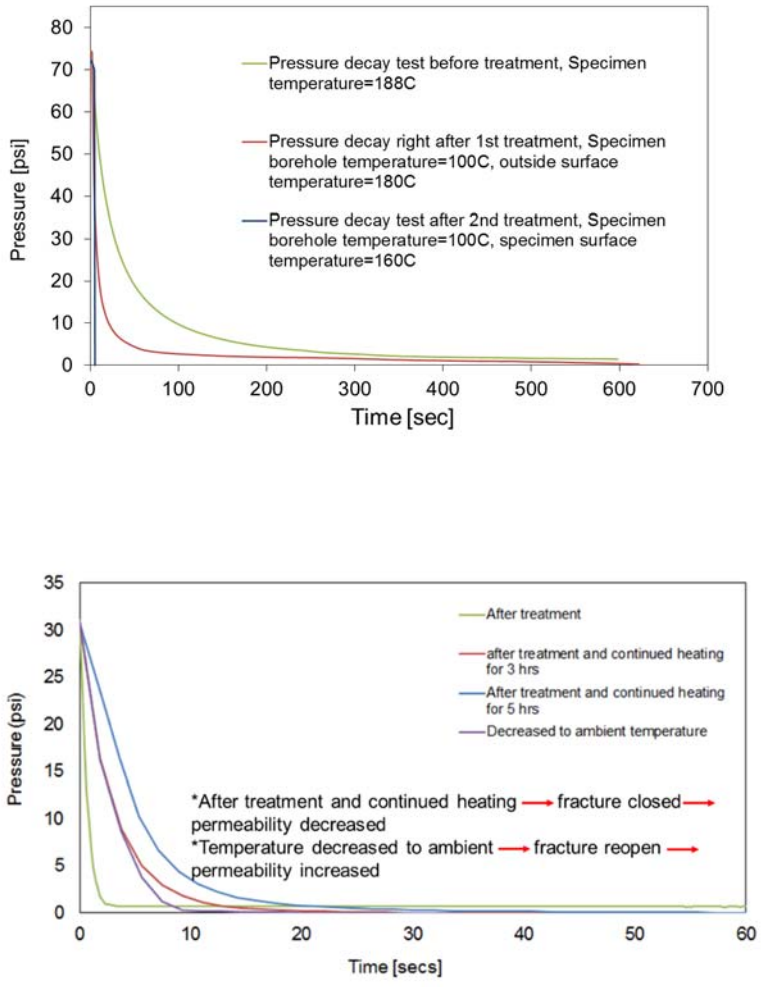


Figure 2.12 Pressure decay test right after the thermal stimulation and continued heating of Specimen 16.

*Bubble leakage tests*

Bubble leakage tests before and after stimulations show that some indications of cracks and permeation paths created due to the thermal stimulation. The borehole is pressurized to about 40 psi by air. The liquid bubble agent used for the bubble tests is sensitive to tiny leaks of gasses and generate bubbles on the leak spots. Leak holes generated near epoxy coat and the wellhead that was created during the thermal stimulation were identified by the massive bubble generation (Figure).

From the Figure 2.17 to Figure 2.21, we could see that massive bubbles generated after thermal simulations, whereas there was no bubble generation before the thermal stimulation. After removing these bubbles, there were visible fractures on the borehole surface. This not only indicates that the thermal stress that caused by cold water injected into hot specimen is strong enough to create the cracks but also proved that these fractures were initiated from the borehole wall and then propagate to outside surface.

In the most situation, where the leakage water is not much, the fractures will be vertical and occur on the face one and three of the specimen. During treatment, the specimen was treated without the confining pressure. Considering of the gravity, the minimum principal stress direction inside the specimen should be horizontal. When the specimen is stimulated with thermal stress, the fracture will initiate and propagate perpendicular to the minimum principal stress. So the vertical direction fracture occurred at our most specimen. The reason that the fractures always occurred on the front and back surface is that the front surface is near the oven door, and its temperature will be easily influenced by the cooling air flow when open the oven door during the heating and testing

to take experimental pictures. Thus the front surface will be weakened by this reason. So it will be easily broken by thermal stress.

We observed that there are several localized permeation spots (or "leaking holes") as shown in Figure 2.15. In Figure 2.16, the bubble leakage test also showed that permeation through the stone was not homogeneous, and there were invisible pathways (cracks, holes, or more permeable regions) that allowed preferential permeation of air/fluid.


Figure 2.13 Observation of several localized permeation spots/cracks.

Figure 2.14 Comparison of the localized permeation crack and massive bubble generation from bubble leakage test (Specimen #7).

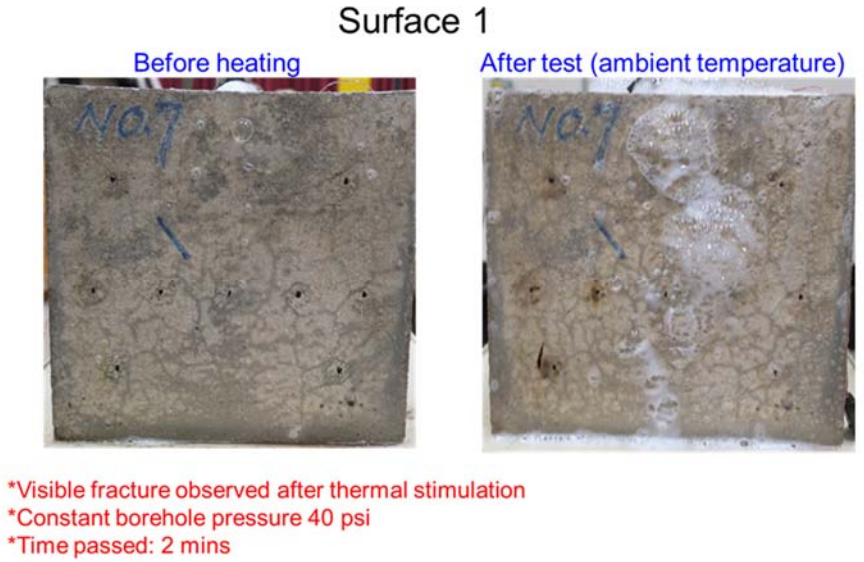


Figure 2.15 Comparison of bubble leakage tests before and after thermal stimulation (Face 1, Specimen #7).

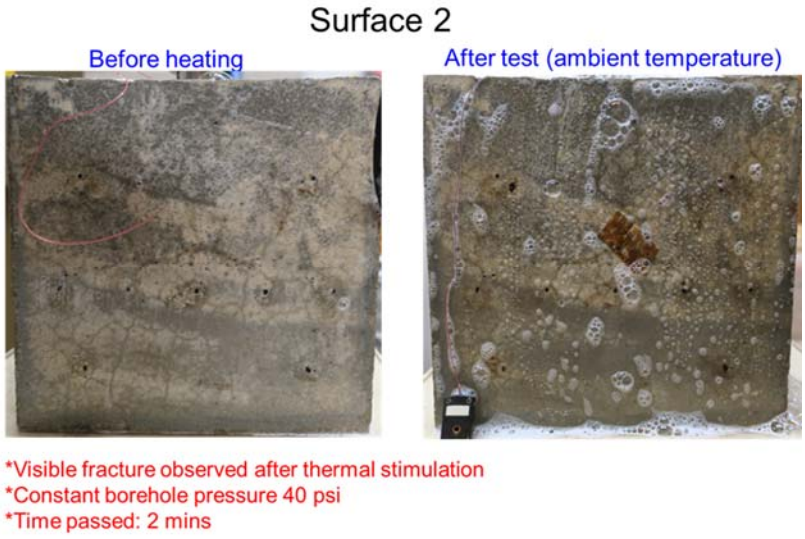


Figure 2.16 Comparison of bubble leakage tests before and after thermal stimulation (Face 2, Specimen #7).

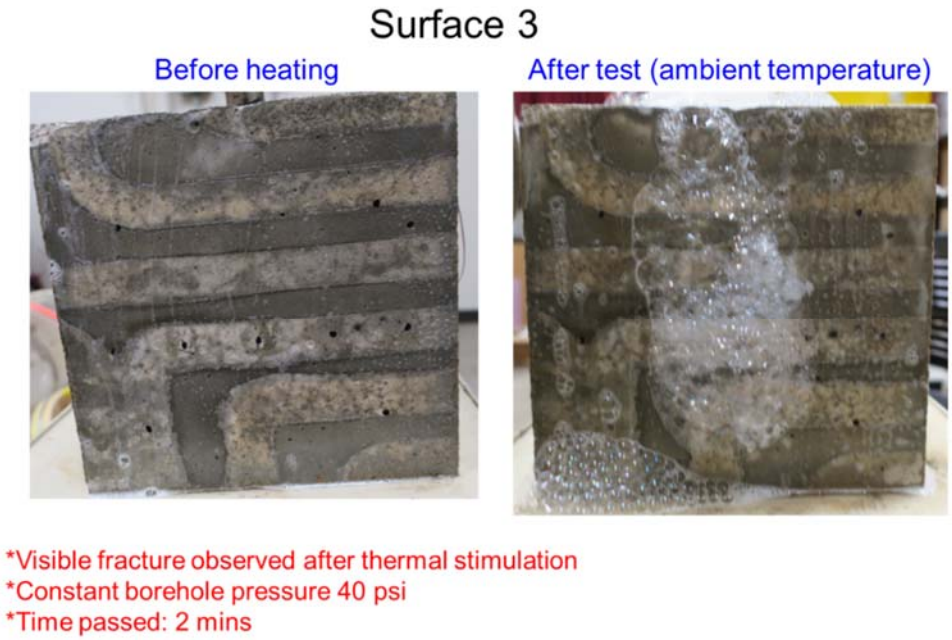


Figure 2.17 Comparison of bubble leakage tests before and after thermal stimulation (Face 3, Specimen #7).

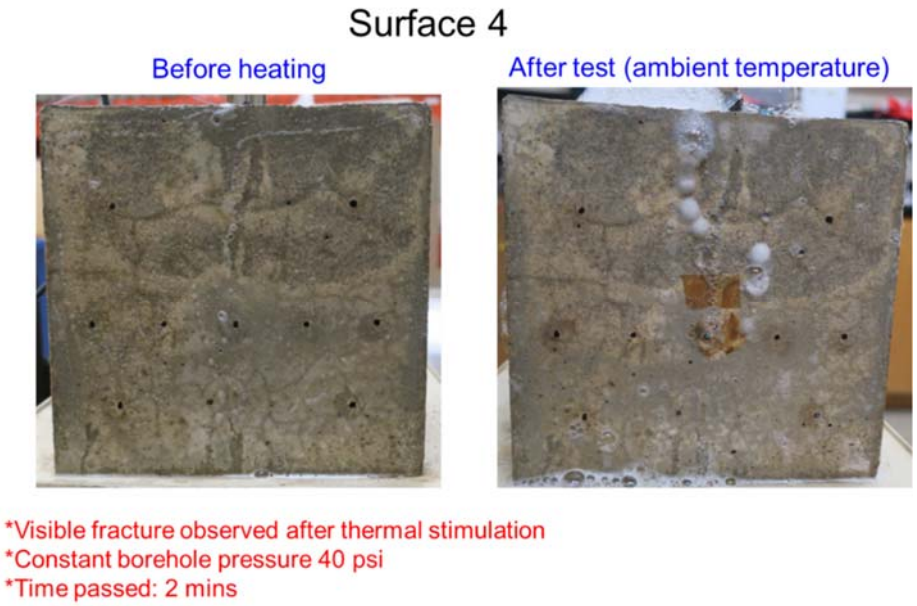


Figure 2.18 Comparison of bubble leakage tests before and after thermal stimulation (Face 4, Specimen #7).

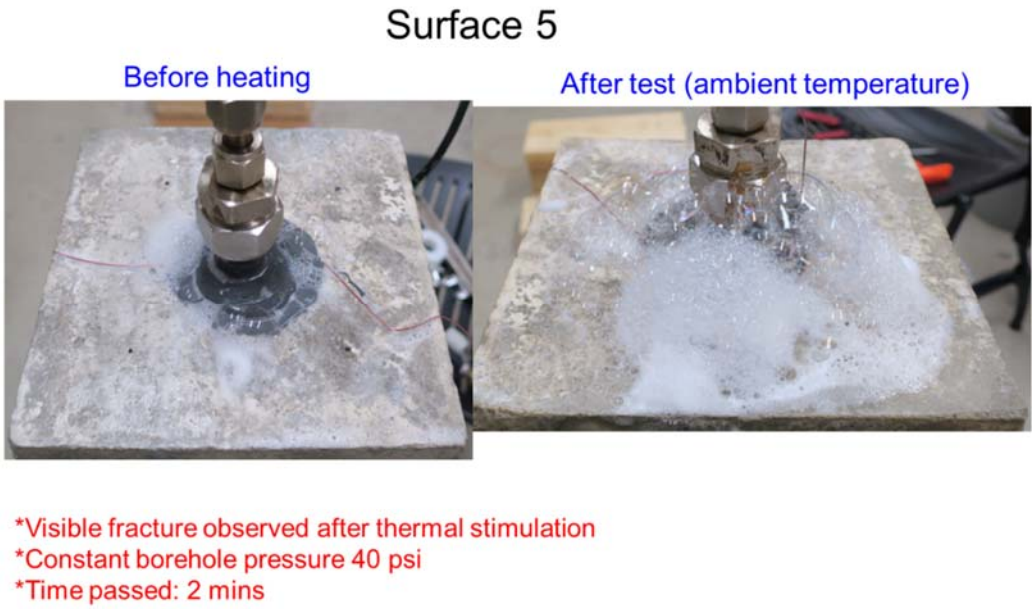


Figure 2.19 Comparison of bubble leakage tests before and after thermal stimulation (Face 5, Specimen #7).

*Characterization from acoustic measurement*

Transmission of compressional (P-waves) and shear (S-) acoustic waves were recorded before and after the treatments. The characteristics of acoustic waves propagating through the medium depend on the mechanical properties of the medium. In particular, the wave velocity in jointed rock masses is a function of the density of fractures (or fracture spacing) (Cha et al., 2009). When other properties such as intact rock properties, density, and joint stiffness are the same, the wave velocity can be used as a monitoring tool to characterize fracture generation.

It is clear that a wave traveling through a crack specimen will, in general, lose energy using scattering. There will be three different methods to travel when the wave

goes through the interface between fracture and specimen: reflection, refraction, and transmission. The first two approaches will scatter the direction of the wave out of the principal direction and cause wave energy loss. Thus the wave attenuation occurs. Distributed macro/micro cracks often give rise to an increase in attenuation. So the precise knowledge of the attenuation of ultrasonic waves in cracked media provides a direct approach for quantifying the material damage. Moreover, the study of elastic wave scattering from cracks is important for various areas of engineering and geophysics, in particular in ultrasonic nondestructive evaluation and materials characterization.

Distributed microcracks induced by the thermal stress will increase the length that wave will travel, thus increase the traveling time, decrease the wave velocity. Changes in the material response due to the reduction of effective elastic stiffness resulting from microcrack damage have a significant influence on the physical properties of the materials.

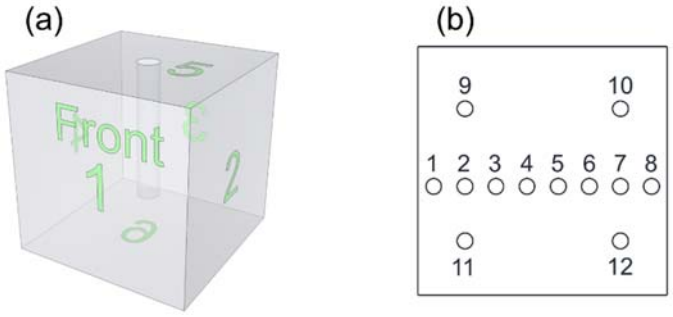


Figure 2.20 Waves measured along Face 1 & 3, 2 & 4, and 5 & 6. (a) Face numbering convention. (b) Locations for acoustic measurement on a face of a specimen.

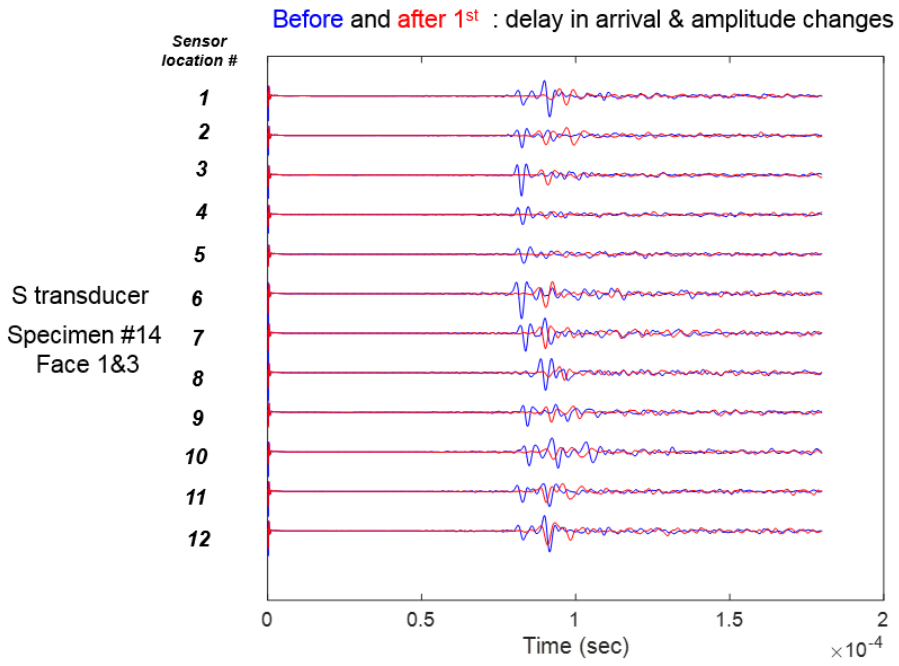


Figure 2.21 Acoustic measurements of Specimen #14 (S-wave, from Face 1 to Face 3).

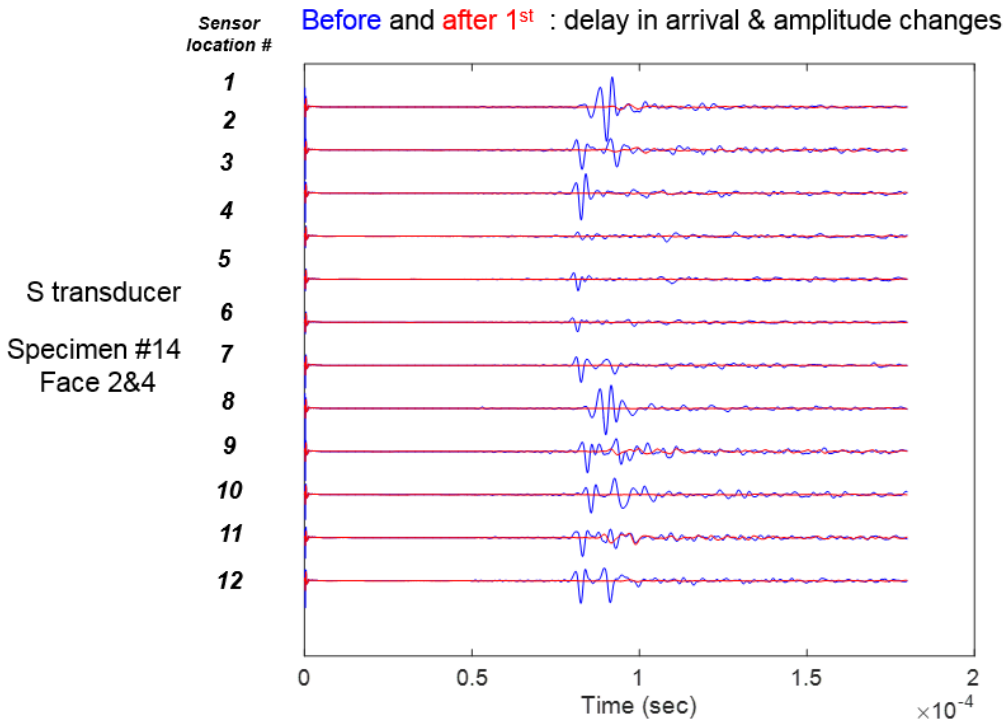


Figure 2.22 Acoustic measurements of Specimen #14 (S-wave, from Face 2 to Face 4).

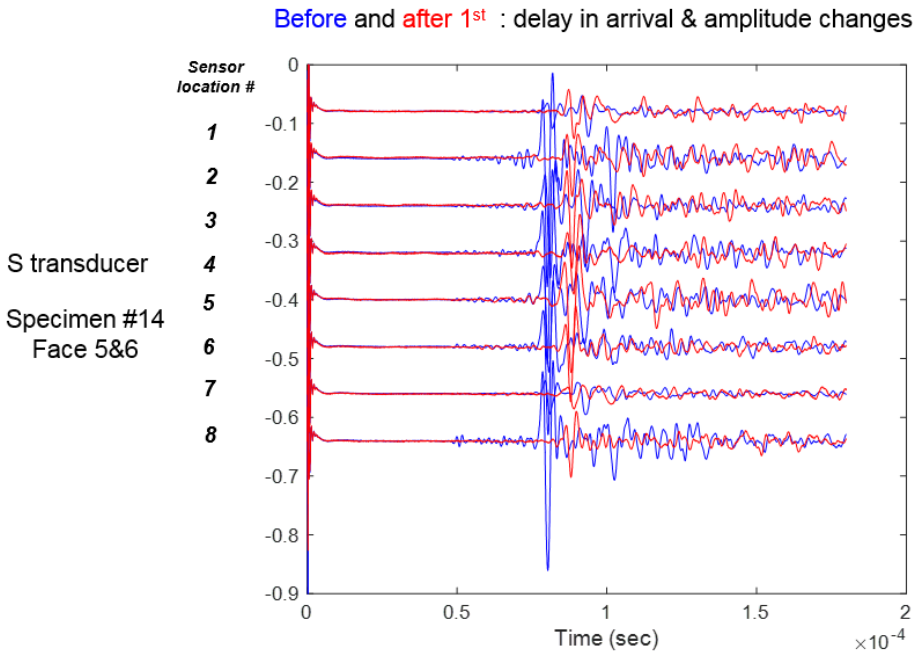


Figure 2.23 Acoustic measurements of Specimen #14 (S-wave, from Face 5 to Face 6).

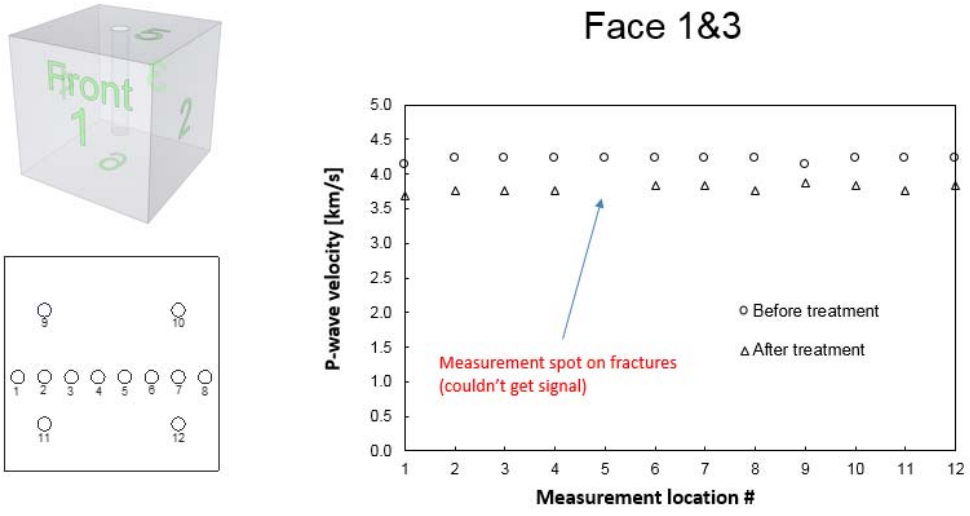


Figure 2.24 P-wave velocity calculation of Specimen #18 (from Face 1 to Face 3).

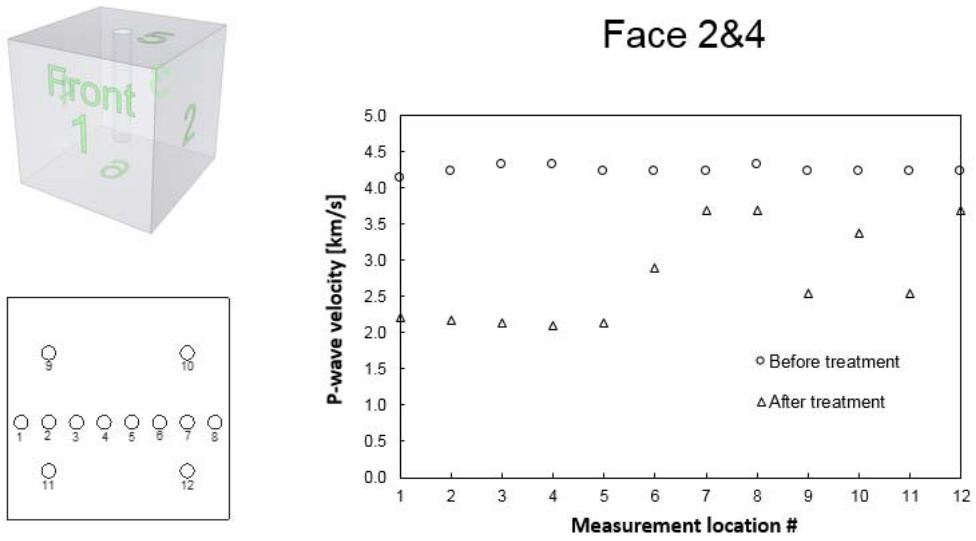


Figure 2.25 P-wave velocity calculation of Specimen #18 (from Face 2 to Face 4).

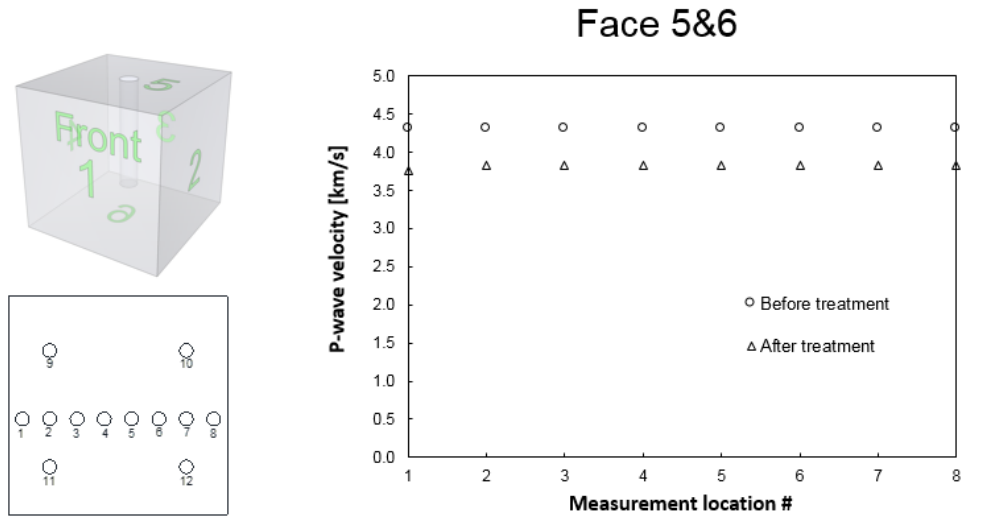


Figure 2.26 P-wave velocity calculation of Specimen #18 (from Face 5 to Face 6).

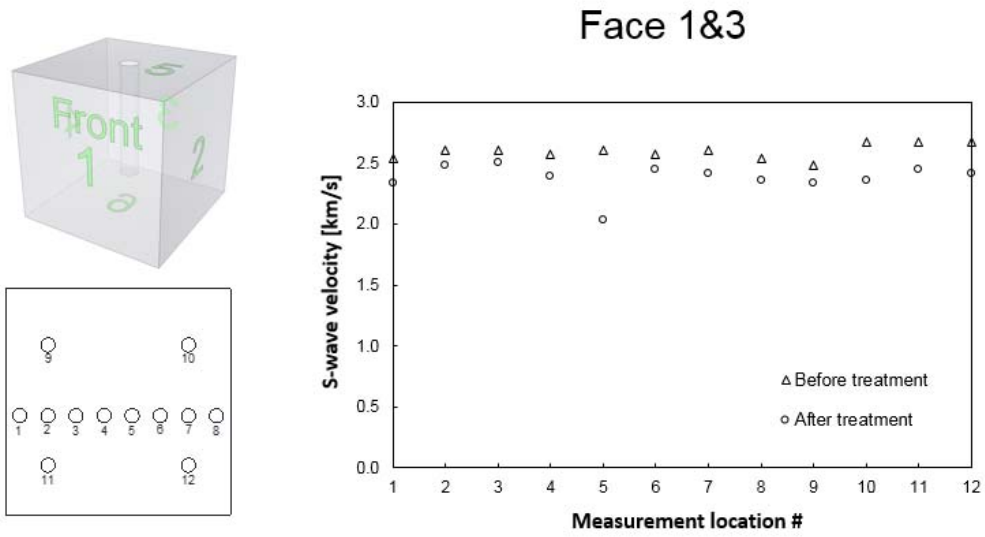


Figure 2.27 S-wave velocity calculation of Specimen #18 (from Face 1 to Face 3).

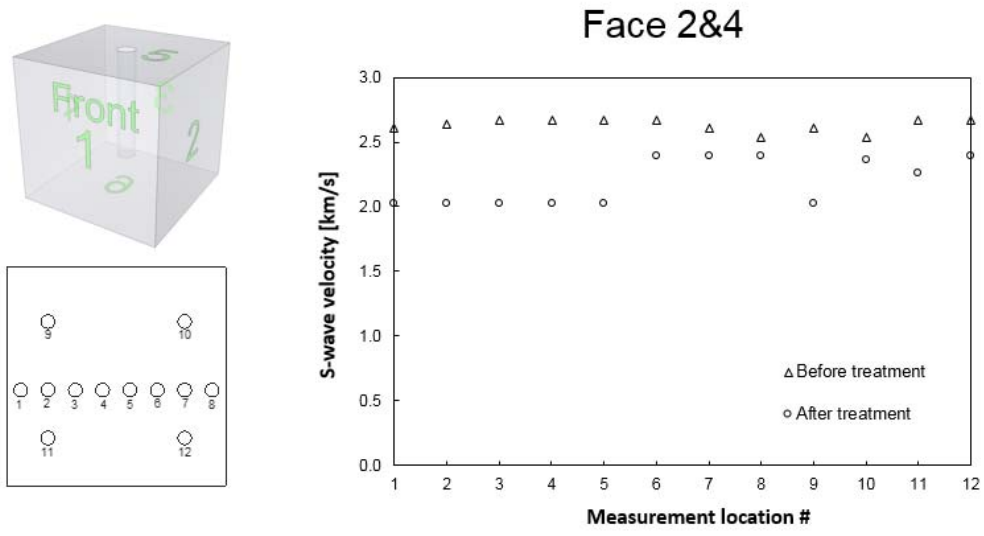


Figure 2.28 S-wave velocity calculation of Specimen #18 (from Face 2 to Face 4).

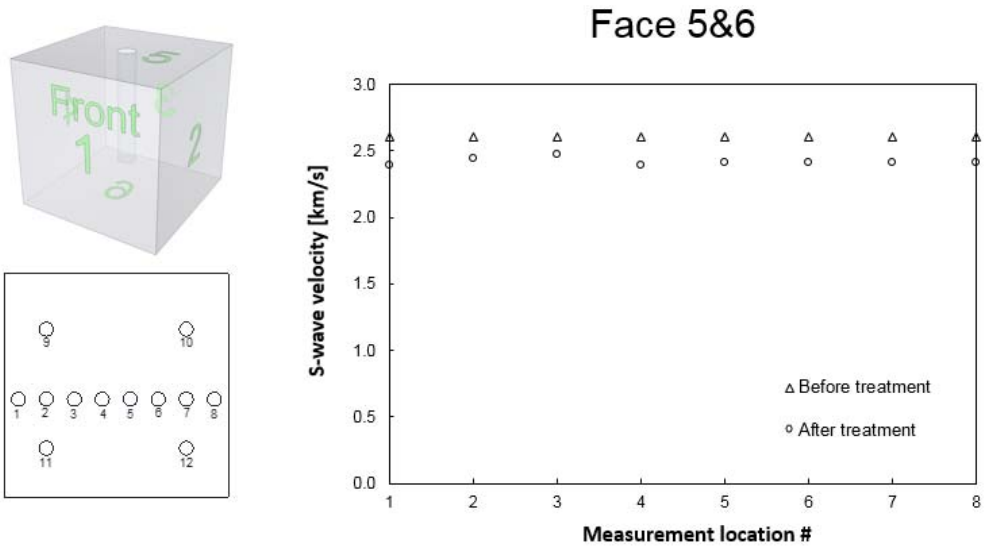


Figure 2.29 S-wave velocity calculation of Specimen #18 (from Face 5 to Face 6).

*Short-cut fractures near the borehole and fracture tortuosity*

Combining the fracture observations in the concrete #12 and concrete #14, we noticed that the fractures would usually initiated from the borehole wall surface near the casing and then propagated onto the top surface. This is likedy caused by the fact that the high-viscosity epoxy as a sealant is not thoroughly applied to fill the gap (about 0.04 inch) between the casing and the borehole, which causes migration of water closer to the top surface leaving shorter distance for crack propagation to the top surface. The different thermal conductivities between the stainless steel casing, epoxy, and concrete may also contribute.

Figure 2.30 "Short-cut" fractures initiate from the borehole and propagate to the top surface (Specimen 14).

The fracture observations also indicate that these fractures on the top surface usually are not straight. They usually are tortuous and even interconnecting with each other. Thus it forms a complex fracture network on the top surface. This fracture tortuosity will influence the movement of fluids through the fractures with low permeability. "Most of the mathematical modeling of flow through a fractured medium assumes that each fracture is smooth, parallel plates that separated by a uniform distance" (Wang et al., 1982). However, "the fracture tortuosity may affect the fluid flow in the fracture and decrease the

connectivity of fluid flow paths, which can further influence the permeability of reservoir" (Tsang, 1984).

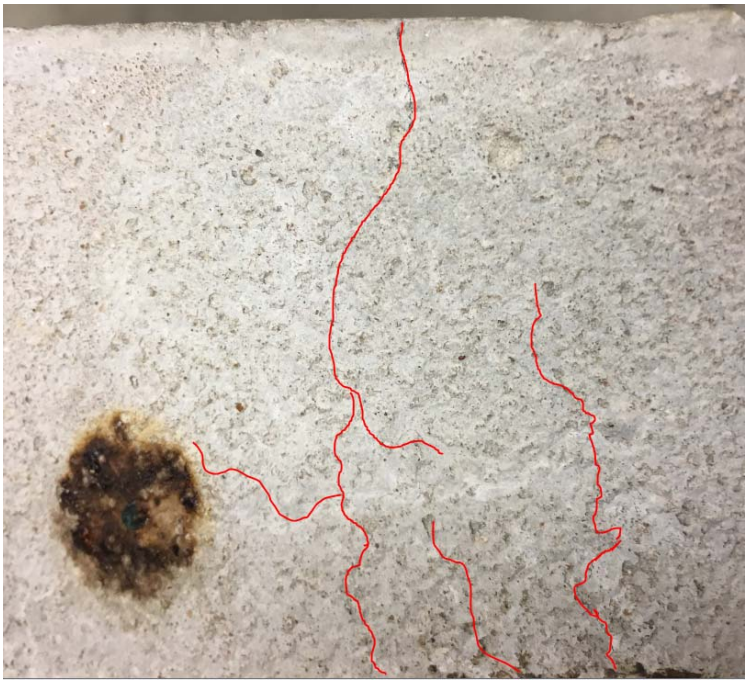

Figure 2.31 Fracture tortuosity on top surface of specimen #18

*Water leakage and bubbles during stimulation*

There were three areas on the top surface where water leaked and bubbled under hot surface temperature during the thermal stimulation. After the test, those three areas were identified where fractures initiated and propagated. During the pressure decay test right after the thermal stimulation, there were many bubbles out of the top surface. However, no bubble was generated on the front face that also had the visible fracture). This behavior proves that the fracture on top surface was initiated from the borehole, and

the fracture on front surface was initiated from outside surface and then propagated into the concrete. However, the fracture initiated on the front face did not connect to the borehole surface.

Figure 2.32 Water bubble indications during pressure decay tests (Specimen #18).

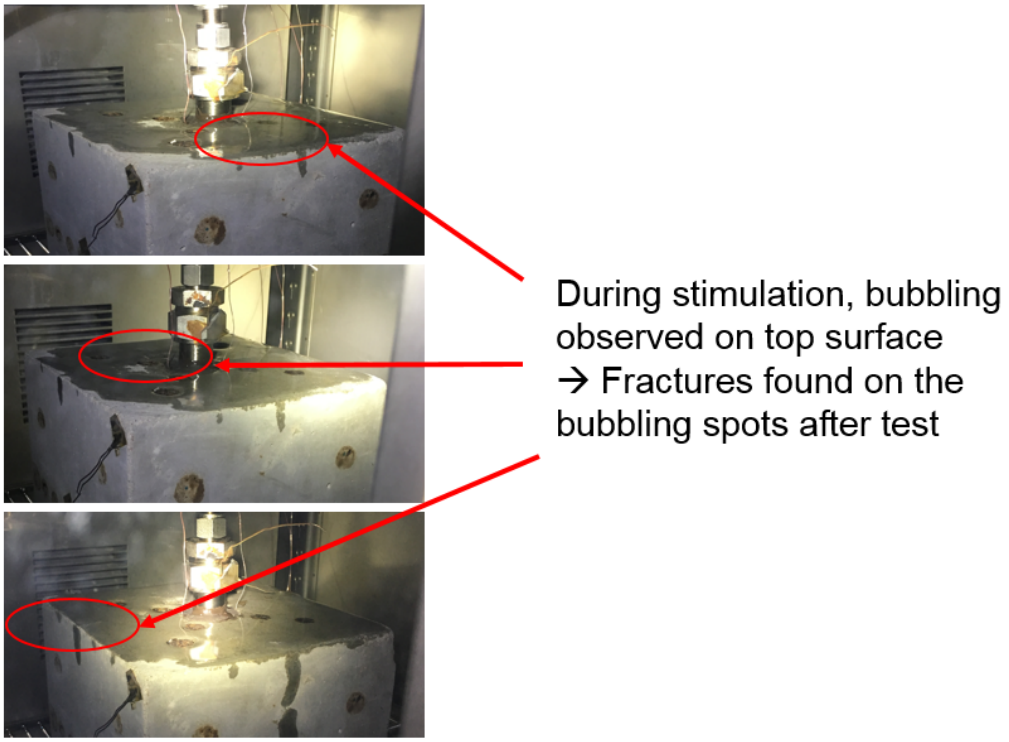


Figure 2.33 Water bubble indications during thermal stimulation (water flow) (Specimen #18).

*Fracture pattern (vertical and transverse directions)*

As shown in Figure 2.35, different from the early specimens (#3,#2,#12,#14), concrete block #15 had transverse direction fracture which showed on the front surface after the treatment. At the meantime, it had the most water leakage during the water flow. The leakage water almost covered the upper half part of the concrete. Moreover, the transverse cracks exactly occurred at the boundary between the leakage water covered part and dry concrete part. Combined with the results of a later test of specimen #18, it indicates that the direction and pattern of cracks on the concrete surface were affected by the amount of water leakage.

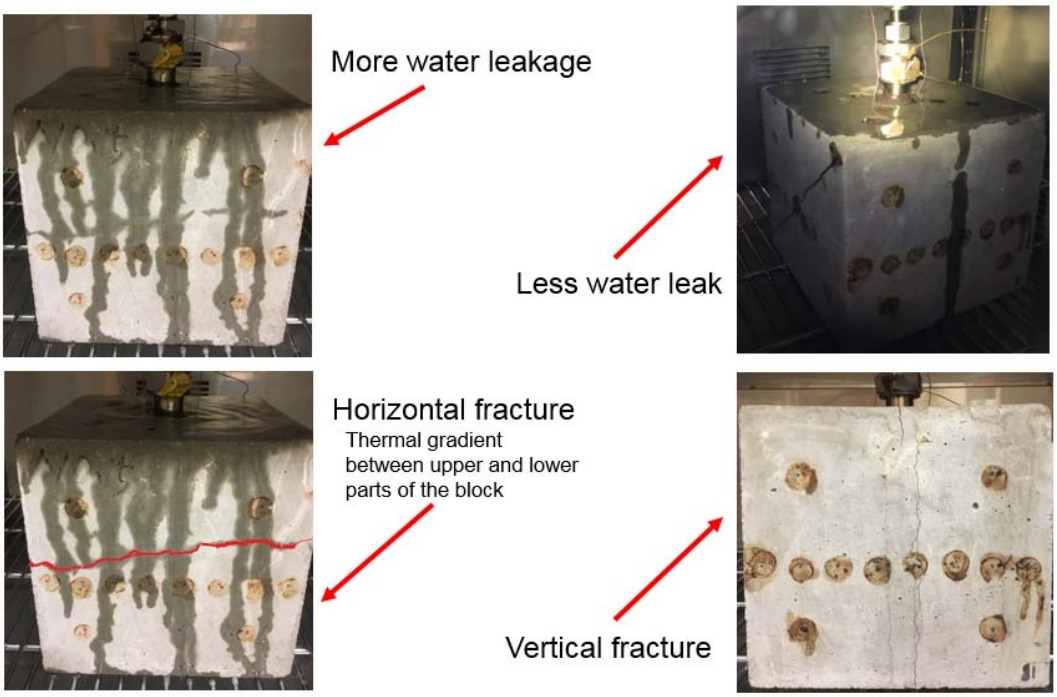


Figure 2.34 Fracture direction comparisons between Specimen #15 (left side in the figure) & #18 (right side in the figure).

The cracks on the outside surface of concrete became wider as the temperature of concrete declined over the cooling period. The concrete surface contracts when its temperature decreases. This shrinkage subjects the surface of the specimen to a tensile stress, which makes the existing fractures on the outside surface wider. As shown in Figure 2.36, this behavior is observed during the cooling (with oven door open) after the thermal stimulation.

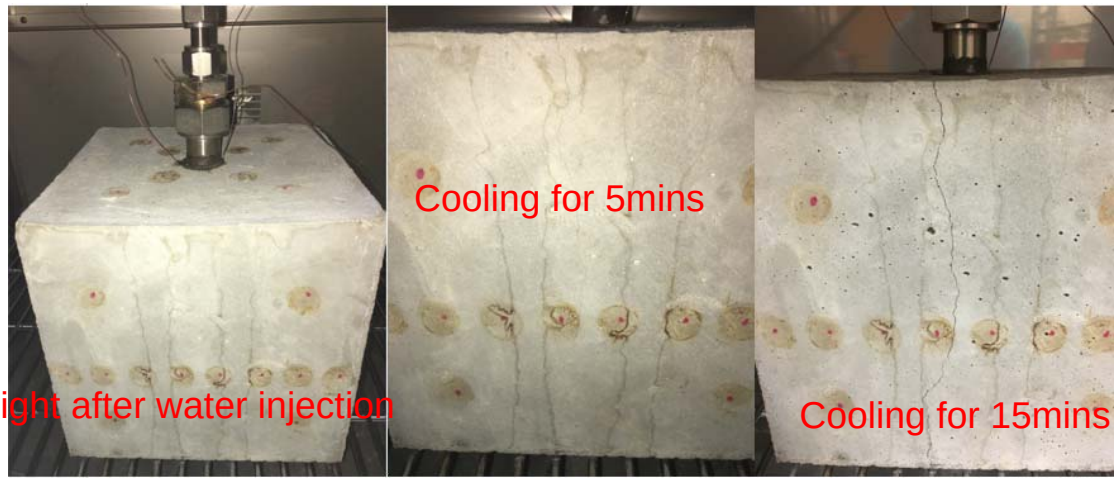


Figure 2.35 Fractures propagated and widened during the cooling period (Specimen 14) (oven door kept open during cooling).

*Area of thermally induced fracture*

By comparing the acoustic signals before and after the thermal stimulation, we attempted to roughly estimate the extent of major fractures caused by thermal stress inside the block. Figure 2.37 shows the fracture front that is estimated by interruption of ultrasonic signals. We also poured the phenolphthalein into the borehole of the treated specimen in order to image internal fractures. When the solutin is fully dried in a few days, we performed the breakdown test. As shown in Figure 2.38, major fractures that are induced by the thermal stimulation are clearly indicated by the area with pink color caused by the exposed surface reacting with phenolphthalein. The thermal fracture front indicates how far the fractures have been propagated. Thus, the speculation about thermal front from the acoustic signal is verified. As shown in Figure 2.39, the analysis about the fracture front that we estimated from the signal (Figure 2. 36) is correct.

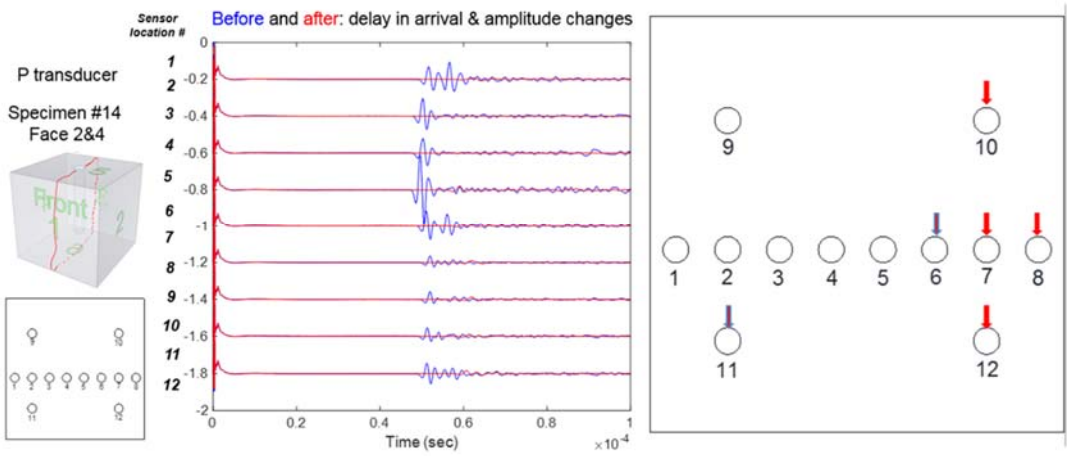


Figure 2.36 Acoustic signals with assumption of thermal front.

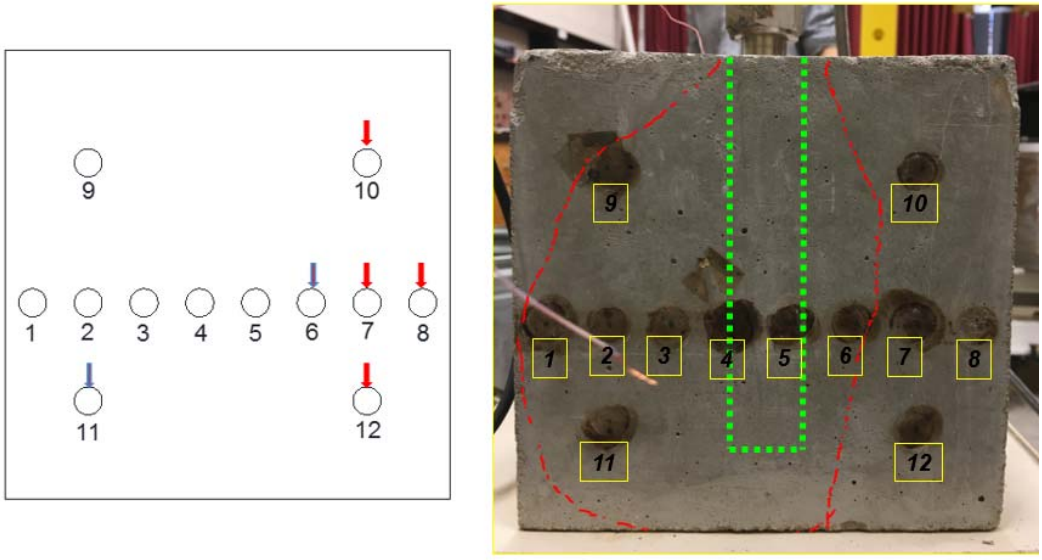


Figure 2.37 Front of fracture was estimated by ultrasonic wave signals (Specimen #18).

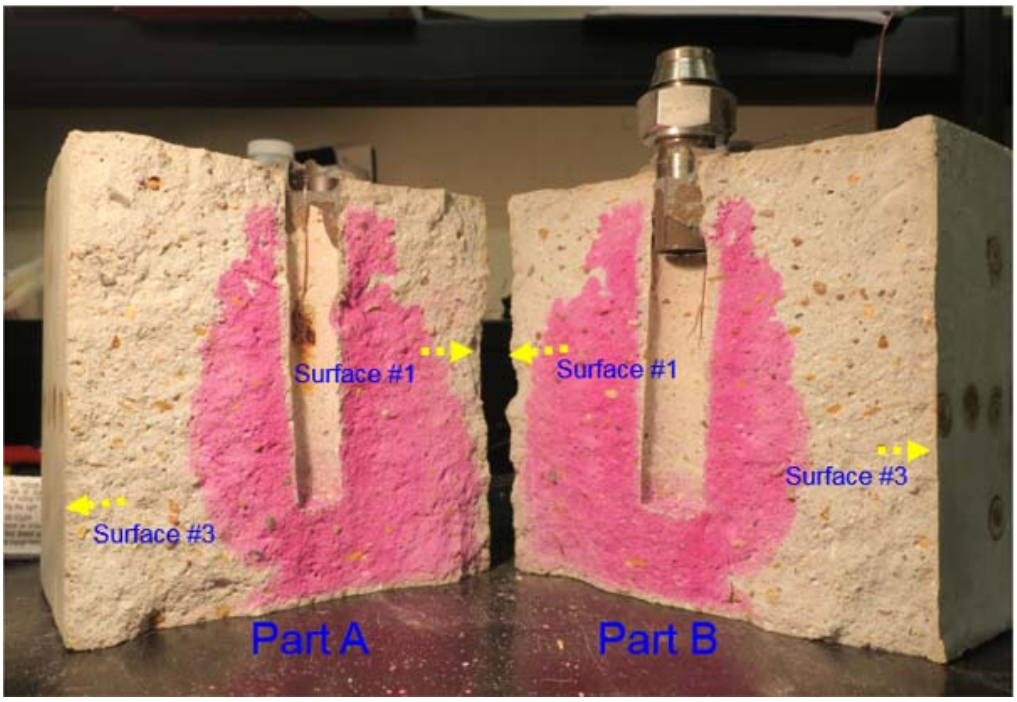


Figure 2.38 Breakdown test results with showing the thermal fracture front (Specimen #18).

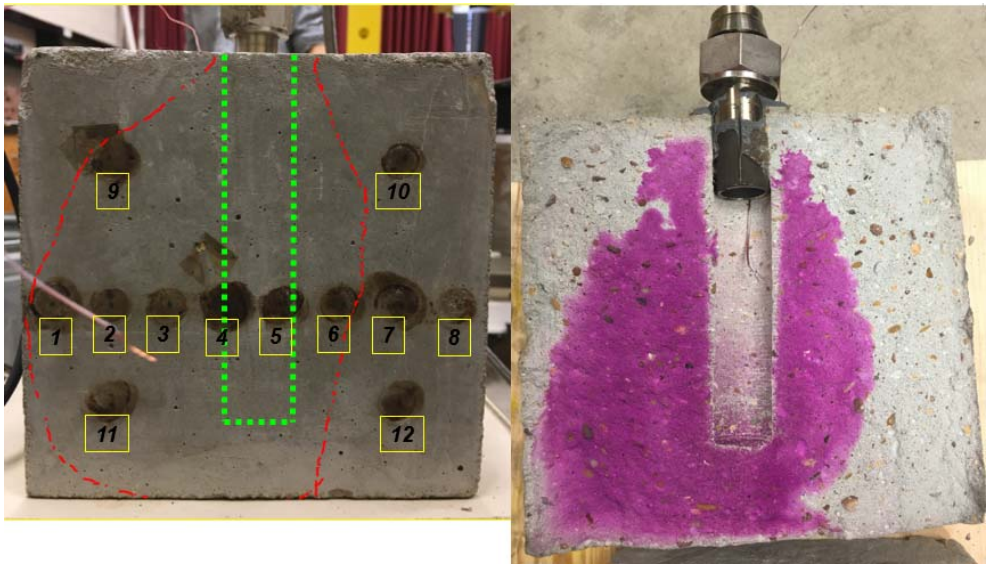


Figure 2.39 Thermal fracture comparision between acoustic analysis and breakdown test (Specimen #18).

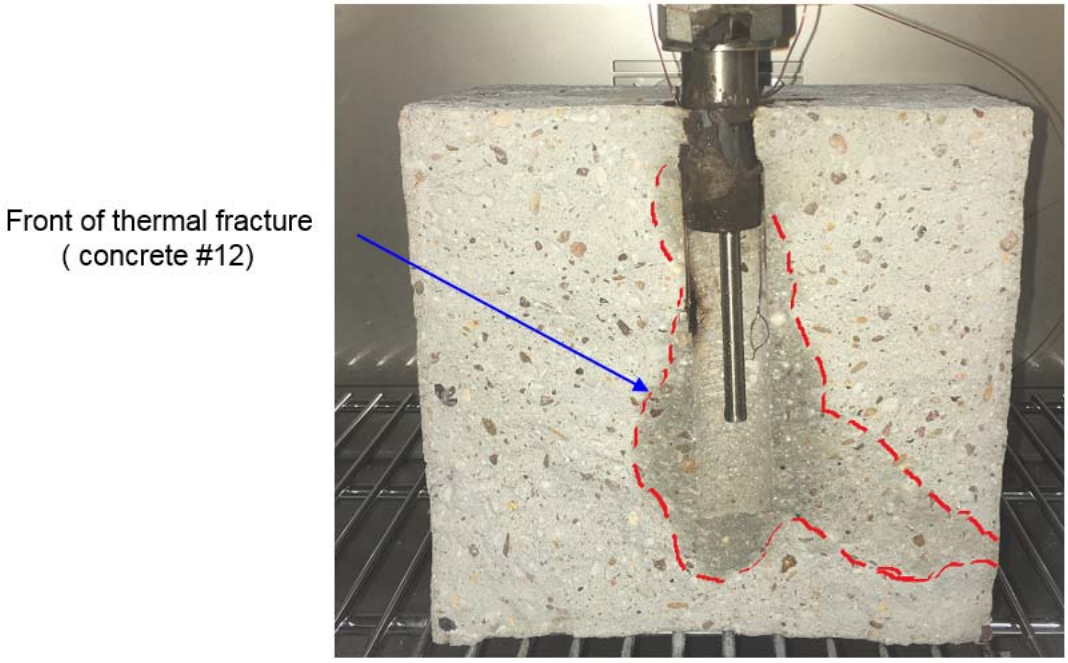


Figure 2.40 Breakdown test results with showing the thermal front (Specimen #12).

Comparing the fractures observation of breakdown test between the Specimen #12 and #18, we could find that the fractures seem always travel from the front surface to back surface (surface one to surface three). This phenomenon may cause by that the front surface is near the oven door, and its temperature will be easily influenced by the cooling air flow when open the oven door during the heating and testing to take experimental pictures. Thus the front surface will be weakened by this reason. So it will be easily broken by thermal stress.

2.3.3 Temperature propagation - Embedded sensors

The thermal stress inside the concrete specimen is caused by thermal gradient. On next step, we want to observe the temperature propagation and thermal gradient inside a specimen during the water flow. We embedded the thermocouples inside the concrete specimen to investigate the temperature propagation inside the specimen. The locations of six thermocouples embedded are shown as number one to six in Figure 2.41. In addition to these, there are four thermocouples placed on the right and left the surface of the specimen, attached to the borehole surface and hanging in the borehole.

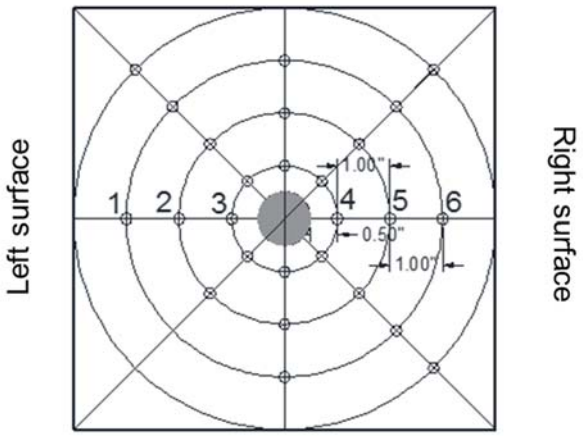


Figure 2.41 Locations of embedded thermocouples at the mid height of the specimen (Plan view).

The Figure 2.42 shows how the temperature propagated from borehole into the specimen. At t = 2 mins, the room-temperature tap water began to flow into the borehole. The temperature of borehole dropped rapidly from 190 °C to 25ºC in about 3 seconds. The

borehole temperature dropped along with first borehole pressure spike (around 30 psi in Figure 2.43) that caused by the rapid evaporation of water when it contacted with the hot borehole surface. After about one minute, the temperature of location 3 and 4 began to drop and also corresponded with the second borehole pressure spike, which was around 65 psi and much higher than the first spike. The fracture occurred, and water evaporation may cause the second spike. When thermal stress is greater than the then tensile strength of the material itself, the fracture will occur. The concrete is described as the thermo-elastic material. It means that the elastic energy inside the concrete will be released when the fracture occurs. This amount of energy will induce the shock wave and propagate along the fractures and tubing, and then captures by the pressure meter. Also, when the new fracture occurs, the cold water will continually contact with the deeper area of the specimen which is still very hot. It will cause the water evaporate again. This may be another reason that the second spike is greater than the first.

Similarly, the third pressure increase during the water flow corresponded with a temperature drop at position 2 & 5 and fourth pressure increase corresponded with a temperature drop at position 1 & 6. This phenomenon indicates when and where the fracture occurred inside the specimen and also showed temperature propagation.

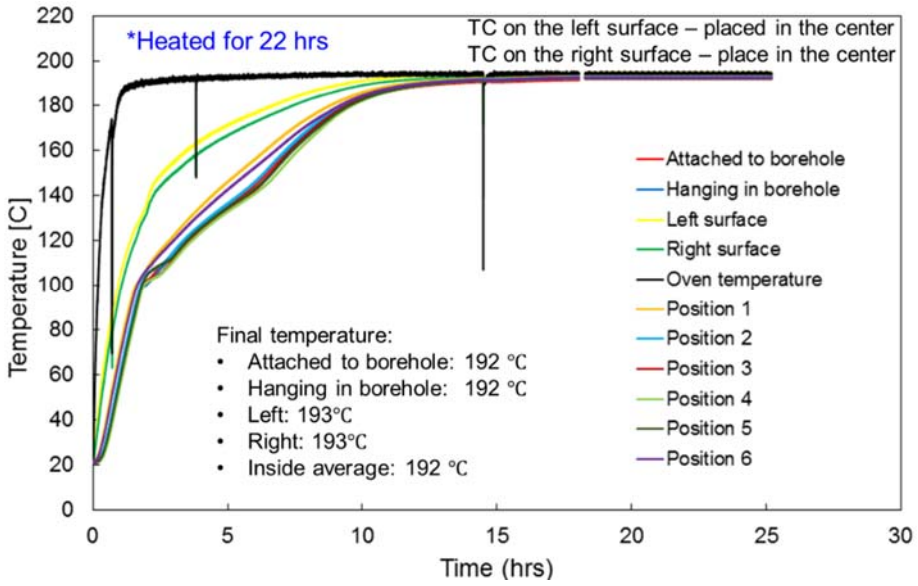


Figure 2.42 Temperature behavior of embedded Specimen #2 during heating period.

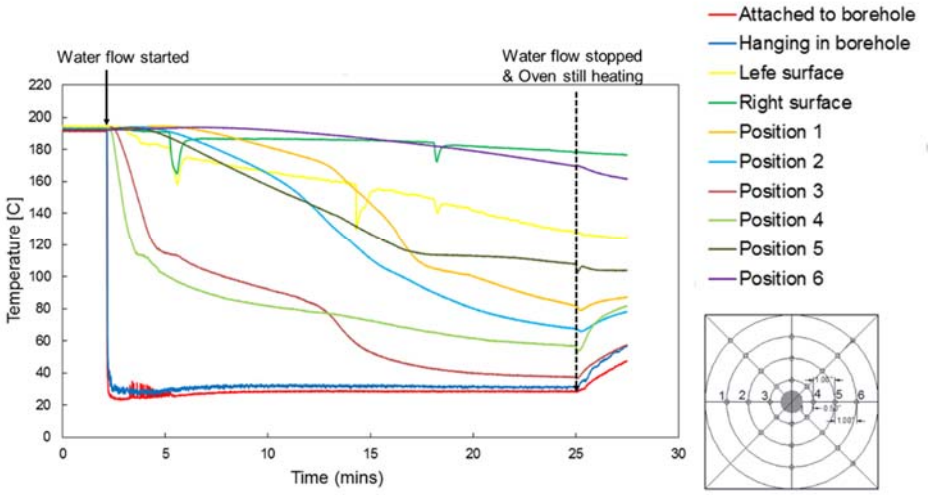


Figure 2.43 Temperatures and borehole pressure of the embedded thermocouples during water flow (embedded thermocouple Specimen #2)

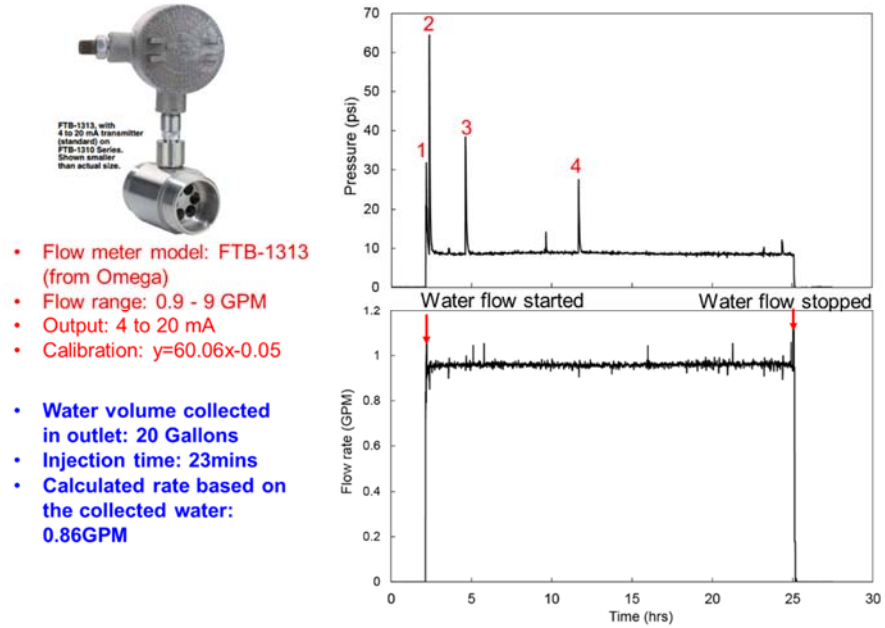


Figure 2.44 Borehole pressure and flow rate of the embedded thermocouples Specimen #2 during water flow.

The thermal gradient results in Figure 2.45 show the thermal gradient at varying locations inside the specimen over time. It indicates that when cold water is flowing into the hot borehole, the thermal gradient initiated from the borehole wall and then propagates to the outside surface. As the flow time went on, the magnitude of thermal gradient inside the specimen decreased, and thermal gradient away from the borehole increased.

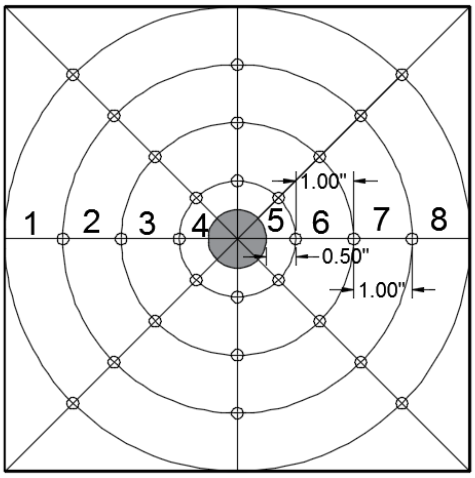


Figure 2.45 Sensor numbering for thermal gradient calculation.

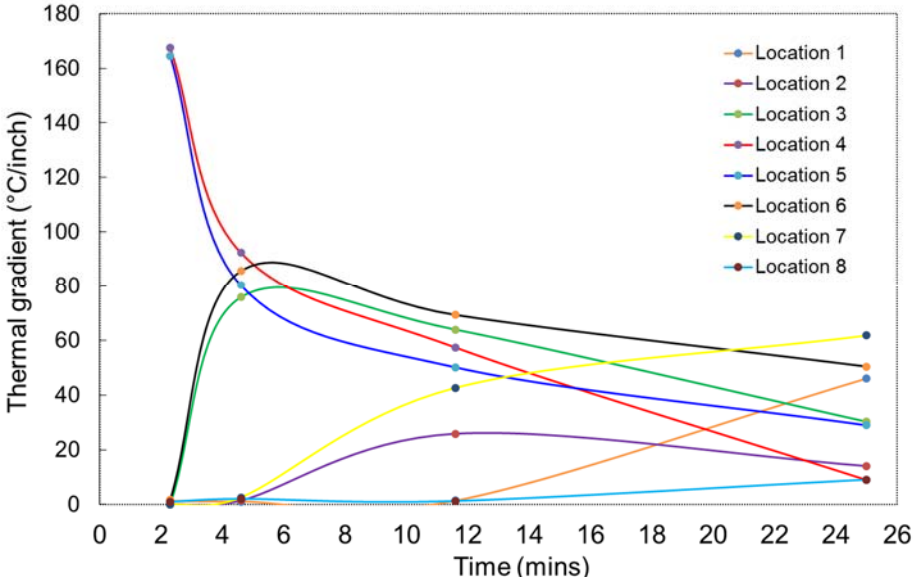


Figure 2.46 Thermal gradient change along with time of each locations

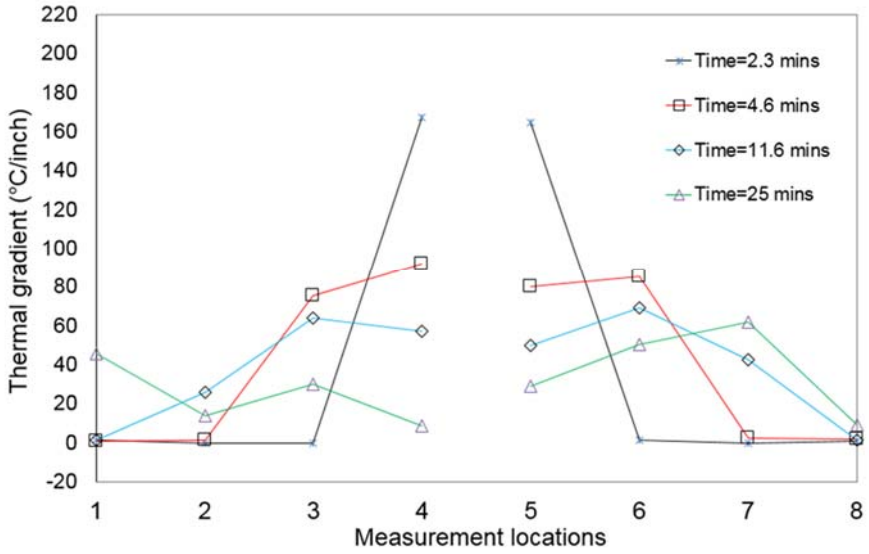


Figure 2.47 Thermal gradients calculated from temperature measured by embedded sensors.

The rock tensile stress and the minimum horizontal stress have a predominant influence on the fracture initiation pressure. There is no confining pressure for our test specimens, the rock tensile strength which can be of the order of 5-10 MPa, will be the main stress to overcome during the thermal fracturing process. In order to elucidate the natural of thermal fracturing, it is necessary to determine how changes in reservoir temperature affect the state of stress of the rock. When the reservoir is cooled, the rock tends to contract and a decrease in original stress of rock occurs. The tangential component of thermal stresses on a planar surface subject to temperature changes is given as (Tarasovs and Ghassemi (2014)):

$$\sigma_{th(z)} = \frac{\mathrm{E}\alpha\Delta T}{1-\upsilon}$$

E is static Young's modulus (MPa), α is linear thermal expansion coefficient (ºC$^{-1}$), $\Delta T$ is the temperature change (ºC), $\upsilon$ is the Poisson's ratio. The properties of our specimen are: $E = 40\times10^{3} MPa$ , $\alpha = 0.55\times10^{-5}$ , $\upsilon = 0.15$ . When the room temperature water is flow through the hot borehole, the thermal stress that applied on the borehole wall is:

$$\sigma_{boreholewall} = 40\times10^{3} MPa \times 0.55\times10^{-5} C^{\circ -1} \times 160C^{\circ} / 1 - 0.15 = 41.41MPa$$

Whereas the tensile strength of concrete is around 2-5 $MPa$ . The thermal stress that caused by the room water injection is much higher that the tensile strength of concrete. So the borehole wall cracked and these fractures continued to propagated into the specimen as the water continuously flow through the borehole. As the cracks continuously propagated into specimen, the thermal stress of location 3&4, 2&5, 1&6 were calculated as followed.

$$\sigma_{3\&4} = 40\times10^{3} MPa \times 0.55\times10^{-5} C^{\circ -1} \times 80C^{\circ} / 1 - 0.15 = 20.70Pa$$

$$\sigma_{2\&5} = 40\times10^{3} MPa \times 0.55\times10^{-5} C^{\circ -1} \times 35C^{\circ} / 1 - 0.15 = 9.05MPa$$

$$\sigma_{1\&6} = 40\times10^{3} MPa \times 0.55\times10^{-5} C^{\circ -1} \times 40C^{\circ} / 1 - 0.15 = 10.35MPa$$

From the above calculation, we could know that once a fracture has been created, it can be propagated with a lower injection pressure.

Our calculation shows that there is a strong possibility of fractures developing when the room temperature water flow through the hot specimen. Furthermore, once the fracture is initiated, cooling in its immediate vicinity is promoted by lower propagation pressure and a large leakoff area, thus encourage further fracture growth.

## 2.4 Analyses and discussions

When heating the specimens from the room temperature to the 190℃ (the target temperature), the specimens (#14, #15, #18, #19 and #20) took almost the same time to arrive the target temperature 190℃ (for both of borehole surface and out surface of concrete). The heating rate details are described in Figure 2.48 and 2.49. The total heating time and heating rate are similar, which may indicate that the specimens before the stimulations were homogeneous and intact.

After the thermal stimulations, although the cooling time and cooling rate may seem similar, there are some slight differences. Figure 2.4 and 2.49 showed that total cooling time and cooling rate when specimen were cooled from 105℃ to 40℃. Note that all the cooling conditions were the same (i.e., oven was turned off, and oven door was open). From these two figures, we noticed that the #14 and #18 cooling time are obviously shorter than other three specimens are. Especially for the borehole cooling time, the specimen #14 and #18 are 30% shorter than other specimens. While the outside surface cooling time of all the five specimens are almost the same. This may be caused by the more open fractures caused by the stimulation during the water flow. Because more open fractures exist in the specimen #14 and #18, there will be more air circulating during the cooling period, which caused the borehole temperature decreased faster compared with other three specimens that have more closed fractures. This phenomenon was also verified by the fracture profiles that showed later in this section. These fracture profiles showed that there more open fractures in Specimen #14 and #18 than Specimen #15, #19 and #29.

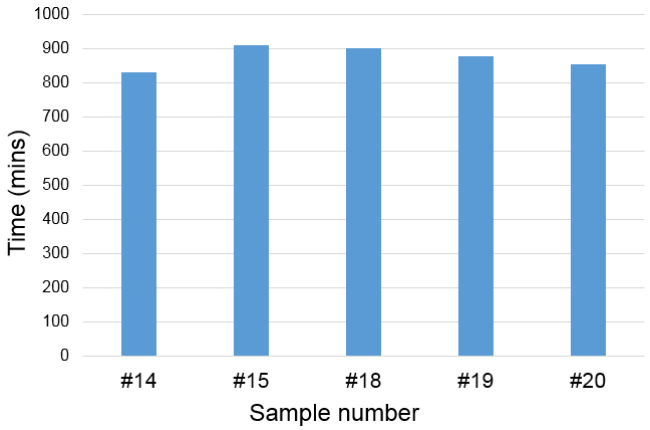


Figure 2.48 Total time for specimen heating (from room temperature to 190°C).

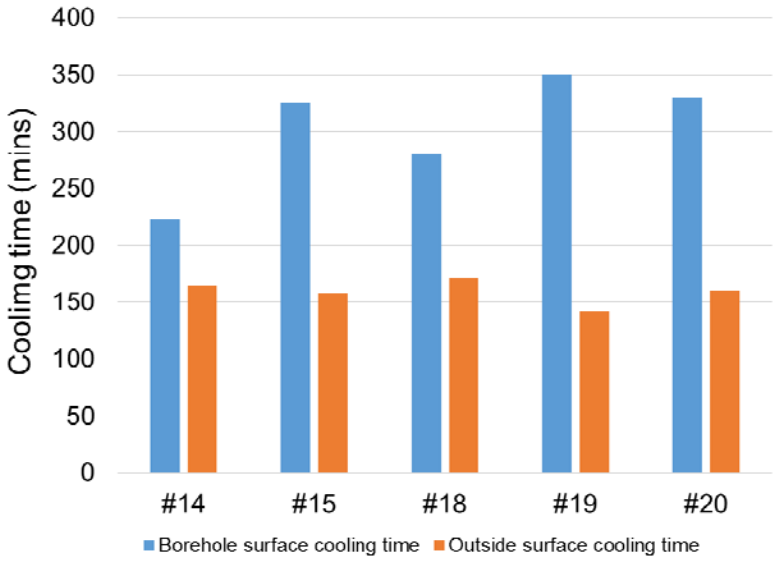


Figure 2.49 Cooling time when specimen borehole surface temperature cooled from 100 ℃ to 40 ℃ and outside surface temperature cooled from 180℃ to 40℃.

All the borehole pressure during the thermal stimulation were collected. However, due to the flow meter failure and repair time, flow data for some specimens were collected.

Also, due to the flow meter malfunction, some flow data were calculated by the collected the flow water volume and flowed time.

In the Figure 2.52, peak borehole pressure and constant (mean) borehole pressure during the thermal stimulation (water flow) are presented. The constant borehole pressure depended mainly on the flow rate, and is caused by the flow pressure/rate when the water is circulated in the borehole and tubing systems. Although the peak pressure also has the similar trend with the flow rate, it is likely to be caused by the quick evaporation of water when the injected cold water first contact with the hot borehole wall. The outlet is open to atmosphere, and the low fluid pressure in the borehole is considered as a minor contributor for initiating and propagating fractures. The initial water evaporation pressure may help to initiate the fractures on the borehole wall. The thermal gradient created by the water flow through the borehole is the major driving force to fracture inside the blocks.

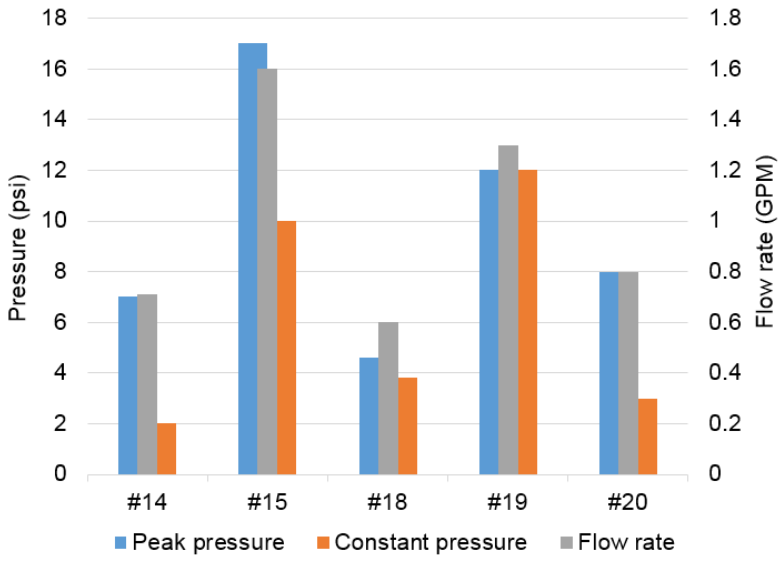


Figure 2.50 Peak borehole pressure, constant (~mean) borehole pressure, and flow rate of each specimen.

The pressure decay tests results have been presented in the section 2.3.2. From these results, we can get the permeability change information (pressure decay rate) due to the thermal stimulation. These data is present in Table 2.3. The method of calculating the pressure decay rate is that we first increase the borehole pressure up to 40 psi and then record the time of the borehole pressure decreases to zero. Then the pressure decay rate equals to borehole pressure (40 psi) over the decreasing time. Table 2.3 shows that the permeability indicated from pressure decay test has been increased after thermal stimulation due to the fractures or microfractures caused by the thermal shock.

Table 2-3 Pressure decay rate before and after thermal stimulation.

| | Before thermal stimulation (psi/sec) | After thermal stimulation (psi/sec) |
|---|---|---|
| #14 | 0.046 | 0.17 |
| #15 | 0.46 | 16.5 |
| #18 | 0.069 | 14.3 |
| #19 | 0.29 | 15 |
| #20 | 0.15 | 22.5 |

The temperature change during the water flow were presented in the first section of this chapter. Here we look into more details to check how much temperature changed during the thermal stimulation. All the specimens were heating to 190℃ and waited for it until the specimen arrive the homogeneous temperature conditions (the borehole and outside temperature both arrive the targeted temperature) before starting the test.

As we can see in the Figure 2.51, the borehole temperature dropped fast after the water was injected into the borehole and became constant around 30 ℃ during the thermal stimulation. However, the outside surface temperature decreased very differently. Several factors may influence the outside surface temperature after the heat stimulation. The first one is the flow time. The #18 had the longest water flow time among the specimens. Therefore its final temperature is the lowest.

The test results also showed that Specimen #18 had the most open fractures among other treated specimen. This indicates that the flowing time not only influences specimen temperature, but it will also affect fractures propagation.

Another factor is the leakage water during the thermal stimulation. There was some leakage water came from the micro-cracks around the casing caused by the thermal stress and the cracks on the epoxy during the water flow.

The water evaporation takes the heat from the specimen and made the temperature of specimen lower (endothermic water evaporation). For example, although Specimen #19 and #20 had the same flow time, there was more leakage water during the test of #20 than #19, so the final temperature of #20 is lower than #19.

An interesting observation is that regardless of the flow time for specimen temperature, the temperature of the water at the outlet was always about 40°C at its steady state.

At its steady state temperature at the borehole, the heat may be continuously transferred from the outside of the concrete to the inner part of the specimen (borehole)

and then transfer to the water that contact with the borehole wall. This phenomenon may be helpful to the EGS topics such as the life span of EGS reservoir.

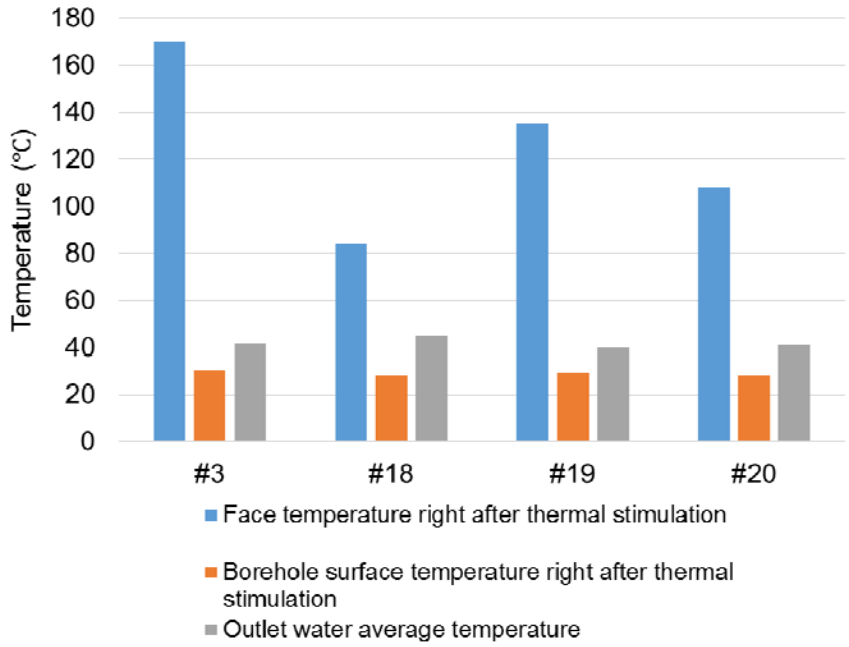


Figure 2.51 Average temperature of face that without leakage water, borehole temperature and outlet water temperature after thermal stimulations.

The breakdown test is performed after thermal stimulation. The aim of this test to know the breakage pressure change due to the thermal stimulation. The fracture profiles before and after the test, pressure profile during the breakdown test and fracture complexity are provided to characterize the fractures.

After the breakthrough test, although the specimen did not fall apart (shown in Figure 2.55), the fractures on the outside surface are wider than before. Most importantly is that the fractures on the bottom of the borehole and the borehole wall are clearly

observed, which was not observed before the breakthrough test (Figure 2.53). It is presumed that the thermal stimulation (thermal stress) initiated the micro-fracture on the borehole wall that previously was not easily observed. When the borehole pressure followed up to induce deeper fracture penetration, the existing micro-fractures became wider. The phenomenon also indicates that the seed fractures created during thermal stimulation will reduce breakdown pressure levels.

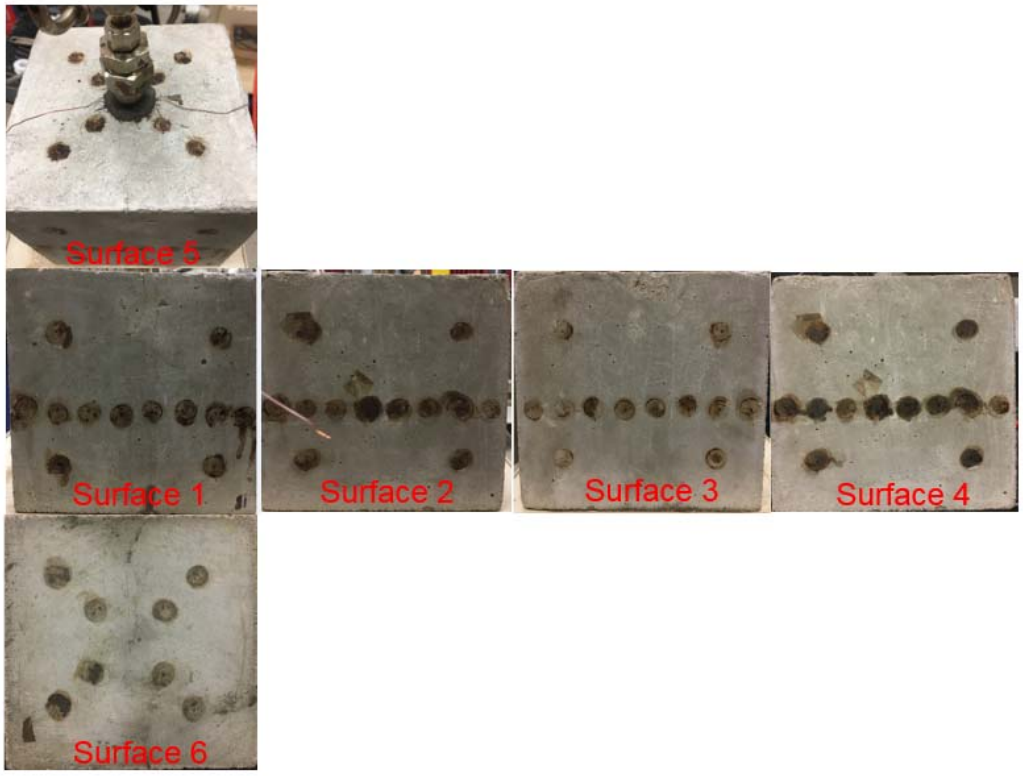


Figure 2.52 Fracture observations after the thermal stimulations (Specimen #18)

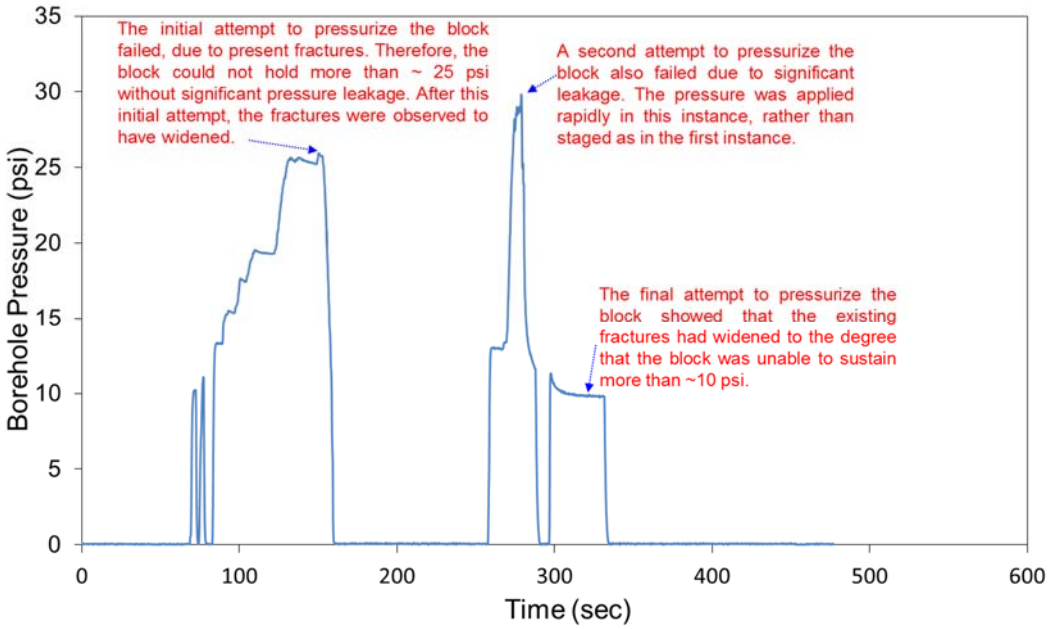


Figure 2.53 Pressure data records when performing the breakdown test (Specimen #18).

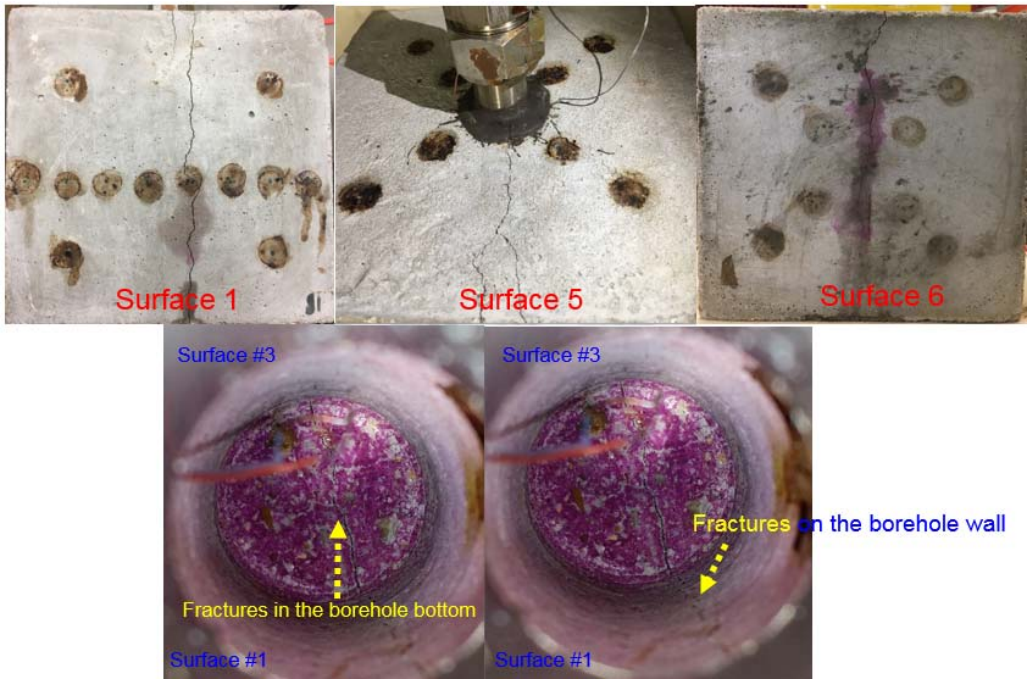


Figure 2.54 Fracture observations after breakdown test (air gas fracturing) (Specimen #18)

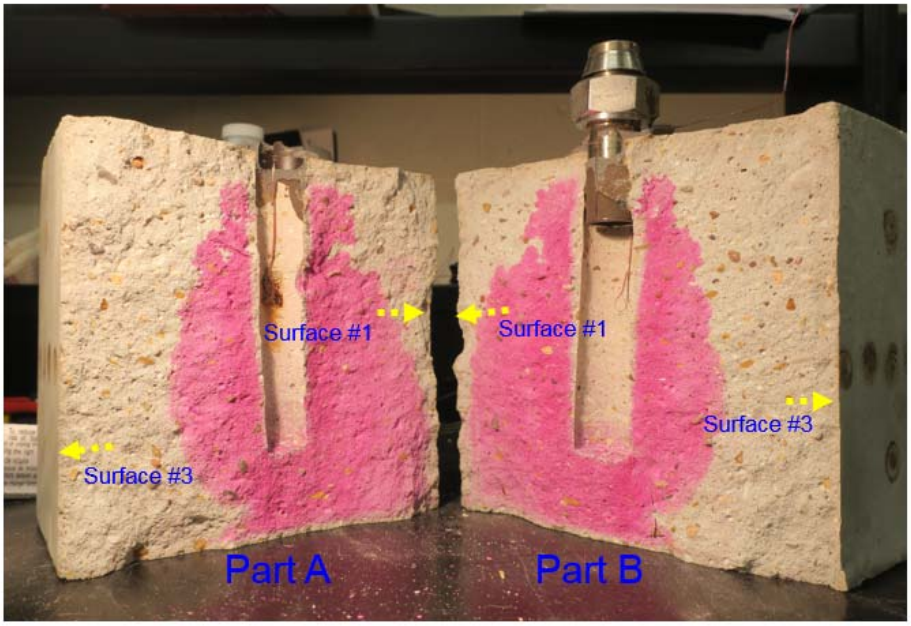


Figure 2.55 Fracture surfaces after specimen breakdown showing the thermal front. The pink area caused by the phenolphthalein shows the extent of the thermally induced fractures. The uncolored areas are opened up by air pressure (Specimen #18).

From our thermal stress calculation, we could know that there is a strong possibility of fractures initiating and propagating when the room temperature water flow through the hot specimen. The maximum thermal stress (around 40 MPa) that generated at the beginning of the water flow is much greater than the tensile stress of the concrete. As the fracture imitated from borehole and continuously propagated into specimen, the thermal stress that generated inside the specimen is lower than the thermal stress that generated on the borehole wall. It indicates that once the pressure that needs for propagation is usually lower than for the initiation.

## 2.5 Conclusions

We developed an experimental rig designed to study thermal stimulations in a laboratory environment resembling EGS downhole conditions. By water flowing, we created fractures in unconfined concrete specimen, thus enhanced its permeability and lower its breakthrough pressure by thermal stimulation. After experiencing the thermal flow, the mechanical and thermal properties are also changed.

- With flowing water continuously through the borehole without pressurization, the borehole is cooled as quickly as possible to maximize the thermal gradient near wellbores, and then injected water become warmed and exit through an outlet.
- The continuous water flow lead to occurrence of different thermal zones (cooled zone, diffusion zone and ambient temperature zone) in the specimens.
- Only minor film boiling effect is observed between the injected water and the much hotter borehole surface with 190°C, as we observed the small temperature difference between borehole space and the borehole wall. This implies efficient temperature conduction from borehole fluid to formation surface, which is favorable for thermal shock treatment.
- Thermally driven fractures were initiated from the borehole surfaces and propagated adjacent to the boreholes to some extent (thermal fracture front is clearly showed by our breakthrough test with phenolphthalein), indicating that borehole pressure may need to follow in order to induce deeper fracture penetration.
- Most of our experimental results showed that we created two-winged fractures after thermal stimulation. For the fracture initiation pressure, the rock tensile stress

and the minimum horizontal stress have a predominant position. Without confining pressure for our test specimens, the overburden pressure (the gravity of specimen itself) will be the maximum pressure and the minimum pressure direction will be horizontal. This explained why the fracture always initiated and propagated from face one to face three.

- The profiles of borehole pressure decay obtained before and after each stage of stimulation show that water flows increase the permeability of treated specimens. Especially, the multiple treatments showed that increasing number of stimulations increases permeability possibly by furthering fracture propagation and creating new fractures.
- Acoustic measurements confirm that the stimulations generate micro-fractures inside the blocks, which will increase the matrix permeability. Bubble leakage tests visually demonstrated localized or distributed permeation spots (or leaking holes) that enhanced permeability.

# 3. WELLBORE THERMAL STIMULATION IN GRANITE BLOCK SPECIMENS

## 3.1 Introduction

The reservoir's permeability can be improved by the sharp thermal gradient that caused by the cold water injected into the hot wellbore. Thermal fractures have been studied by many researchers. However, fracture formation as a result of rapid cooling of rock formation at downhole conditions in Enhanced Geothermal Systems is not well understood. In this study, we present laboratory results of emulating thermal stimulation under downhole conditions to give a deeper understanding of thermal fracturing mechanism.

To have more understanding that how thermal stimulation in EGS may occur, we designed and developed an integrated system to emulate thermal stimulation under wellbore condition in laboratory scale. We developed an apparatus to allow granite to be heated to 200 - 300°C without the confining pressure and rapidly injecting the cold water into the borehole in the specimen. We present a laboratory study of the role of thermal stress on fracture imitation and propagation. The acoustic amplitude and acoustic velocity are profiled to describe the physical properties. Thermal conductivity, expansion of thermal diffusivity are also measured before and after the thermal stimulation. Our results indicate that through thermal stimulation, especially after cycles of thermal simulations, porosity increased, density decreased, acoustic waves attenuated and the mechanical properties changed. We conclude that through our methods we have confirmed the process believed to be responsible for the application of successful thermal stimulation in geothermal fields.

## 3.2 Experimental studies

### 3.2.1 Experimental design and equipment

For the experimental design of granite block specimens, we designed the borehole thermal shock with the tubing and fitting system. The cold water is injected into 1-inch diameter boreholes, which are drilled 6 inches deep from the center of the top face into the eight cubic specimens. Cracking by borehole thermal shock only uses tensile stress resulting from sharp thermal gradient at borehole surfaces to initiate fractures. With flowing water continuously through the borehole under low fluid pressure, the borehole will be cooled as quickly as possible to maximize the thermal gradient across the contact surface.

Water flows from the tap water to the specimen, and injected into the borehole and then directed to an outlet at atmosphere pressure. A pressure transducer is attached to the wellhead to monitor the borehole pressure. Because borehole pressure will not exceed 100 psi throughout all stimulation tests and pressure decay tests, it can be safely applied to unconfined specimens. This experiment equipment employs specialized water rate transport, control, and measurement systems. We have set up real-time monitoring and logging of various parameters inside the borehole including pressure, water flow rate and consumption, temperature and acoustic signal. During the thermal shock tests, several thermocouples were attached to the inlet, borehole, outlet and Specimen surface to monitor the dynamic evolution of temperatures.

### 3.2.2 Specimens

It is important that all the specimens were prepared in a similar way. To ensure this, all the granite specimens to be tested are processed into 8-inch cubic blocks, an intermediate scale between cores and reservoirs. Westerly granite was chosen as the test material because they are common and inexpensive, and its properties are well known. The outside surface and borehole wall surface were polished at the factory. Several researchers (Yu et al., 2014, Haimson and Chang, 2000, Yong and Wang, 1980) have studied the change of mechanical and thermal properties of granite when it is heated to high temperature. According to their results, the granite's mechanical and thermal properties at room temperature are stated in Table 3.1.

Table 3-1 Mechanical and thermal properties of granite at room temperature.

| Properties | |
|---|---|
| Density (g/cm³) | 2.5-2.8 |
| Unconfined compressive strength (MPa) | 200-300 |
| Tensile strength (MPa) | 8-20 |
| Dynamic Young's Modulus (GPa) | 60-80 |
| Dynamic constraint Modulus (GPa) | 40-90 |
| Dynamic shear Modulus (GPa) | 15-30 |
| Poisson's ratio | 0.2-0.3 |
| P-wave velocity (Km/s) | 4.6-6 |
| S-wave velocity (Km/s) | 2.5-3.5 |
| Thermal conductivity(W/m·K) | 2-5 |
| Volumetric specific heat (MJ/(m³K) | 1.5-4.0 |
| Thermal diffusivity ($mm^2/s$) | 1.5-1.8 |
| Coefficient of thermal expansion (/K) | $2 \times 10^{-5}$ |

Table 3-2 Mechanical and thermal properties of the granite specimens tested in Chapter 3 at room temperature.

| Properties | |
|---|---|
| Density (g/cm³) | 2.6-2.7 |
| Dynamic constraint Modulus (GPa) | 42-44 |
| Dynamic shear Modulus (GPa) | 16-17 |
| P-wave velocity (Km/s) | 4-4.1 |
| S-wave velocity (Km/s) | 2.5-2.6 |
| Thermal conductivity(W/m·K) | 3.0-3.1 |
| Volumetric specific heat (MJ/(m³K) | 1.9 |
| Thermal diffusivity ($mm^2/s$) | 1.60 |
| Coefficient of thermal expansion (/K) | $2.2 \times 10^{-5}$ |

3.2.3 Procedures

For the assessment of fractures, the methods used for the concrete specimens in Chapter 2 were employed for the granite specimen tests as well. Procedures followed for the experiments of wellbore thermal stimulation in granite block specimens are detailed below.

① Before heating

- Before putting the Specimens the oven

    1) Pressure decay test with the short rig

    2) Leak detection test (at 50 psi constant borehole pressure) with the short rig

- After putting the Specimens the oven and fully assembling the rig

1) Pressure decay test

② During heating

- Data logging: Temperature (slow logging)
- Observe epoxy damage/contacts
- Pressure decay test right before treatment
- For granite block specimen, should heat at least for 20 hrs.

③ During treatment

- Flow rate (2-3 options: e.g. 1, 2, 3 GPM)
- Flow duration (2-3 options: e.g., 20, 40, 60 minutes)
- Target temperatures (Two options: 200 °C and 280 °C (max))
- Data logging: Temperature, flow rate and borehole pressure (intermediate)
- Observe processes and take photos

④ After treatment

- Pressure decay test right after treatment
- Two intermediate pressure decay tests
- Data logging: Temperature (slow logging)
- Continue heating for 6-10 hours
- Pressure decay test right before cooling

⑤ Cooling (two options: closed oven door / open oven door)

- Data logging: Temperature (slowest logging)
- One pressure decay test when the specimens are cooled a bit, but still warm (maybe after 3-5 hrs).

- Cool down specimen ambient temperature (75 °F or 24 °C). Then do pressure decay test
- Take out the specimen, and then perform:

    1) Pressure decay test with the short rig

    2) Leak detection test (again at 50 psi borehole pressure) with the short rig

## 3.3 Results

### 3.3.1 System behavior – temperature / pressure / flow

We are trying to emulate in a laboratory scale the thermal stimulation under wellbore condition that is conducted in the enhanced geothermal system field. Therefore, the system behaviors are important for us to observe and analyze. In this section, we will present temperature evolution during a whole test, which includes initial heating, water flow, continued heating, and cooling, and flow and present pressure data recorded during the flow period. Pressure decay tests are performed in each period above.

*Temperature*

A specimen is placed in the oven, and then the oven is turned on for gradual heating (Figure 3.2). If the specimen is placed while the oven is at its target temperature, the specimen will undergo high thermal loading at the surface, which is undesirable. Upon the flow of water, the borehole temperature decreased rapidly from ~190°C to ~25°C in 3-5 seconds. This rapid heat transfer creates a sharp thermal gradient and thermal shock to the borehole surface. Through the whole treatment that lasted about 5-20 minutes, the temperature difference between the inside of borehole and the block face is observed to

be large (about 160°C). Thus, the average thermal gradient between the borehole surface and the outside of the block is maintained high. The thermal gradient caused by cold water injected into the hot borehole is considered as the major driving force to initiate cracks inside the blocks. It is observed that compared with concrete specimens, granite specimens have slightly faster rates of heating and cooling (compared with Figure 2.4 and Figure 3.1) This may be caused by different thermal properties - thermal capacity, thermal conductivity and thermal expansion coefficient - between concrete and granite. This is because the granite has higher thermal diffusivity (1.6 $mm^2/s$) than that of the concrete (1.1 $mm^2/s$); temperature is better propagated in the granite blocks.

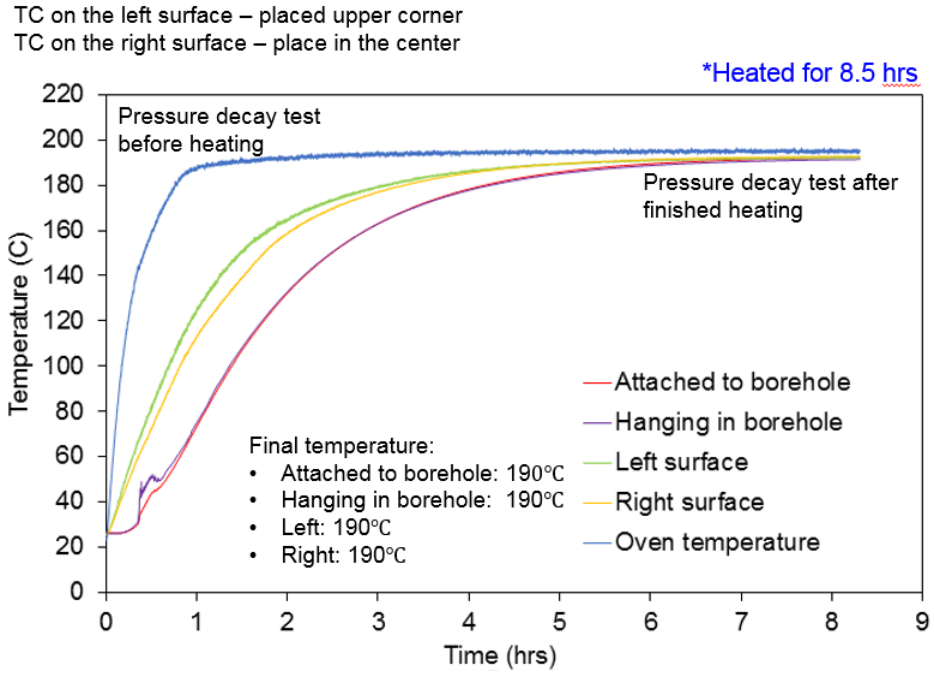


Figure 3.1 Temperature during heating of granite block Specimen #2 (the first stimulation).

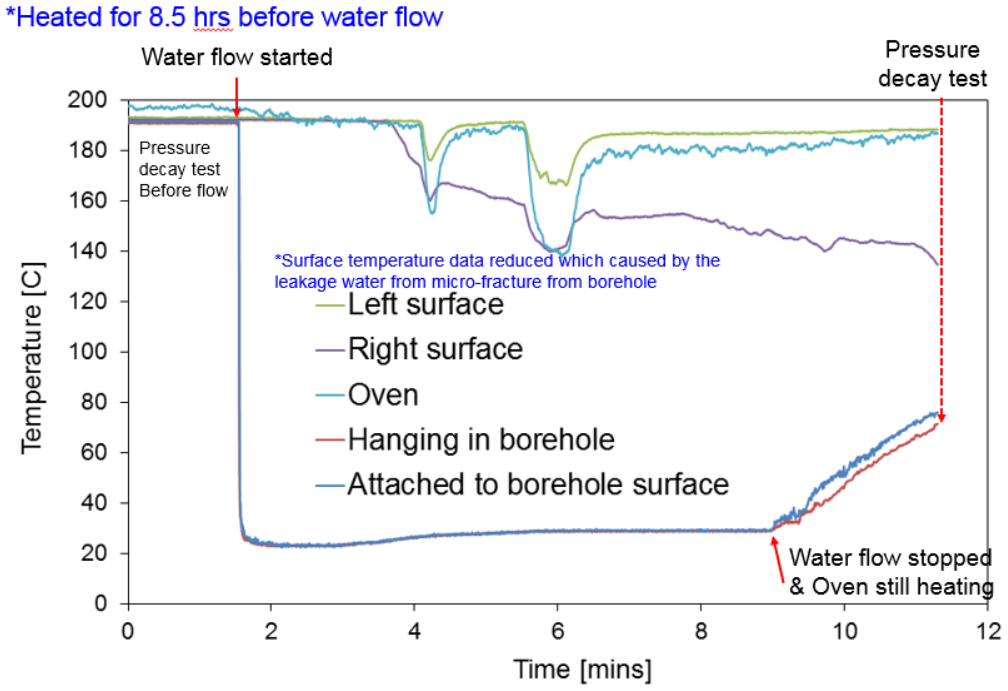


Figure 3.2 Temperature changes during thermal stimulation (flow of tap water) of granite block Specimen#2 (the first stimulation).

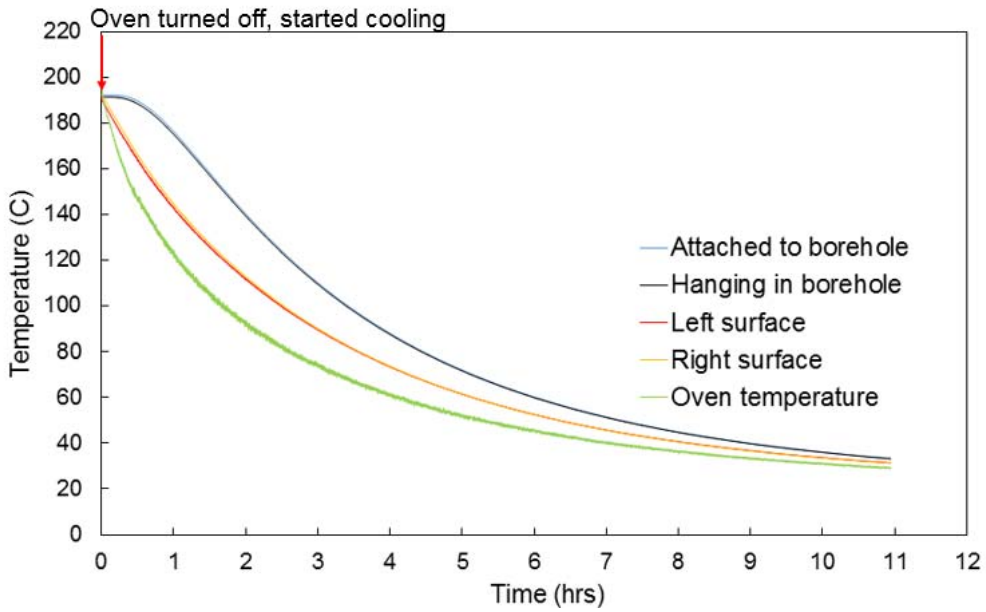


Figure 3.3 Temperature changes after stopping water injection of granite block Specimen#2 (the first stimulation).

*Borehole pressure and flow rate*

The pressure inside the borehole first tends to increase possibly due to the rapid water evaporation and then decrease to the more constant pressure governed by flow pressure (Figure 3.4 and 3.5). During the flow of water, spikes of borehole pressure that reached up to 80-160 psi. The outlet is open to atmosphere, and the average fluid pressure in the borehole (around 30 psi) would contribute little to fracture propagation. The magnitudes of the flow rates apparently affected the fluid pressures in the borehole. Lower flow rates corresponded to lower borehole pressure, and higher flow rate corresponded to higher borehole pressure, as the outlet is open to atmosphere. Water was collected at the outlet during the stimulation and compared with flow meter data (Figure 3.4). The flow rate calculated from the collected water is a bit higher than the flow rate from the meter. This may be caused by the turbulent flow created along the flow line.

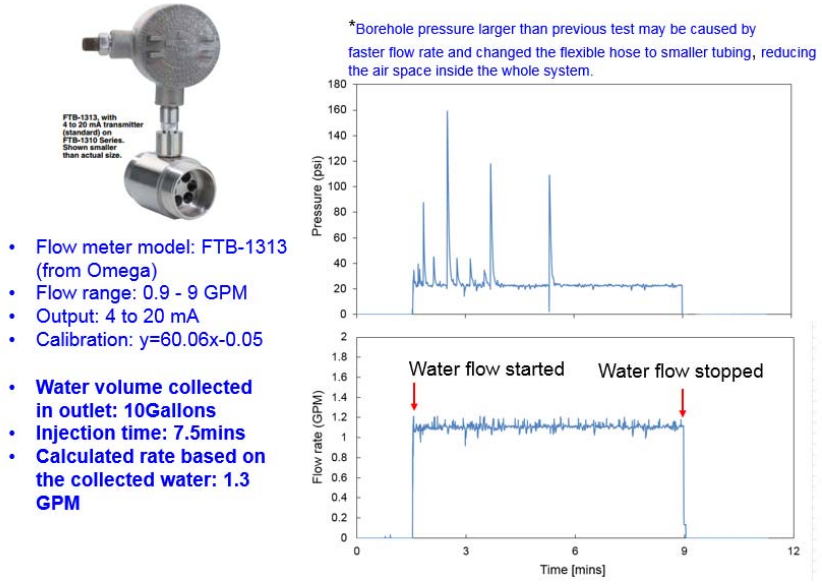


Figure 3.4 Borehole pressure and flow rate during thermal stimulation (water flow, Specimen#2-first stimulation).

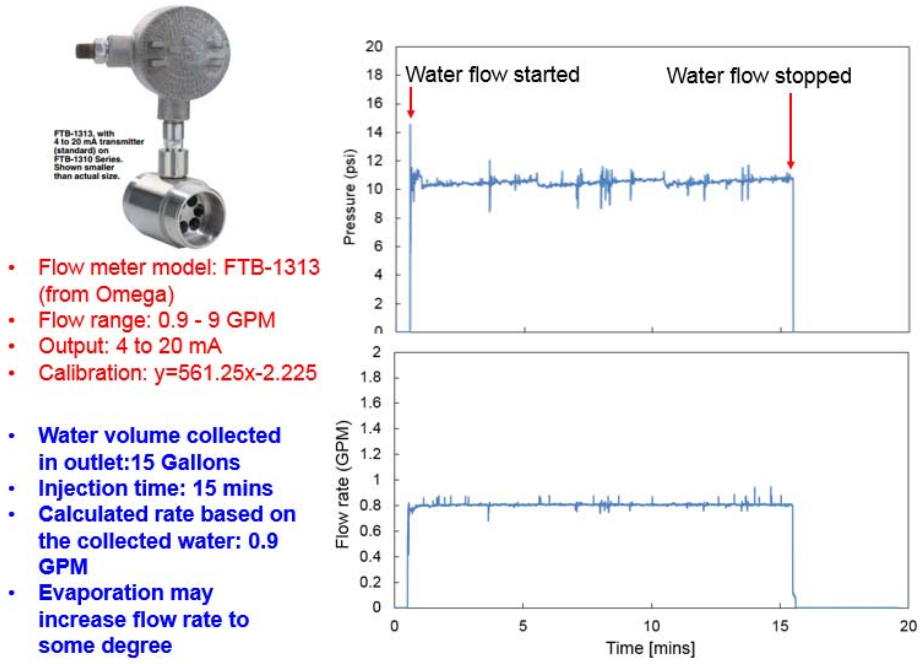


Figure 3.5 Borehole pressure and flow rate during thermal stimulation (water flow, Specimen#1-third stimulation).

### 3.3.2 Fracture Characterization

*Pressure decay tests*

The permeability of a specimen increased right after the treatment, indicated by faster decay in pressure decay tests (Figure 3.2). This is because the fractures created by the thermal shock, and the fractures will increase the air flow path when doing the pressure decay tests. However, after stopping the water injection, the permeability of the specimen will decrease back, as the wellbore become heated up. The disappearance of the thermal gradient closes fractures, and thus permeability decreased. However, when the specimen cooled down to room temperature, it is found that the permeability of the specimen

increased again. It is possible that either fracture were created during gradual cooling or simply fractures were reopened at room temperature.

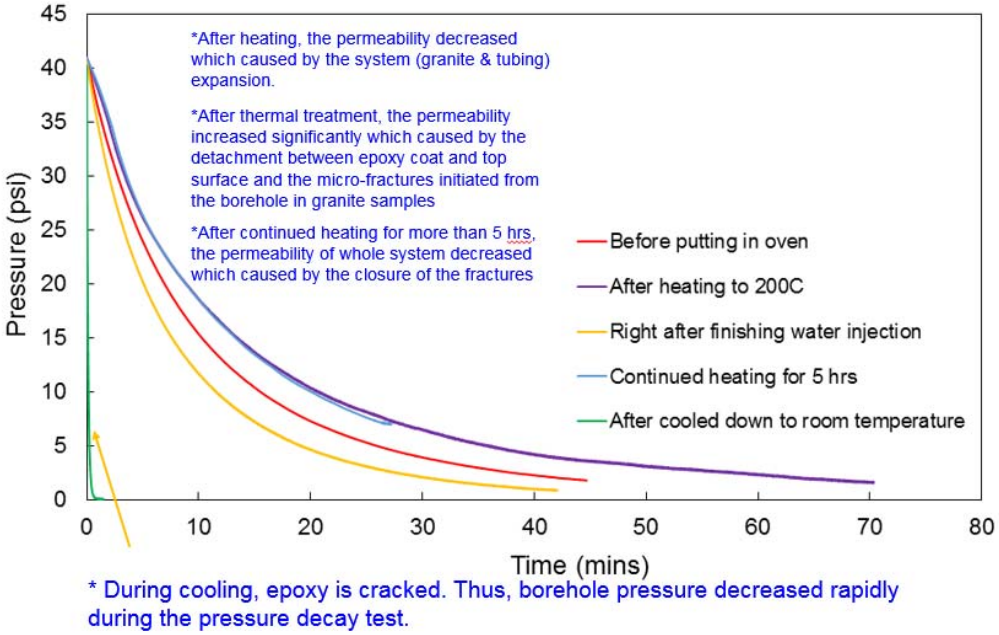


Figure 3.6 Pressure decay test results for Granite #2 (the first stimulation).

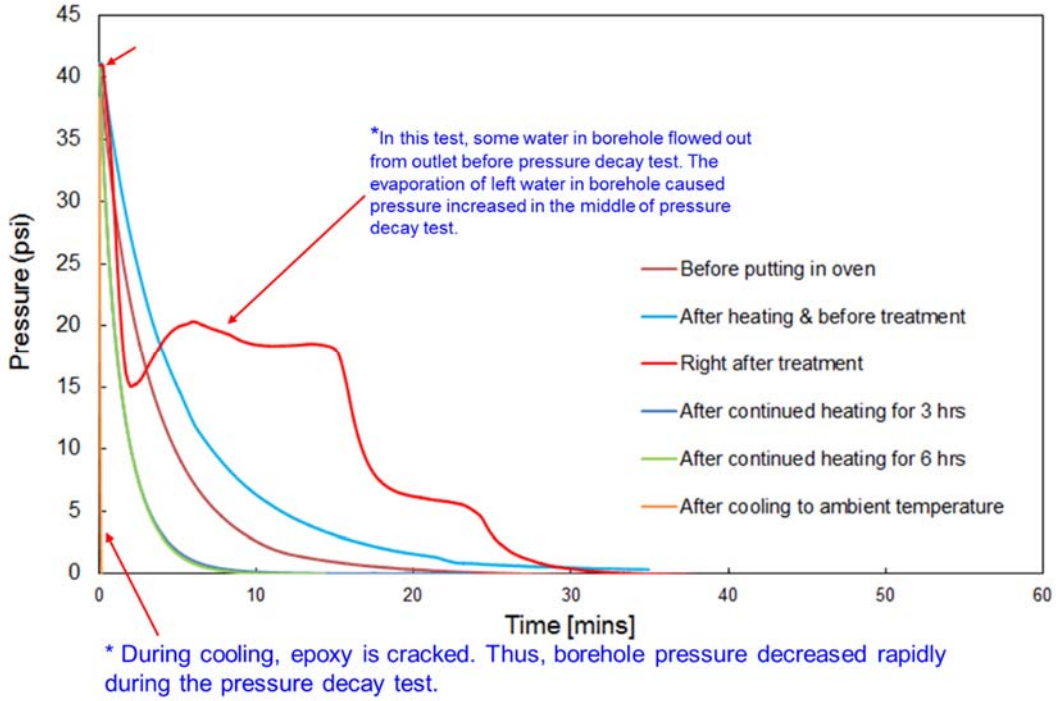


Figure 3.7 Pressure decay test results for Granite #1 (the third stimulation).

Table 3-3 Changes in permeability of granite block for a different phase.

"-" permeability decreased
"+" permeability increased

| Permeability | Before heating | After heating | Before treatment | After treatment | Before heating for 3 hrs | After heating for 3 hrs | Before heating for 6 hrs | after heating for 6 hrs | Back to ambiment |
|---|---|---|---|---|---|---|---|---|---|
| | Phase 1 | | Phase 2 | | Phase 3 | | Phase 4 | | Phase 5 |
| G1-1 | _ | | + | | _ | | _ | | + |
| G1-2 | _ | | _ | | + | | _ | | + |
| G1-3 | _ | | + | | _ | | _ | | + |

- For phase 1&3&4: Granite permeability decreased after heating. This may be caused by thermal expansion of granite/tubing/epoxy, causing closure of micro cracks.
- For Phase 2: Granite permeability increased after treatment. This may be caused by thermal shock caused micro cracks inside the specimen. The reason that G1-2 is different from others may cause by the presentence of water in the cracks. It prevents the pathway of air.
- For Phase 5: Granite permeability increased dramatically after completing the test. It is caused by the cracks on epoxy.

*Bubble leakage tests*

Bubble leakage tests can show changes in permeability due to the thermal stimulation before and after the treatments, by detecting the leaking crack. The liquid used for the bubble tests is specially formulated for sensitive leak tests in pressurized equipment such as Dewar or gas tank. Leak holes created during the thermal stimulation is located from the massive bubble generation. Then the bubbling agent is applied all over the faces to detect the leak cracks before the borehole is pressurized to about 40 psi by air.

Intuitively, more cycles of thermal treatments will increase the chances that cracks are generated, and cracks formed during previous treatment may propagate, which further weaken the specimen. Increasing the cycles of thermal treatment and waiting for the thermal recovery between each treatment are also suggested by the industrial geothermal field. It has been proved an efficient method to open up new fractures or widen the existing fractures in the reservoir (Bradford et al., 2015).

The results from the leakage bubble test showed the permeability changed significantly after the first water injection. It is speculated that thermal fracturing method may destroy the microstructures of grains inside the granite block during the first treatment. However, after completing four treatments to Granite #1, there are no further fractures observed on outside faces of granite. During the treatment and pressure decay test, there were no indications of short-cut cracks occurred on the borehole surface near the casing. At least regarding bubble leakage tests, with increasing cycles of treatment on granite blocks, the number and massiveness of leak points outside granite specimens only slightly increased.

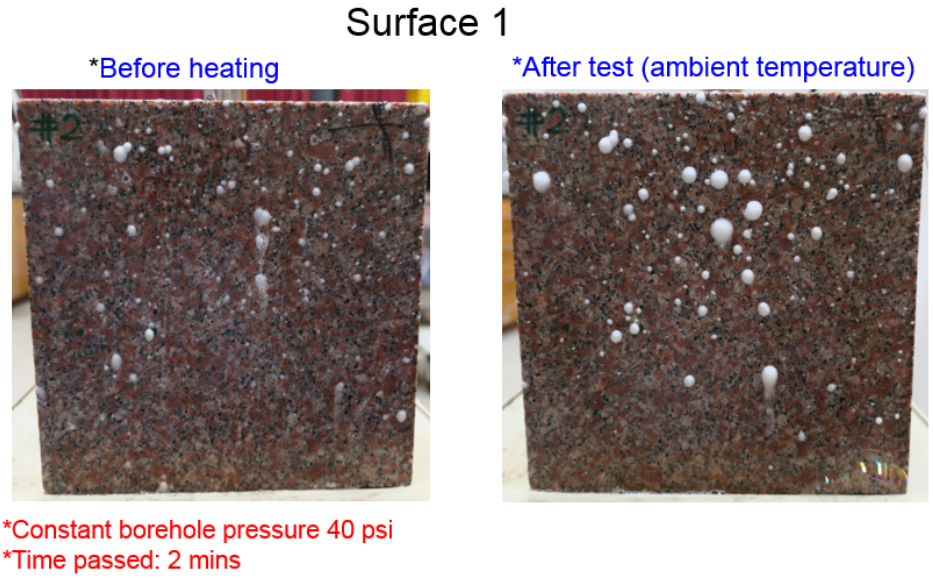


Figure 3.8 Comparison of bubble leakage before and after the first stimulation (Face 1, granite Specimen#2).

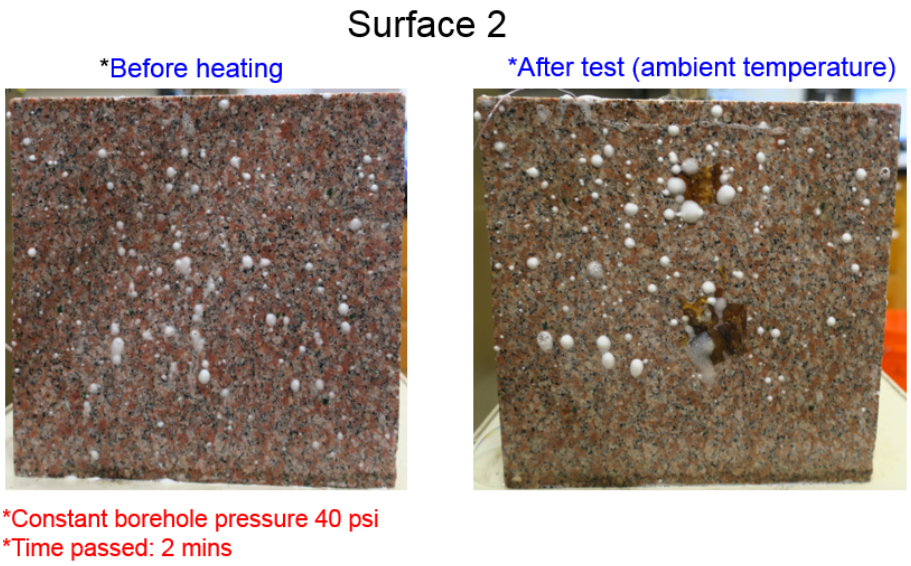


Figure 3.9 Comparison of bubble leakage before and after the first stimulation (Face 2, granite Specimen#2).

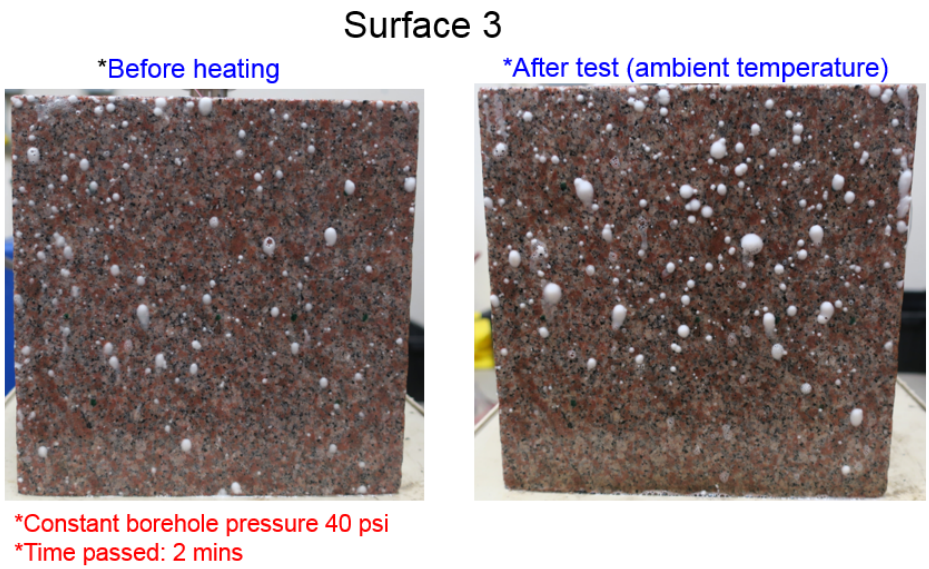


Figure 3.10 Comparison of bubble leakage before and after the first stimulation (Face 4, granite Specimen#2).

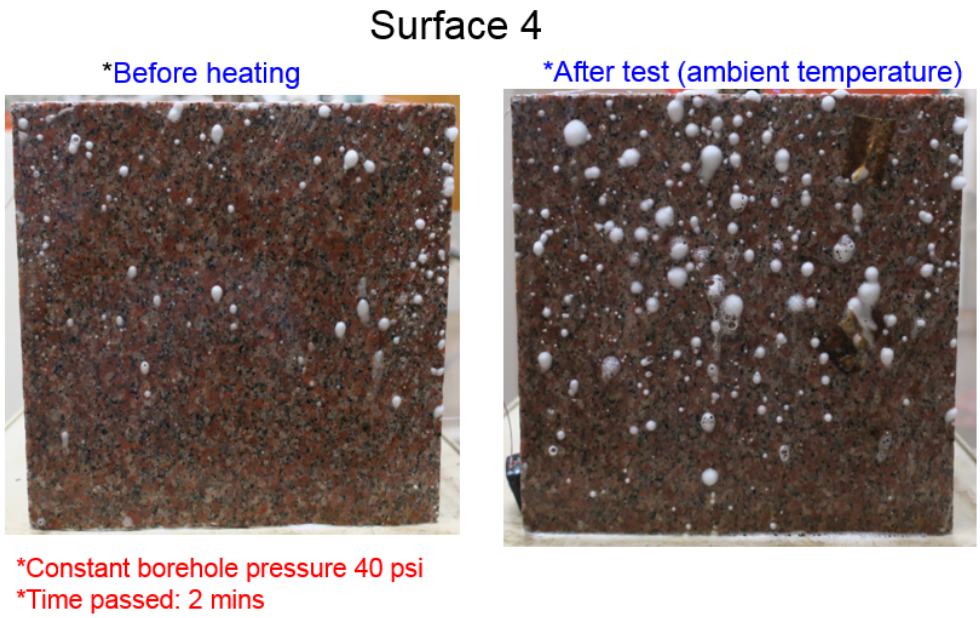


Figure 3.11 Comparison of bubble leakage before and after the first stimulation (Face 4, granite Specimen #2).

*Acoustic measurement results*

Transmission of compressional (P-waves) and shear (S-) acoustic waves were recorded before and after the treatments. The characteristics of acoustic waves propagating through the medium depend on the mechanical properties of the medium. In particular, the wave velocity in jointed rock masses is a function of the density of fractures (or fracture spacing) (Cha et al. 2009). When other properties such as intact rock properties, density, and joint stiffness are the same, the wave velocity can be used as a monitoring tool to characterize fracture generation.

A wave traveling through a cracked specimen, in general, loses energy faster due to dissipation and scattering. When the wave goes through the interface and fractures in the specimen, three modes of wave travel path includes reflection, refraction, and

transmission. The first two will scatter the direction of the wave out of the principal direction and cause wave energy loss, and the wave attenuation occurs. Distributed macro/micro cracks often give rise to an increase in attenuation. The knowledge of the attenuation of waves in cracked media provides an approach for quantifying the material damage.

The results from our acoustic measurement before and after the treatment confirms that the influence of thermal shock on the granite specimen. After all the treatments in our studies, the amplitudes of waveforms decreased significantly, which means the wave energy was dissipated through cracks and damages generated by the thermal stimulation. According to our measurement data, the range of reduction percentage for P-wave is from 20% to 85% and for S-wave is from 10% to 80%.

Distributed microcracks induced by the thermal stress will increase the length that wave will travel, thus increase the traveling time, decrease the wave velocity. Changes in the material response due to the reduction of effective elastic stiffness resulting from microcrack damage have a significant influence on the physical properties of the materials.

All the signals showed the time delays, which mean the velocities, were decreased (P-wave velocity decreased about 25%-40% and S-wave velocity decreased about 15%-30%. There is an inverse relation between the velocities and the damage induced by the thermal shock.

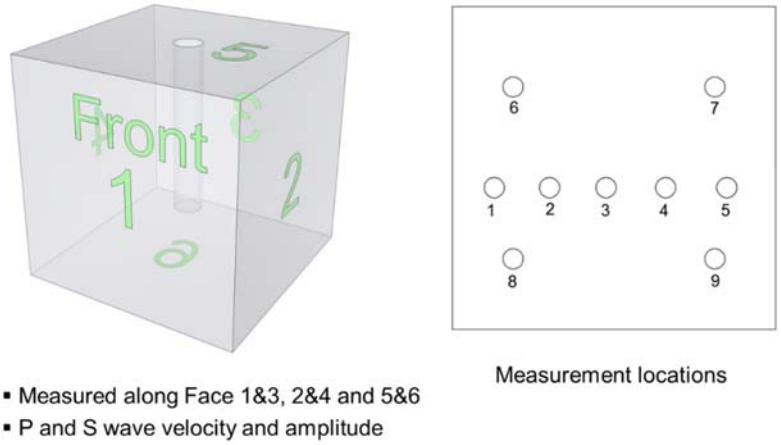


Figure 3.12 Locations for acoustic measurements.

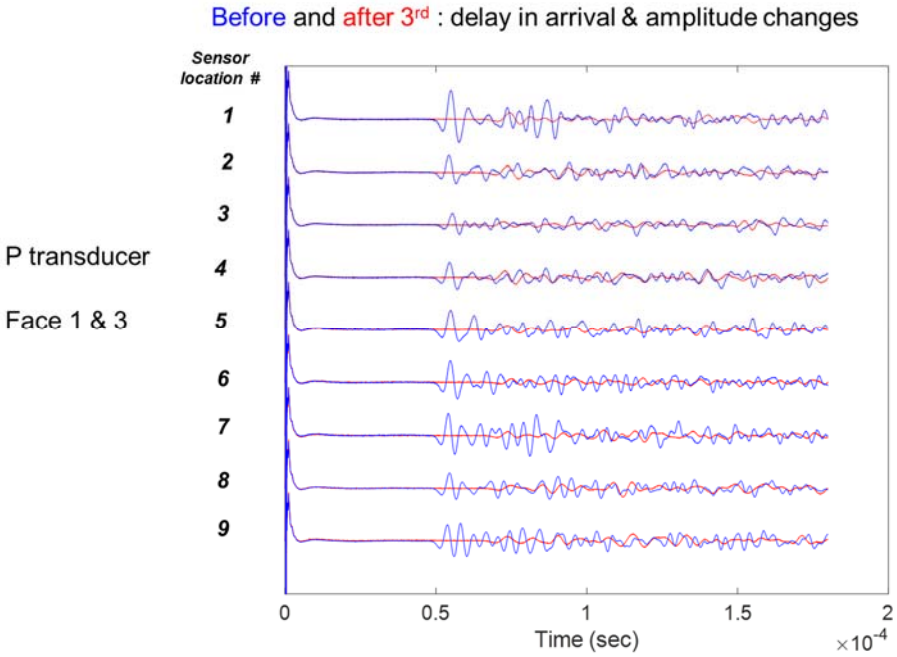


Figure 3.13 Acoustic waveforms of granite Specimen#1 after the third stimulation (P-wave, from Face 1 to Face 3).

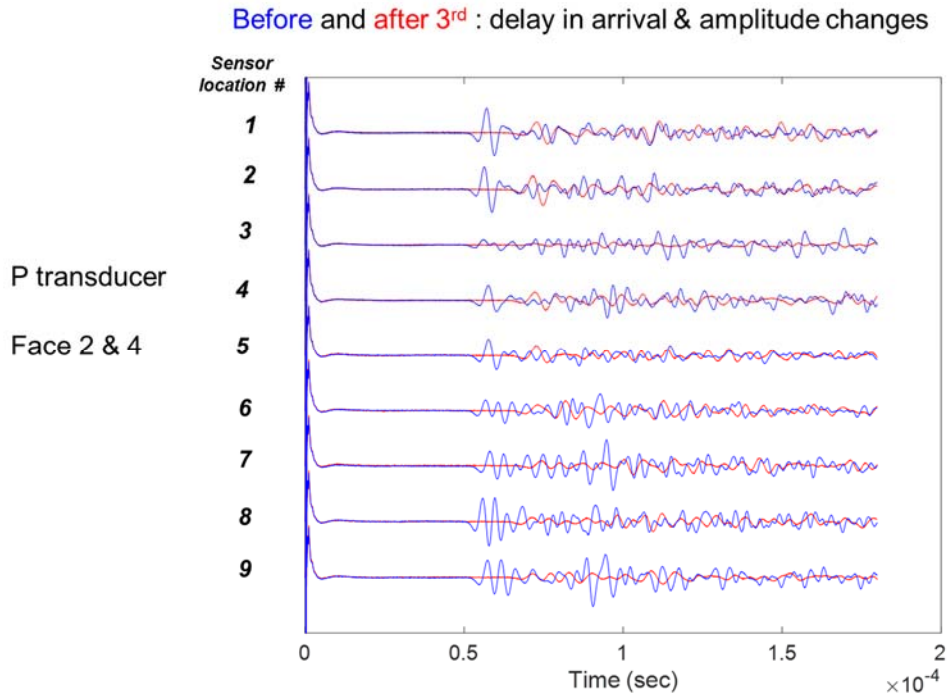


Figure 3.14 Acoustic waveforms of granite Specimen#1 after the third stimulation (P-wave, from Face 2 to Face 4).

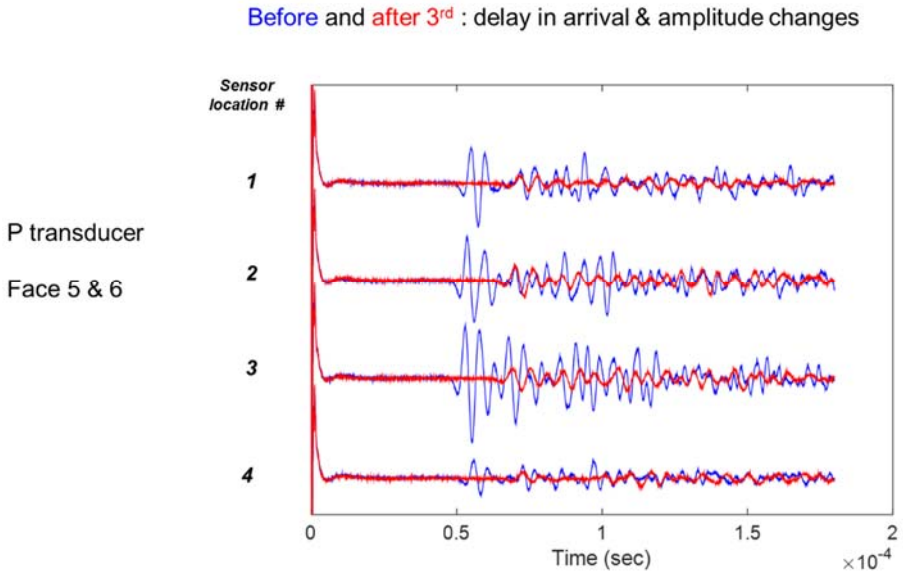


Figure 3.15 Acoustic waveforms of granite Specimen#1 after the third stimulation (P-wave, from Face 5 to Face 6)

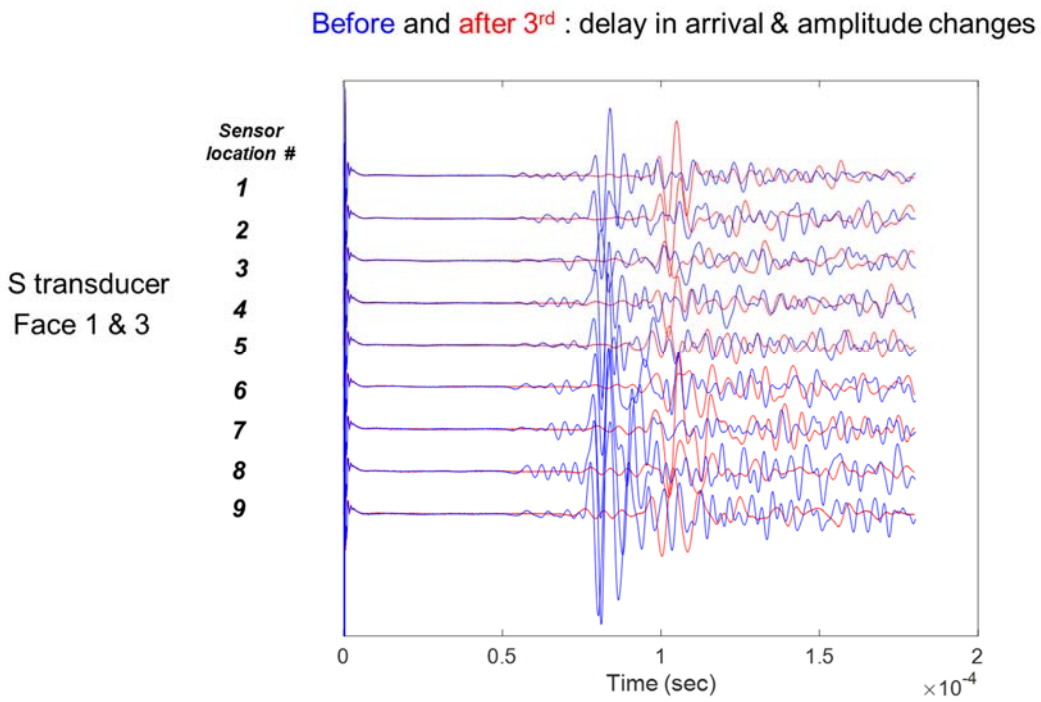


Figure 3.16 Acoustic waveforms of granite Specimen#1 after the third stimulation (S-wave, from Face 1 to Face 3).

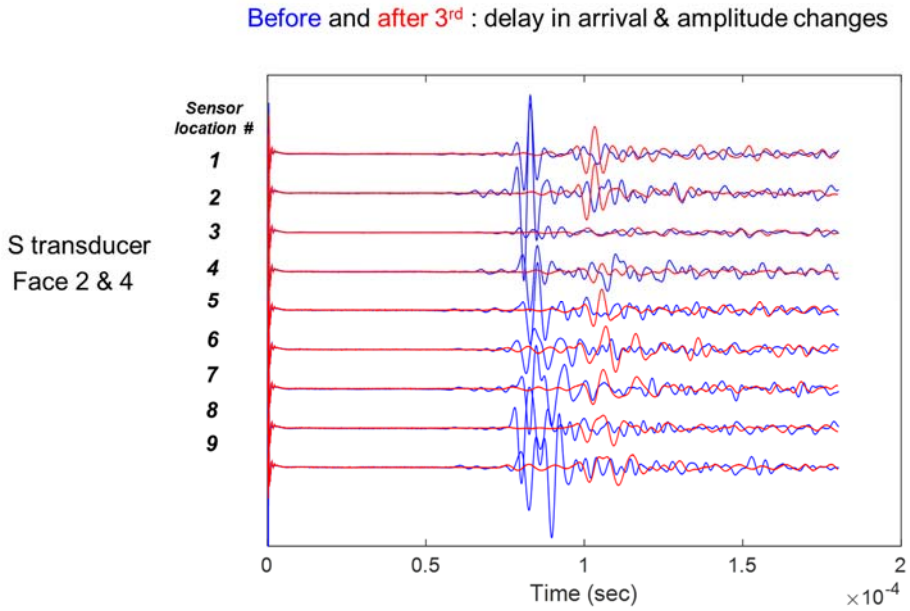


Figure 3.17 Acoustic waveforms of granite Specimen#1 after the third stimulation (S-wave, from Face 2 to Face 4).

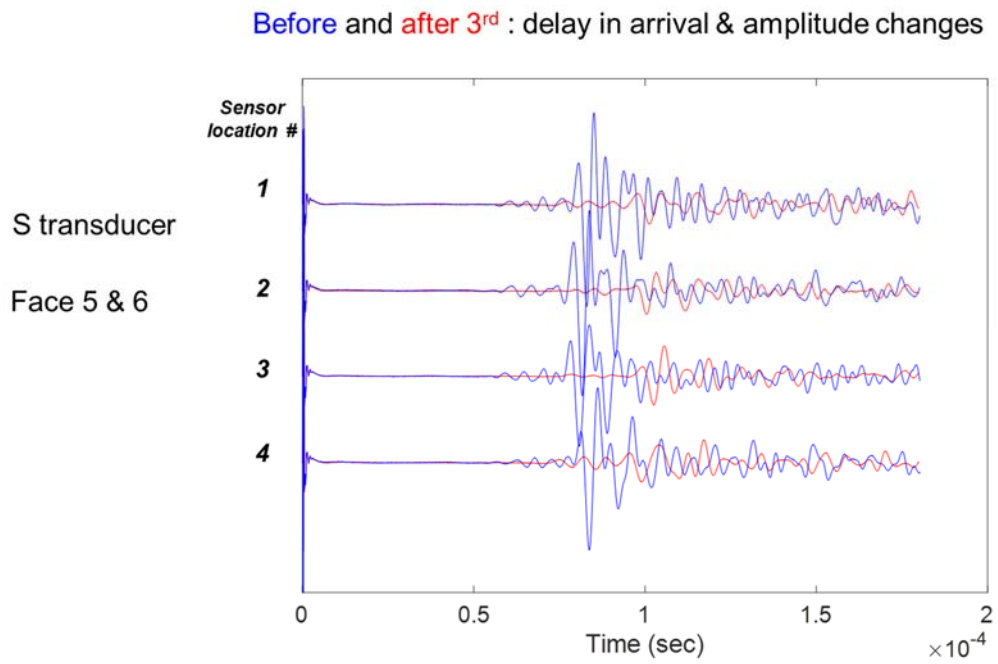


Figure 3.18 Acoustic waveforms of granite Specimen#1 after the third stimulation (S-wave, from Face 5 to Face 6).

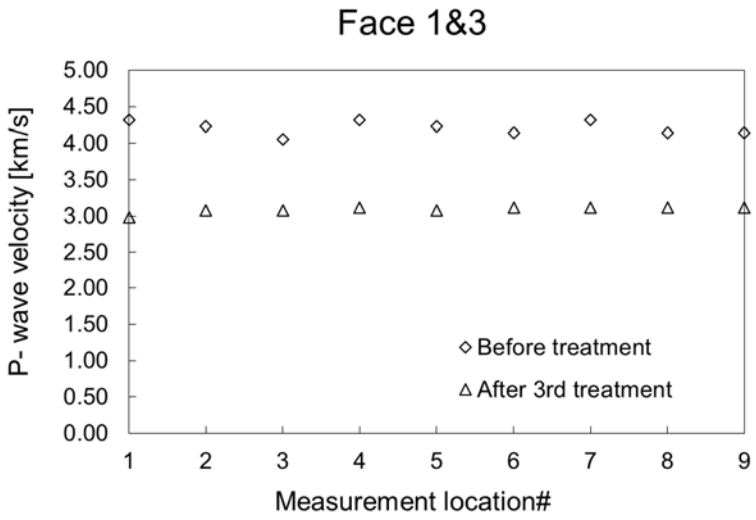


Figure 3.19 P-wave velocities of granite Specimen#1 after the third stimulation (from Face 1 to Face 3).

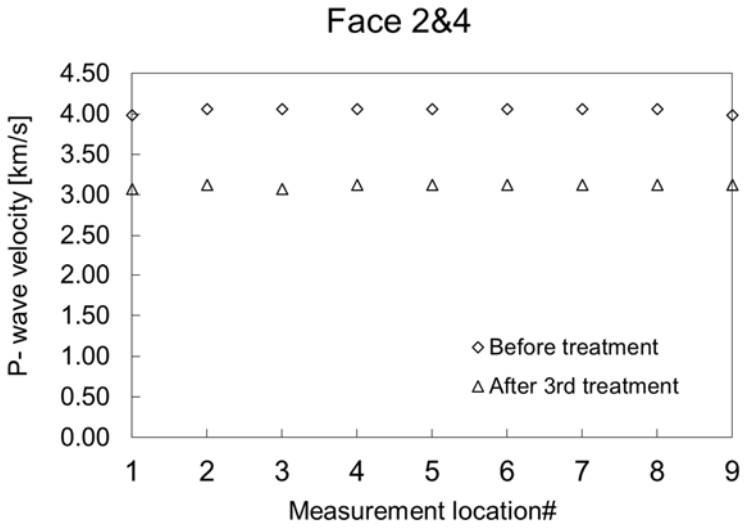


Figure 3.20 P-wave velocities of granite Specimen#1 after the third stimulation (from Face 2 to Face 4).

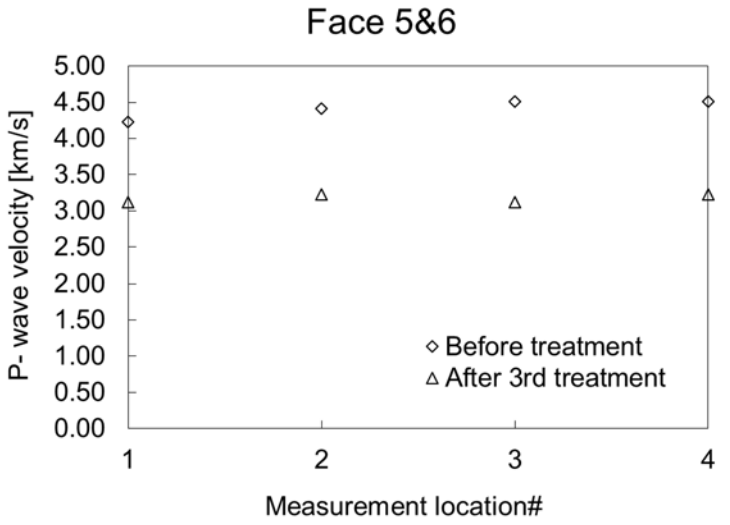


Figure 3.21 P-wave velocities of granite Specimen#1 after the third stimulation (from Face 5 to Face 6).

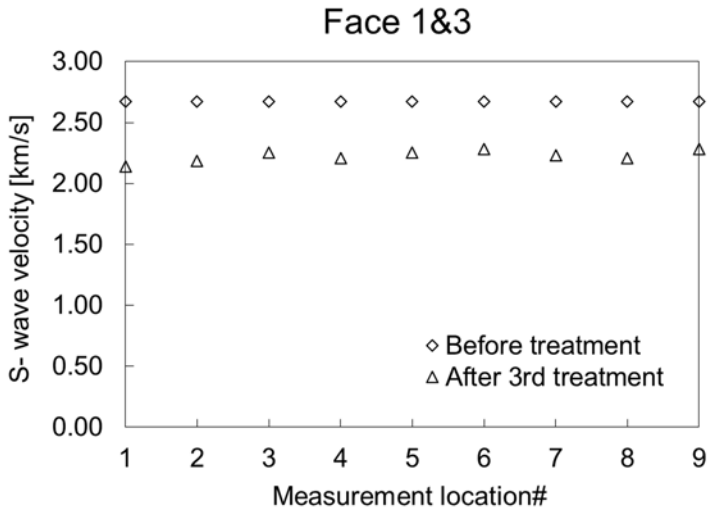


Figure 3.22 S-wave velocities of granite Specimen#1 after the third stimulation (from Face 1 to Face 3).

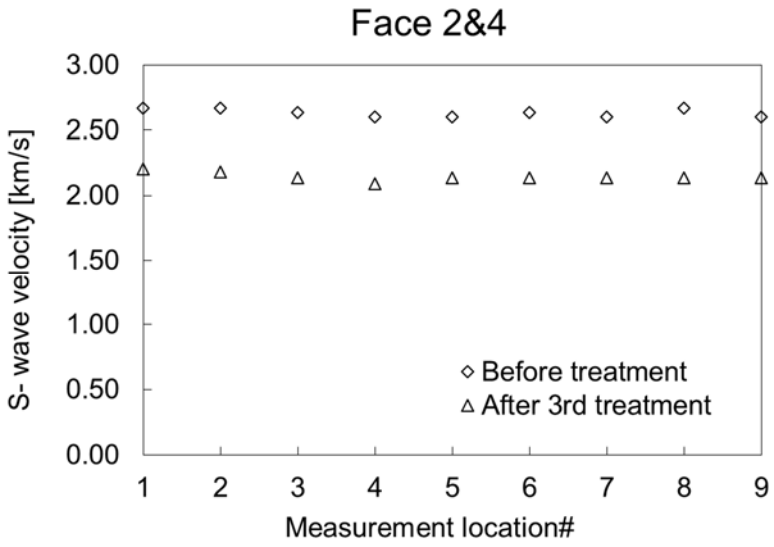


Figure 3.23 S-wave velocities of granite Specimen#1 after the third stimulation (from Face 2 to Face 4).

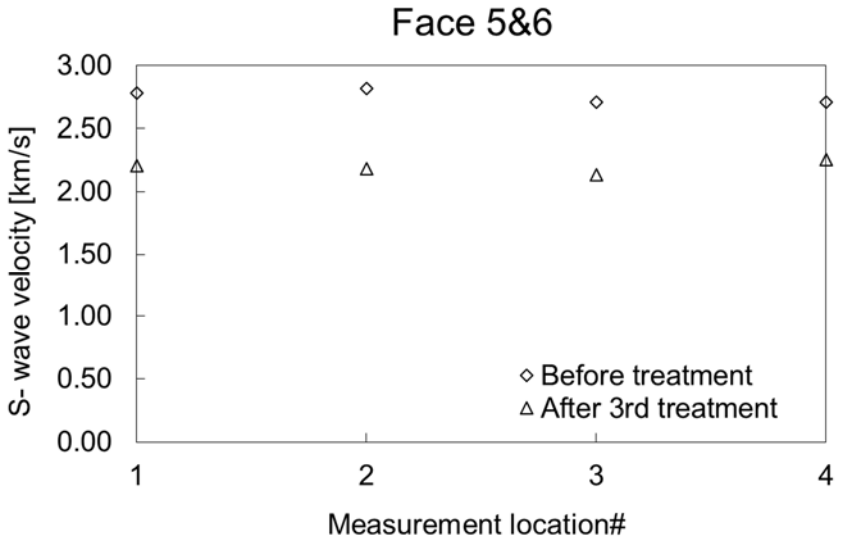


Figure 3.24 S-wave velocities of granite Specimen#1 after the third stimulation (from Face 5 to Face 6).

*Thermal properties*

After thermal stimulation, the thermal properties, especially thermal conductivity (shown in Figure 3.25), are reduced by the thermal stress. The seven measurement locations are at different locations on the top surface and around surfaces. After the water flow through the borehole, the thermal conductivity on the top surface, especially the area near the casing, significantly reduced by the thermal stress. The thermal conductivity on face one to face four, which are away from the borehole and didn't have stronger thermal gradient, didn't reduced much. The reason that caused the face one and face two have the different value of thermal conductivity with face three and four may cause by the leakage water.

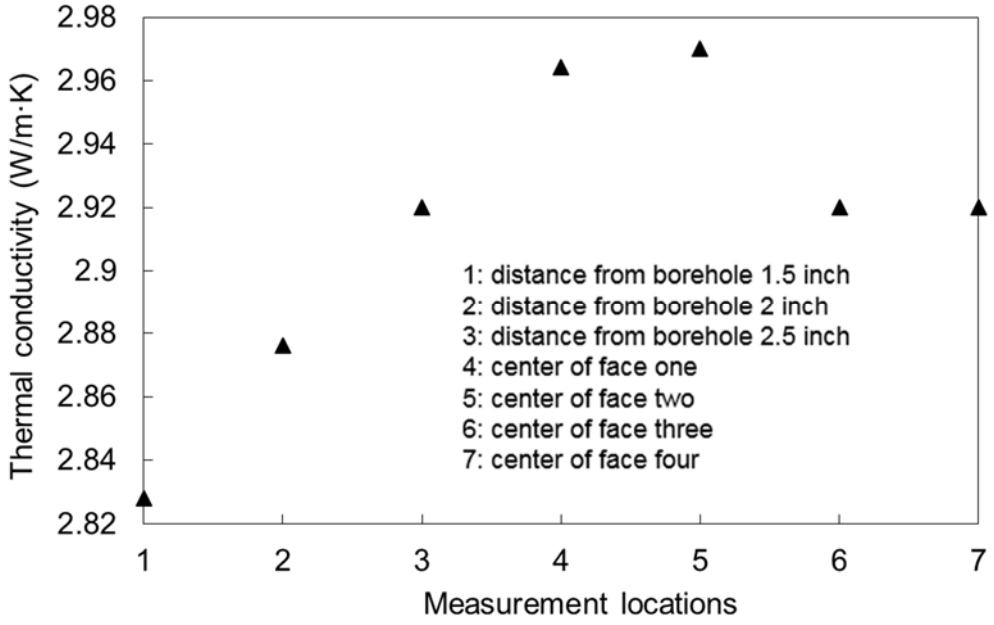


Figure 3.25 Thermal conductivity changed after thermal treatment.

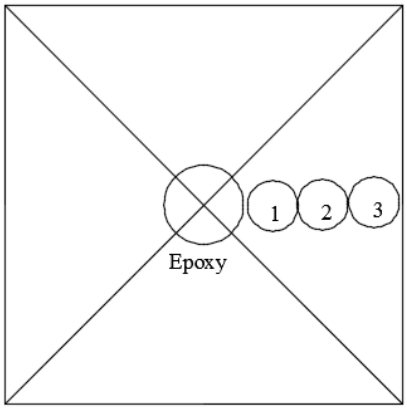


Figure 3.26 Thermal properties measurement locations 1-3 on the top surface

## 3.4 Conclusions

In this chapter, we successfully applied thermal stress into downhole condition of the unconfined granite specimen by water flowing. By using the thermal stress, we created the micro fractures to enhance permeability of the specimen. Also, the mechanical and thermal properties are changed after experiencing the thermal flow.

- Different from the concrete specimen, we didn't create visible fractures on granite due to its stronger mechanical properties (higher tensile strength and Young's modulus). But the profiles of borehole pressure decay obtained before and after each stage of stimulation show that water flows increase the permeability of treated specimens.
- Results from our Micro-CT showed that the permeability change is caused by micro fractures that caused by thermal stress. These small fractures that have formed during thermal treatment, which added up, significantly weakened the specimen. Also, this micro-fracturing in rocks is an indication of the occurrence of a failure, which could further lower the breakthrough pressure.
- Acoustic measurements confirm that the stimulations generate micro-fractures inside the blocks, which will increase the matrix permeability. Bubble leakage tests visually demonstrated localized or distributed permeation spots (or leaking holes) that enhanced permeability.
- Thermal treatment also changes the mechanical and thermal properties of granite, the effect enhanced with increasing number of cycles of the treatment. The thermal shock treatment decreased density (thus increasing porosity) and reduced acoustic

amplitudes and velocities (thus decreasing elastic constants). The thermal shock decreased thermal conductivity and specific heat of the treated specimens. This is because the treatment created minute cracks, and thus creating air voids, which have lower thermal conductivity and specific heat than mineral solids.

# 4. THERMAL STIMULATION OF CORE SPECIMENS - CHANGES IN PHYSICAL PROPERTIES

## 4.1 Introduction

In previous chapters, we conducted thermal stimulations to wellbores in large block specimens. In this chapter, we applied thermal shock on granite core specimens by heating and quenching them. Then we observed how micro and macro properties are altered by some methods. Granite core specimens were heated in the oven to the temperature of 150°C or 280°C and then submerge into the room-temperature water to rapidly cool the specimens. We characterized mechanical and thermal properties before and after quenching tests. The physical properties measured include elastic wave velocities, dynamic modulus, thermal conductivities, the coefficient of thermal expansion, specific heat, and surface texture. We also utilize micro-CT to evaluate the alterations of microstructure in 3D of the specimens and supplement our macro property investigations. The results of our investigation and implications for well stimulation in enhanced geothermal system are also discussed in this chapter.

## 4.2 Experimental studies

### 4.2.1 Specimens

All the granite core specimens are processed into 4-inch length and 2-inch diameter cylinder shape. Westerly granite was chosen because they are relatively inexpensive and its properties are known. Also, they are a kind of granite, which is the most common target formation for EGS. Both end surfaces were polished for the convenience of the acoustic and thermal measurements.

Researchers (Yu et al., 2014, Haimson and Chang, 2000, Yong and Wang, 1980) have studied the change of mechanical and thermal properties of granite when it is heated to high temperature. According to their results, the granite's mechanical and thermal properties at room temperature are stated in Table 4.1.

Table 4-1 Mechanical and thermal properties of granite at room temperature

| properties | |
|---|---|
| Density (g/cm³) | 2.5-2.8 |
| Unconfined compressive strength (MPa) | 200-300 |
| Tensile strength (MPa) | 8-20 |
| Dynamic Young's Modulus (GPa) | 60-80 |
| Dynamic constraint Modulus (GPa) | 40-90 |
| Dynamic shear Modulus (GPa) | 15-30 |
| Poisson's ratio | 0.2-0.3 |
| P-wave velocity (Km/s) | 4.6-6 |
| S-wave velocity (Km/s) | 2.5-3.5 |
| Thermal conductivity(W/m·K) | 2-5 |
| Specific heat (J/(kg·K)) | 1.5-4.0 |
| Coefficient of thermal expansion (/K) | $2\times10^{-5}$ |

Table 4-2 Mechanical and thermal properties of the granite core specimen tested.

| Properties | |
|---|---|
| Density (g/cm³) | 2.6-2.7 |
| Dynamic constraint Modulus (GPa) | 42-44 |
| Dynamic shear Modulus (GPa) | 16-17 |
| P-wave velocity (Km/s) | 4-4.1 |
| S-wave velocity (Km/s) | 2.5-2.6 |
| Thermal conductivity(W/m·K) | 3.0-3.1 |
| Specific heat (J/(kg·K) | 1.9 |
| Coefficient of thermal expansion (/K) | $2.2\times10^{-5}$ |

4.2.2 Experimental design and procedures

The experiment is performed to assess overall cracks and damages due to thermal shock that is induced by submerging heated granite core specimens into room-temperature water (quenching). The granite core specimens instrumented with temperature sensors at an outer surface were placed in the oven to slowly heat the specimen. After the internal temperature of the specimen reached the target temperature and become steady state, the core is submerged into tap water. The core is kept underwater for about 1 hour. Before and after tests, acoustic and thermal properties are measured. CT scans are performed for selected specimens to visualized internal microcracks, and microscopy is utilized to observe surface cracks and textures.

Detailed procedures for the experiments of quenching granite core specimens are as follows:

① Before heating

- Measure the volume and mass (to calculate density).
- Using microscopy to observe target area and save the picture (focusing on surface textures, color, and cracks).
- Acoustic measurement (using alcohol to clean the coupling agent after measurement).
- Place thermocouple on the specimen (glue and tape).

② During heating

- Set up the target temperature, for example, one specimen 280C and another 150C.
- To avoid creating the thermal shock, place specimen in the oven first and then turn on the oven. Do not place specimen while the oven temperature is already very hot.
- Data logging: temperature & time (to calculate heating rate).

③ During treatment

- Quenching time: according to the cooling data from previous block specimen (oven turn off & oven door closed & cooling in the air), it will take around 10 hrs to cool from 200C to room temperature. If the specimen is quenched in the water and cool down to room temperature, it will probably take 5 hours.
- Data logging: temperature & time (to calculate cooling rate).

④ After treatment

- Measure the volume and mass (to calculate density).

- Using microscopy to observe target area and save the picture (focusing on surface textures, color, and cracks).
- Acoustic measurement

### 4.2.3 Measurements

*Acoustic measurement*

In an ultrasonic transmission test, pulse energy generated from an ultrasonic transducer located at one end of a core specimen propagates through the core and is received by another transducer placed at the opposite end of the core specimen. A timing device measures the transmit time of the ultrasonic pulse through the material. With known propagation length, the pulse velocity can be calculated from the path length divided by the transmit time. Acoustic measurements give the velocity of compressional and shear waves that inside materials. By comparing these velocities before and after performing the thermal stimulation, the existence of cracks and damages within the rock specimen medium can be qualitatively assessed. Additionally, with known density rock density, the dynamic elastic modulus and Poisson's ratio can be calculated from these two velocities.

*Micro-CT scan*

As shown in Figure 4.1, the ZEISS Xradia 520 Versa Micro-CT is a non-destructive imaging technique capable of reproducing 3D material microstructure from shadow images based on X-ray absorption by material volume elements through the mechanism of contrast formation. A computer processing of the projected shadow pictures of different intensity is then used to reconstruct the 3D microstructure of the object. In our

project, the micro CT-scanner is used to get high-resolution 3D images of fracture planes and fracture network connectivity before and after thermal treatment.

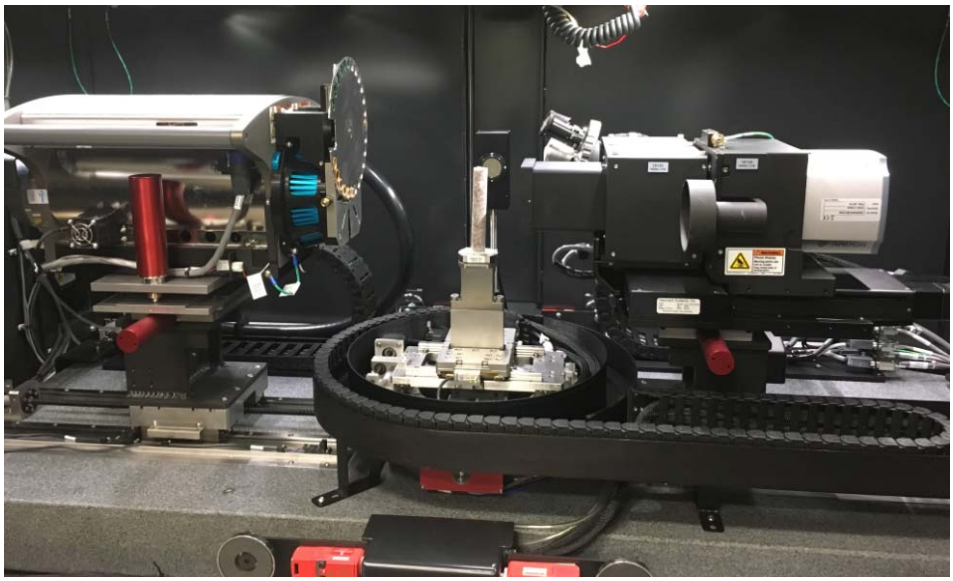

Figure 4.1 X-ray microtomography device (ZEISS Xradia 520 Versa Micro-CT)

The boundaries of mineral grains in the rock will determine a possible location that will occur the thermally induced cracks. Because in these boundaries, different mineral components will have different thermal expansion. When the microscopic fracturing connected to a network, the macroscopic permeability and the fluid transport properties of the rock changed remarkably. So two mechanisms have been suggested for thermal cracking. First, most rock-forming minerals are anisotropic, and, if there is a mismatch in the thermo-elastic behavior of minerals across a grain boundary, internal stresses may be generated as the rock is subjected to different temperatures and the stresses may be large enough to cause the formation of new cracks. The second model considers the effect of

the temperature gradient. Local variations in the temperature gradient in rocks generate thermal stress that in turn will initiate the new fractures or propagate the existing cracks.

*Thermal properties*

The hot disc thermal conductivity analyzer we used can provide thermal properties including coefficient of thermal expansion, thermal conductivity (0.001 to 1000 W/mK), thermal diffusivity, and volumetric specific heat. Applicable types of materials include solid, liquid, paste, and powder. It can also measure directional (axial & radial) properties, and can cover homogeneous, heterogeneous, isotropic, and anisotropic orientations.

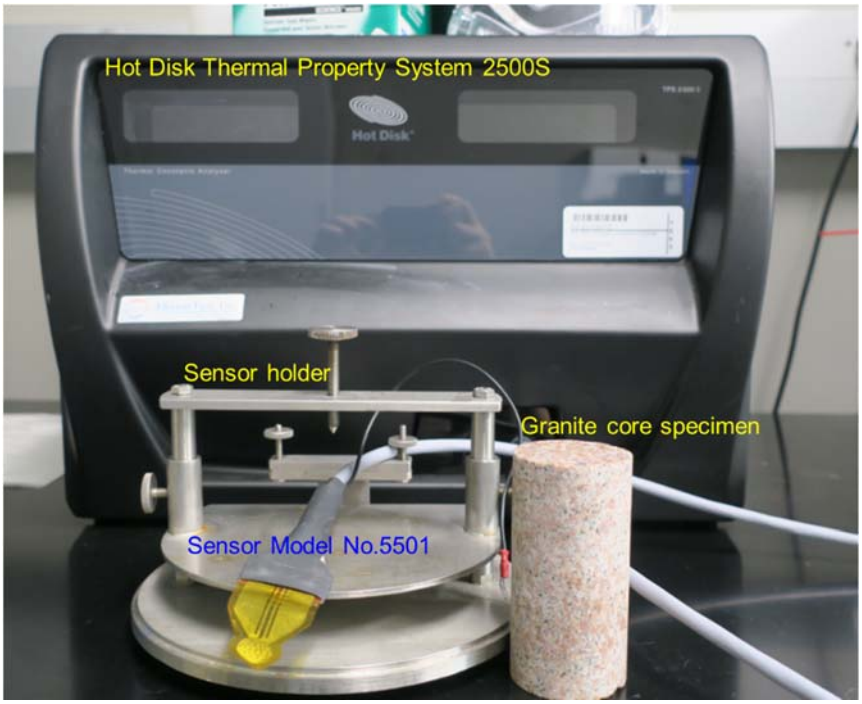


Figure 4.2 Hot Disc Thermal Property System (Model Number 2500S)

## 4.3 Experimental results

### 4.3.1 Temperatures

The thermocouple was attached to the specimen surface to measure the temperature during the heating and quenching. To ensure the specimen is thoroughly heated internally to targeted temperature, the cores are heated for at least 16 hours before the quenching (Figure 4.5). Once the hot specimen was submersed into the water, the temperature of specimen dropped rapidly, and the temperature of water increased slightly (Figure 4.6 and 4.7). The quenching will create thermal stress to the specimen, and micro fractures will be created.

Figure 4.3 Thermocouples attached on core specimen with glue - the glue cured for 12 hours before starting to heat (Granite Core Specimen #1 and Specimen #2).

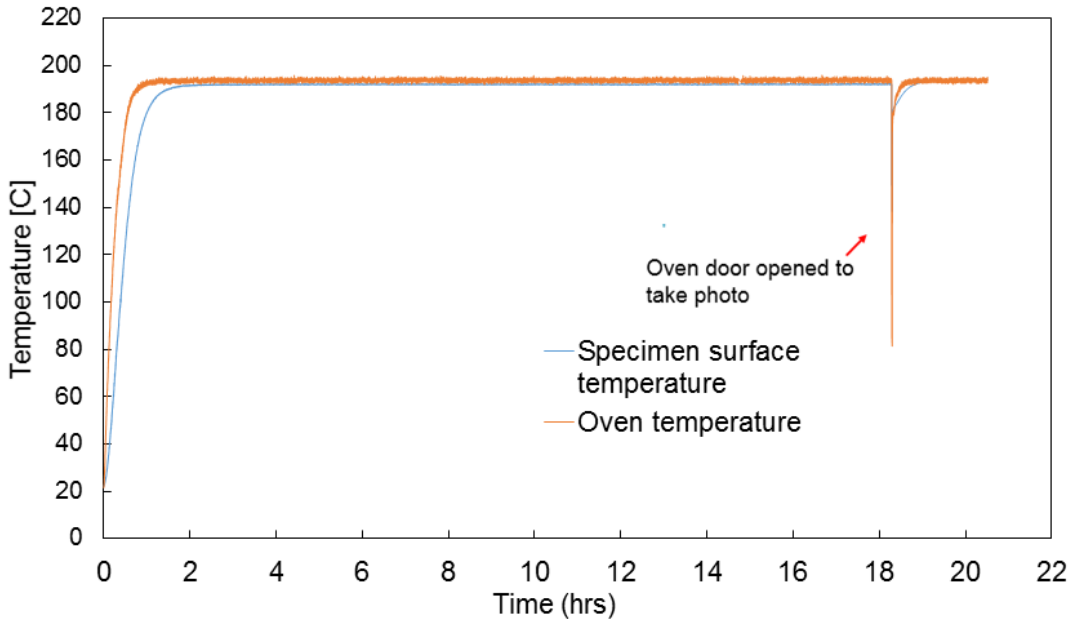


Figure 4.4 Temperature of granite core Specimen #1 during heating: total heating for about 20 hours before quenching.

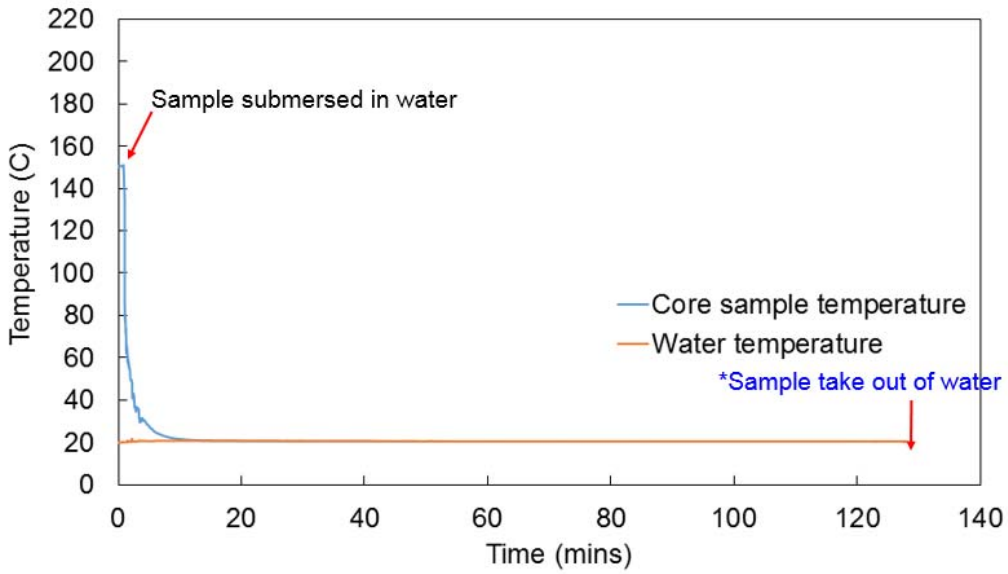


Figure 4.5 Temperature changes of granite core Specimen #1 during quenching test.

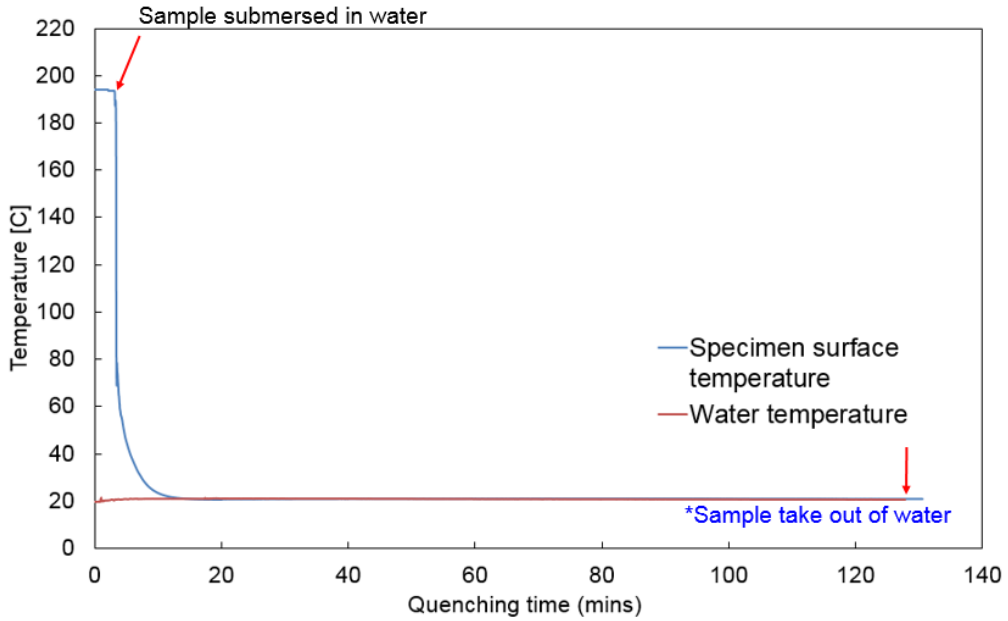


Figure 4.6 Temperature changes during the quenching test (granite core specimen #2).

4.3.2 Elastic wave velocity and density

The results showed that ultrasonic velocities decreased after thermal stimulation. Distributed microcracks induced by the thermal stress will decrease equivalent modulus of the specimen, and thus increase travel time, and decrease the wave velocity. Calculated wave velocities are shown in Figure 4.8 and Figure 4.9. It indicates that the thermal stimulation decreased the wave velocities.

Table 4-3 Specimen temperature before quenching tests

| | Core #1 | Core #2 | Core #3 |
|---|---|---|---|
| Temperature before quenching (ºC) | 150 | 190 | 270 |

The granite core specimens #1, #2 and #3 were heated to a different temperature (Table 4.2). When the target temperature of the specimen is higher, it will cause stronger thermal stress when performing the quenching test. Thus, the more thermal damage will occur on the specimen. Combining the Table 4.2 and Figure 4.8 and Figure 4.9, we see that there is an inverse relation between the specimen temperature and ultrasonic velocity after the thermal stimulation. For comparison or as the control experiment, Granite Core #4 is heated to 200ºC, and then slowly cooled to room temperature. This gradual heating and cooling (without quenching) will also create micro fractures and change core properties. Because most rock-forming minerals are anisotropic, and, if there is a mismatch in the thermo-elastic behavior of minerals across a grain boundary, internal stresses may be generated as the rock is subjected to different temperatures and the stresses may be large enough to cause the formation of new cracks.

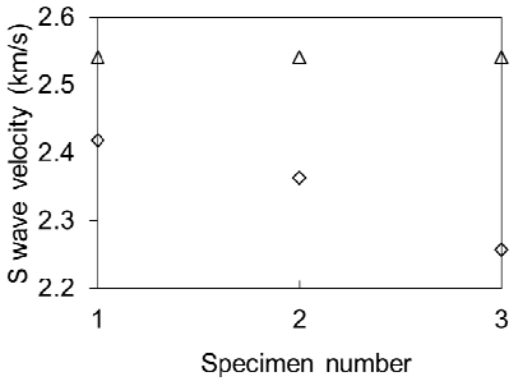


Table 4-4 S-wave velocity changes before and after treatment (Core #1 to #3)

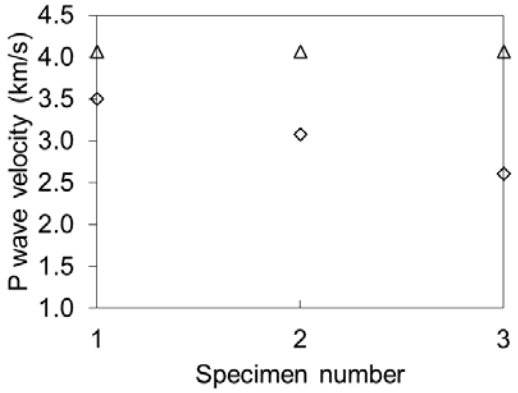


Table 4-5 P-wave velocity changes before and after treatment (Core #1 to #3)

Cracks and damages existing in specimens, in general, tend to dampen wave energy. A wave traveling through these discontinuities loses energy due to scattering. There are three modes of a wave traveling through the interfaces and fractures in specimens: reflection, refraction, and transmission. The first two will scatter the direction of the wave out of the principal direction and cause loss of wave energy. Thus, distributed macro/micro cracks often give rise to an increase in attenuation. From the results in Figure 4.8 to Figure 4.13, the amplitudes of both P and S waves dampened after the specimens that underwent quenching. Amplitudes before and after quenching compare by percentages in Table 4.3.

Table 4-6 Ultrasonic amplitude reduction by percentage.

| | Core #1 | | Core #2 | | Core #3 | | Core #4 | |
|---|---|---|---|---|---|---|---|---|
| | P-wave | S-wave | P-Wave | S-wave | P-Wave | S-wave | P-Wave | S-wave |
| Deduction percengate | 44% | 40% | 75% | 80% | 75% | 87.5% | 35% | 0% |

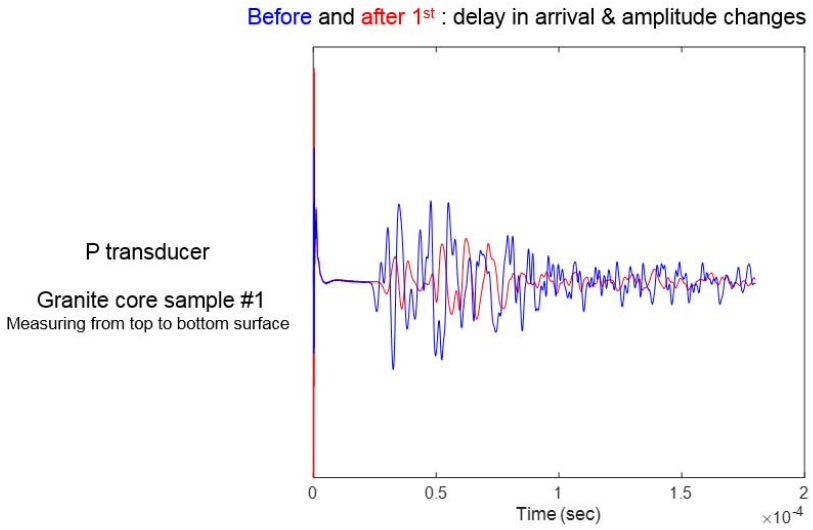


Figure 4.7 P-wave signature before and after quenching (Granite Core #1).

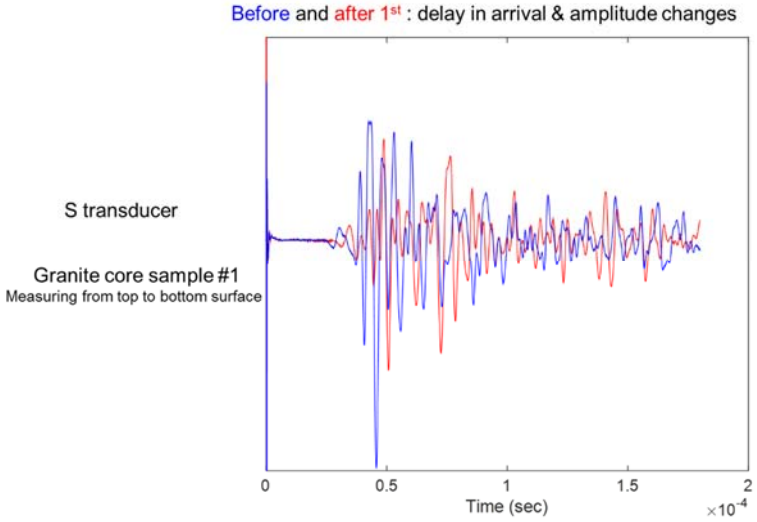


Figure 4.8 S-wave signature before and after quenching (Granite Core #1).

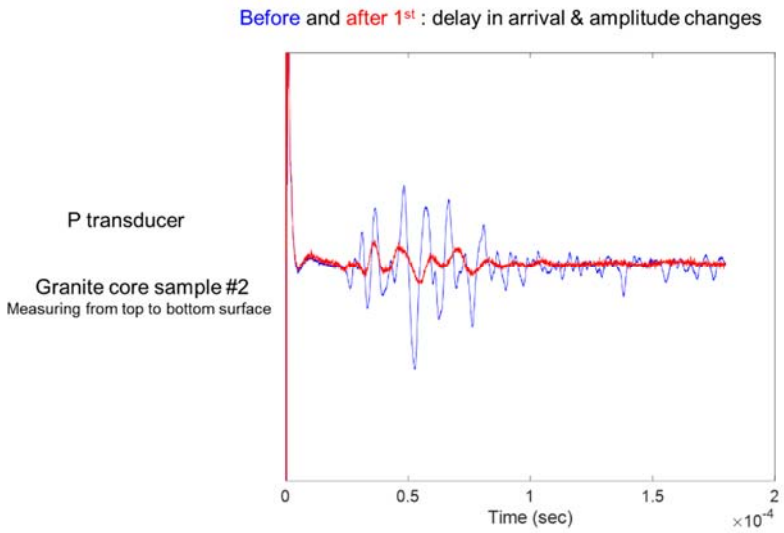


Figure 4.9 P-wave signature before and after quenching (Granite Core #2).

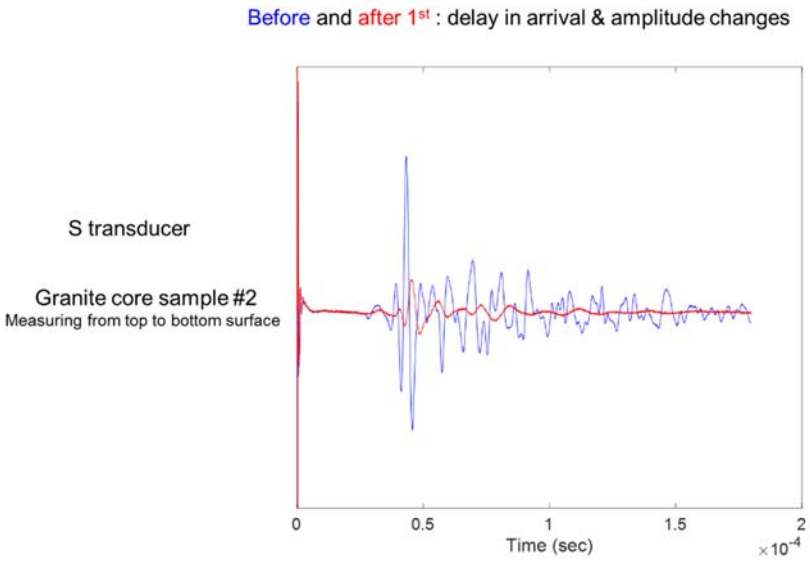


Figure 4.10 S-wave signature before and after quenching (Granite Core #2).

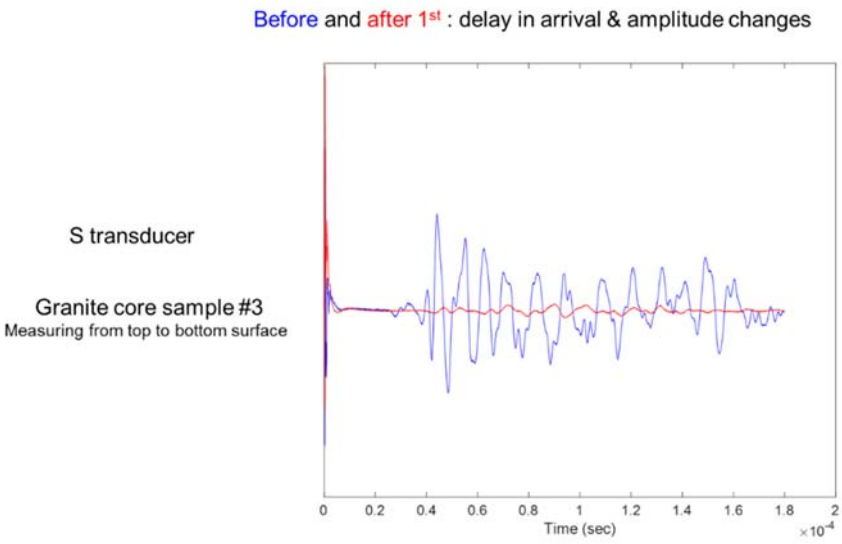


Figure 4.11 S-wave signature before and after quenching (Granite Core #3).

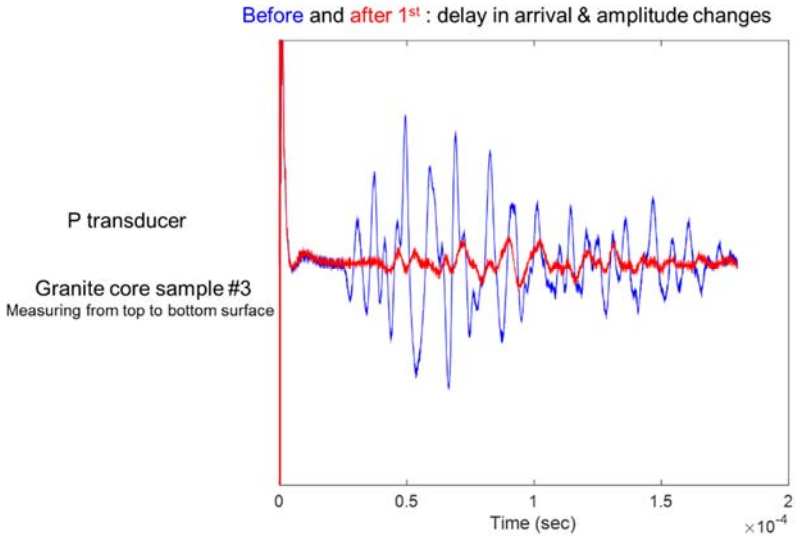


Figure 4.12 P-wave signature before and after quenching (Granite Core #3).

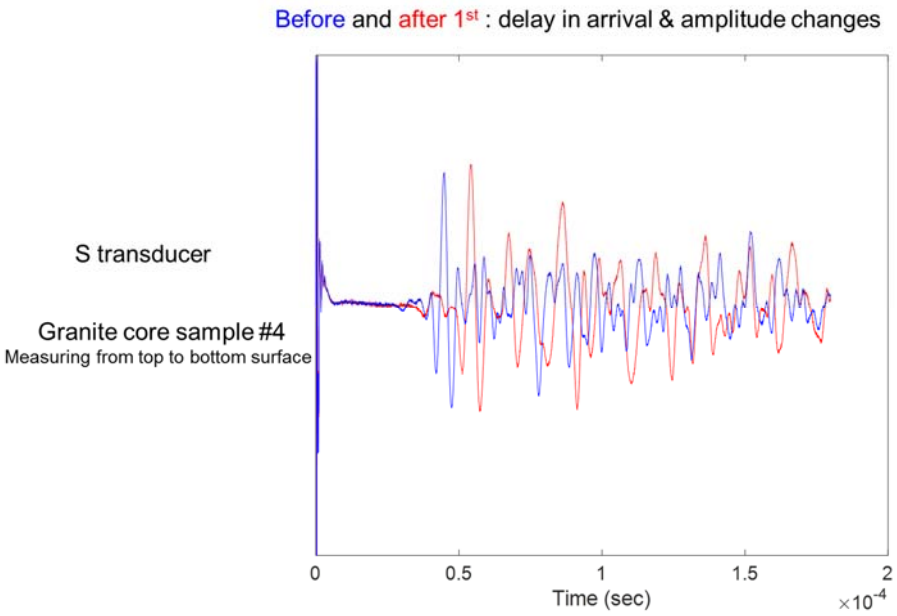


Figure 4.13 S-wave signature before and after quenching (Granite Core #4; just heating and cooling cycle without quenching).

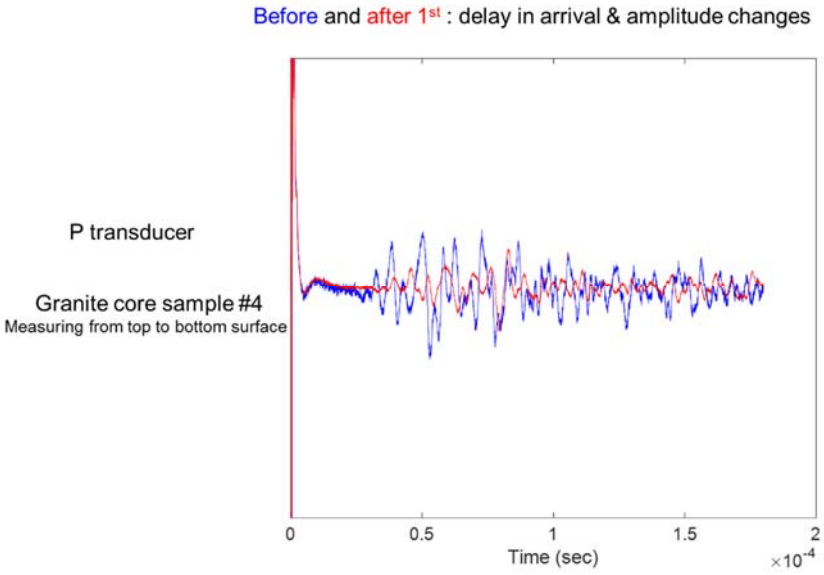


Figure 4.14 P-wave signature before and after quenching (Granite Core #4; just heating and cooling cycle without quenching).

As shown in Table 4.4, the thermal stimulation that occurred during the quenching test decreased the specimen density. We observed density decreases in all specimens subject to thermal treatment. Furthermore, a decrease in density of the rapidly quenched specimen is slightly greater than those that were slowly cooled (Specimen #4 in Table 4.4 is slowly cooling in the oven without quenching). The quenching will create a greater thermal stress that will induce microfractures inside the specimen, which is also the mechanism that may be responsible for the density decrease. Besides, the thermal gradient may also induce the dissolution of quartz and feldspar and re-deposition of this mineral within the specimen, which will also lead to the density decrease (Arshad et al., 2016).

Table 4-7 Density change before and after treatment

| Density ($g/cm^3$) | Specimen #1 | Specimen #2 | Specimen #3 | *Specimen #4* |
|---|---|---|---|---|
| Before treatment | 2.70 | 2.66 | 2.65 | 2.65 |
| After treatment | 2.65 | 2.64 | 2.62 | 2.63 |
| Density change percentage | 0.46% | 0.54% | 1.09% | 0.40% |

4.3.3 Micro-CT scan

Microscopic cracks of the granite specimen may be associated with the macroscopic property changes. The leakage bubble tests showed that macroscopic permeability changed after we perform the thermal stimulation on the granite specimen. Our micro-CT scan shows the microscopic fractures that caused by thermal stress

connected to a network after the thermal stimulation. So the results of micro-CT explain why the macroscopic permeability and the fluid transport properties of the rock changed remarkably after thermal stimulation. This phenomenon also indicates that the implication of thermal fracturing to the enhanced geothermal system is very important.

Two mechanisms have been suggested for thermal cracking. First, most rock-forming minerals are anisotropic, and, if there is a mismatch in the thermo-elastic behavior of minerals across a grain boundary, internal stresses may be generated as the rock is subjected to different temperatures and the stresses may be large enough to cause the formation of new cracks. The second model considers the effect of the temperature gradient. Local variations in the temperature gradient in rocks generate thermal stress that in turn will initiate the new fractures or propagate the existing cracks.

4.3.4 Thermal properties

Thermal gradient leads to a differential contraction of the rock, which in turn creates thermal stresses. It could conclude that this thermal stresses that happened during the thermal stimulation process will lead to the reduction of thermal conductivity of the rock, the shear modulus and constrained modulus, the tensile strength and the density. The changes of thermal properties before and after the quenching tests are listed in Table 4.5 and Table 4.6. The main reason behind the decreased thermal conductivities after quenching tests can be explained by micro cracks generated in the specimens due to quenching. Micro cracks introduce air or void in the specimen. The air has lower thermal conductivity (0.024 W/(m·K)) than the mineral comprising the granite, thus lowering

overall thermal conductivities of the treated granite. Similarly, the volumetric specific heat of the air is much lower than the granite.

Table 4-8 Changes in thermal conductivities before and after the quenching tests

| Thermal conductivity (W/m·K) | Specimen #1 | Specimen #2 | Specimen #3 | *Specimen #4* |
|---|---|---|---|---|
| Before | 3.012 | 3.056 | 3.042 | 3.014 |
| After | 2.964 | 2.876 | 2.814 | 2.980 |

Table 4-9 Changes in volumetric specific heat before and after the quenching tests

| Specific heat ($MJ/m^3K$) | Specimen #1 | Specimen #2 | Specimen #3 | *Specimen #4* |
|---|---|---|---|---|
| Before | 1.989 | 1.978 | 1.951 | 1.967 |
| After | 1.951 | 1.832 | 1.813 | 1.879 |

## 4.4 Conclusions

In our research, we successfully applied thermal shock on granite core specimens by heating and quenching them. The micro and macro properties alternation indicates that the thermal fracturing is efficient for enhancing the permeability of granite core specimen. The thermal stimulation mechanism can not only create new fractures but also will change the mechanical and thermal properties of our original material. Through thermal stimulation, especially after many cycles of thermal stimulations, we have increased porosity and permeability, decreased density, attenuated acoustic velocities, decreased

Shear Modulus and Constrained Modulus, decreased compressive and tensile strength, decreased thermal conductivity and specific heat.

Above results clearly show that by changing the properties of the granite, the thermal fracturing mechanism could maximum the hydraulic fracturing by further enhancing reservoir permeability, lowering breakthrough pressure level and improving fracturing efficiency. This also implies that circulation of cold water in the wellbore at low pressure in the enhanced geothermal system can be applied as a near-wellbore formation damage remediation mechanism. The thermal fracturing offers much promise as a new fracturing mechanism will potentially increase the permeability of reservoir in Enhanced Geothermal System and ultimately make it economically exploitable.

# 5. CONCLUSIONS

## 5.1 Key findings of the thesis

This research investigated the effect of thermal stimulation on fracture creation and permeability changes by laboratory studies. We developed an experimental rig designed to study thermal stimulations in a laboratory environment resembling EGS downhole conditions. Water is flown through wellbores of unconfined hot dry granite and concrete blocks. Unlike pressure-based fracturing, such as hydraulic fracturing, in this study, the wellbore is subject to continuous flow under flow pressure to maximize thermal shock effects. Additional insights are obtained by quenching tests using core-sized specimens. We have reached the following key conclusions.

- Only minor film boiling effect is observed between the injected water and the much hotter borehole surface with 190°C, as we observed the small temperature difference between borehole space and the borehole wall. This implies efficient temperature conduction from borehole fluid to formation surface, which is favorable for thermal shock treatment.
- Temperature propagation into the rock formation is significantly delayed during both the heating and water flow as expected. In terms of laboratory testing, this means significantly more heating is required after the boundary measurements reached the target temperature.
- Thermally driven fractures were initiated from the borehole surfaces and propagated adjacent to the boreholes to some extent, indicating that borehole pressure may need to follow in order to induce deeper fracture penetration. The

seed fractures created during thermal stimulation may reduce breakdown pressure levels.

- The profiles of borehole pressure decay obtained before and after each stage of stimulation show that water flows increase the permeability of treated specimens. Multiple treatments showed that increasing number of stimulations increases permeability possibly by furthering fracture propagation and creating new fractures.
- Acoustic measurements confirm that the stimulations generate micro-fractures inside the blocks, which will increase the matrix permeability.
- Bubble leakage tests visually demonstrated localized or distributed permeation spots (or leaking holes) that enhanced permeability. Permeation through the rock was not homogeneous, and there were invisible pathways (cracks, holes, or more permeable regions) that allowed preferential permeation of air/fluid.
- Mechanical and thermal properties of formation rock affect the effect of thermal stimulations. The granite blocks were harder to create fractures and increase permeability with the same amount of temperature difference and water flow.
- The core specimens manifested indirect indications of cracks - changes in mechanical and thermal properties - after experiencing the thermal flow. The effect enhanced with increasing number of cycles of the treatment.
- The thermal shock treatment decreased density (thus increasing porosity) and reduced acoustic amplitudes and velocities (thus decreasing elastic constants).

- The thermal shock decreased thermal conductivity and specific heat of the treated specimens. This is because the treatment created minute cracks, and thus creating air voids, which have lower thermal conductivity and specific heat than mineral solids.

## 5.2 Implications and future study

The knowledge obtained in this study may be applicable to wellbores that need stimulation such as enhanced geothermal wellbores and other underground resources and environmental projects. Thermal fracturing may also be used in combination with other stimulation technologies. In particular, the technique may help in the field to lower the breakdown pressure by creating seed fractures prior to a pressure-based treatment. Thus, the thermal fracturing mechanism may potentially increase the efficiency of hydraulic fracturing.

If lower breakdown pressure is achieved due to thermally induced fractures, It may also related to reduce environmental concerns (e.g., by reduced induced seismicity) associated with fracturing, and possibly lower stimulation cost, although economic analysis is needed to verify.

To further develop this thermal fracturing mechanism, future research must go past the unconfined testing presented in this study. A few topics for further studies have been identified. Thermal fracturing at reservoir stress levels by thermal shock and the added effect of borehole pressurization such as hydraulic loading are still poorly understood. The effect of stress level and stress anisotropy on the characteristics of thermal fracturing can be investigated by using a triaxial loading system. The effects of various material

properties on fracturing behavior should be thoroughly investigated. A dimensional analysis considering relevant parameters will serve as a frame of understanding and will guide the scaling up of laboratory studies to potential field applications.

# REFERENCES


Alqahtani, N. B., Miskimins, J. L., Huang, C. & Cha, M. (2017) 3D Finite Element Modeling of Thermally-induced Stress during a Cryogenic Fracturing Experiment In *Proceedings of 51st US Rock Mechanics/Geomechanics Symposium, American Rock Mechanics Association*.

Alqatahni, N. B., Cha, M., Yao, B., Yin, X., Kneafsey, T. J., Wang, L., Wu, Y.-S. & Miskimins, J. L. (2016) Experimental Investigation of Cryogenic Fracturing of Rock Specimens Under True Triaxial Confining Stresses. In *SPE Europec featured at 78th EAGE Conference and Exhibition*.) Society of Petroleum Engineers.

Arshad, M., Nakagawa, M., Jahanbakhsh, K. & Dunnington, L. (2016) An Insight in Explaining the Stress Distribution in and around EGS. *arXiv preprint arXiv:1611.00596*.

ASTM (2008a)D2845-08 Standard Test Method for Laboratory Determination of Pulse Velocities and Ultrasonic Elastic Constants of Rock, ASTM International.

ASTM (2008b)D3967 Standard Test Method for Splitting Tensile Strength of Intact Rock Core Specimens.

ASTM (2014a)ASTM C192/C192M Standard Practice for Making and Curing Concrete Test Specimens in the Laboratory.

ASTM (2014b)D7012 Standard Test Methods for Compressive Strength and Elastic Moduli of Intact Rock Core Specimens under Varying States of Stress and Temperatures.

Bazant, Z. P. & Kaplan, M. F. (1996) *Concrete at high temperatures: material properties and mathematical models.* Longman.

Bradford, J., Moore, J., Ohren, M., Mclennan, J., Osborn, W. L., Majer, E., Nash, G., Podgorney, R., Freifeld, B. & Nye, R. (2015) Recent Thermal and Hydraulic Stimulation Results at Raft River, ID EGS Site. In *40th Workshop on Geothermal Reservoir Engineering*.), pp. 561-571.

Cha, M., Alqahtani, N., Yao, B., Wang, L., Yin, X., Wu, Y. & Kneafsey, T. (2016a) Studying cryogenic fracturing process using transparent specimens In *Proceedings of The 1st International Conference on Energy Geotechnics, August 29-31, 2016*, pp. 211-216.

Cha, M., Alqahtani, N. B., Yao, B., Yin, X., Wu, Y. S. & Kneafsey, T. J. (2016b) Development of laboratory system for cryogenic fracturing study In *Proceedings of ICEGT 2016*, pp. 381-388.

Cha, M., Cho, G.-C. & Santamarina, J. C. (2009) Long-wavelength P-wave and S-wave propagation in jointed rock masses. *Geophysics* 74(5):E205-E214.

Cha, M. & Cho, G. C. (2007) Compression wave velocity of cylindrical rock specimens: engineering modulus interpretation. *Japanese Journal of Applied Physics Part 1-Regular Papers Brief Communications & Review Papers* 46(7B):4497-4499.

Cha, M., Yin, X., Kneafsey, T., Johanson, B., Alqahtani, N., Miskimins, J., Patterson, T. & Wu, Y.-S. (2014) Cryogenic fracturing for reservoir stimulation–Laboratory studies. *Journal of Petroleum Science and Engineering* 124:436-450.

Duchane, D. & Brown, D. (2002) Hot dry rock (HDR) geothermal energy research and development at Fenton Hill, New Mexico. *Geo-Heat Centre Quarterly Bulletin* 23(4):13-19.

Enayatpour, S. & Patzek, T. (2013) Thermal Shock in Reservoir Rock Enhances the Hydraulic.) Unconventional Resources Technology Conference (URTEC).

Fragaszy, R., Santamarina, J., Amekudzi, A., Assimaki, D., Bachus, R., Burns, S., Cha, M., Cho, G., Cortes, D., Dai, S., Espinoza, D., Garrow, L., Huang, H., Jang, J., Jung, J., Kim, S., Kurtis, K., Lee, C., Pasten, C., Phadnis, H., Rix, G., Shin, H., Torres, M. & Tsouris, C. (2011) Sustainable development and energy geotechnology — Potential roles for geotechnical engineering. *KSCE Journal of Civil Engineering* 15(4):611-621.

Haimson, B. & Chang, C. (2000) A new true triaxial cell for testing mechanical properties of rock, and its use to determine rock strength and deformability of Westerly granite. *International Journal of Rock Mechanics and Mining Sciences* 37(1):285-296.

Lamond, J. F. & Pielert, J. H. (2006) Significance of tests and properties of concrete and concrete-making materials.) ASTM West Conshohocken, PA.

Pasikki, R. G., Libert, F., Yoshioka, K. & Leonard, R. (2010) Well stimulation techniques applied at the salak geothermal field. In *Proceedings of the World Geothermal Congress*.), pp. 11.

Powers, T. C. (1969) The properties of fresh concrete.

Siratovich, P., Cole, J., Heap, M., Villeneuve, M., Reuschlé, T., Swanson, K., Kennedy, B., Gravley, D. & Lavallée, Y. (2015) Experimental thermal stimulation of the Rotokawa Andesite.

Siratovich, P. A. (2014) Thermal Stimulation of the Rotokawa Andesite: A Laboratory Approach.

Siratovich, P. A., Sass, I., Homuth, S. & Bjornsson, A. (2011) Thermal stimulation of geothermal reservoirs and laboratory investigation of thermally-induced fractures. In *Proc., Geothermal Resources Council Annual Meeting*.), pp. 1529-1535.

Tarasovs, S. & Ghassemi, A. (2014) Self-similarity and scaling of thermal shock fractures. *Physical Review E* 90(1):012403.

Tsang, Y. (1984) The effect of tortuosity on fluid flow through a single fracture. *Water Resources Research* 20(9):1209-1215.

Wang, J., Tsang, C. & Sterbentz, R. (1982) The state of the art of numerical modeling of thermohydrologic flow in fractured rock masses. *Environmental Geology* 4(3-4):133-199.

Wang, L., Yao, B., Cha, M., Alqahtani, N. B., Patterson, T. W., Kneafsey, T. J., Miskimins, J. L., Yin, X. & Wu, Y.-S. (2016) Waterless fracturing technologies for unconventional reservoirs-opportunities for liquid nitrogen. *Journal of Natural Gas Science and Engineering* 35:160-174.

Yong, C. & Wang, C. Y. (1980) Thermally induced acoustic emission in Westerly granite. *Geophysical Research Letters* 7(12):1089-1092.

Yu, W., Bao-Lin, L., Hai-Yan, Z., Chuan-Liang, Y., Zhi-Jun, L. & Zhi-Qiao, W. (2014) Thermophysical and mechanical properties of granite and its effects on borehole stability in high temperature and three-dimensional stress. *The Scientific World Journal* 2014.